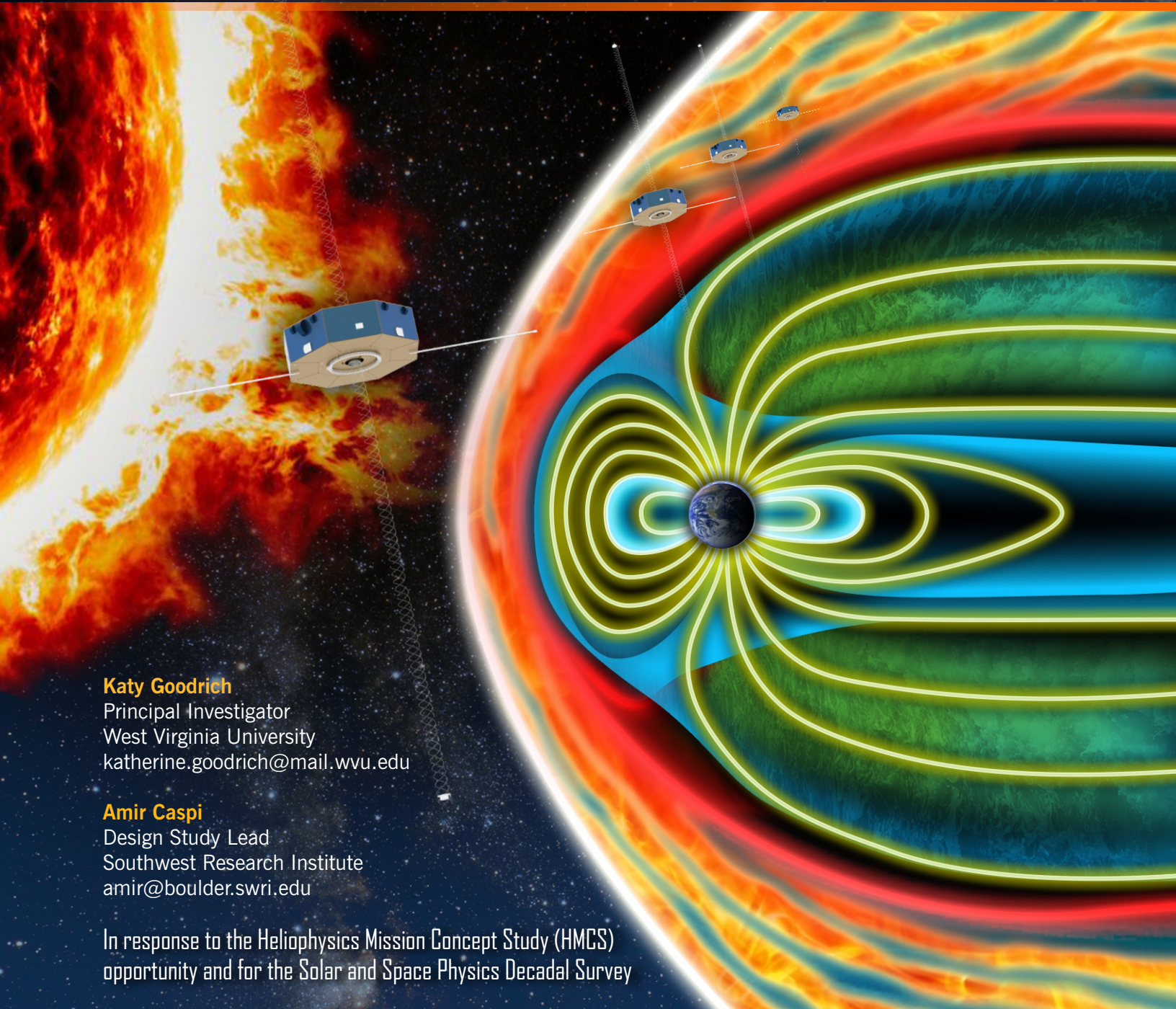




MISSION CONCEPT STUDY REPORT

# MAKOS

Multi-point Assessment of the Kinematics of Shocks



**Katy Goodrich**  
Principal Investigator  
West Virginia University  
katherine.goodrich@mail.wvu.edu

**Amir Caspi**  
Design Study Lead  
Southwest Research Institute  
amir@boulder.swri.edu

In response to the Heliophysics Mission Concept Study (HMCS) opportunity and for the Solar and Space Physics Decadal Survey



## Table of Contents

---

<b>Table of Contents</b>	<b>i</b>
<b>Executive Summary</b>	<b>iii</b>
<b>FOLDOUT: MAKOS mission summary</b>	<b>iv</b>
<b>1 Science Overview</b>	<b>1</b>
1.1 Outstanding Science Questions	1
1.2 Background and Motivation	1
1.3 Current Knowledge of Collisionless Shocks	1
1.4 Outstanding Questions and Necessary Measurements	2
1.5 MMS Limitations	6
1.6 Expected Scientific Impact	7
<b>2 Mission Concept Implementation</b>	<b>9</b>
2.1 Overview	9
2.2 Technology Maturity	9
2.3 Key Trades	10
<b>3 Technical Overview</b>	<b>11</b>
3.1 Payload Description	11
3.1.1 <i>Solar Wind Ions (SWI)</i>	11
3.1.2 <i>Solar Wind Electrons (SWE)</i>	12
3.1.3 <i>Suprathermal Ions (STI)</i>	14
3.1.4 <i>Suprathermal Electrons (STE)</i>	15
3.1.5 <i>Energetic Particles (EP)</i>	15
3.1.6 <i>Fluxgate Magnetometer (FGM)</i>	16
3.1.7 <i>Search Coil Magnetometer (SCM)</i>	17
3.1.8 <i>Electric Fields (EF)</i>	18
3.2 Concept of Operations and Mission Design	19
3.2.1 <i>Mission Design</i>	19
3.2.2 <i>Concept of Operations</i>	23
3.3 Flight System (Spacecraft)	25
3.3.1 <i>Instrument Accommodation</i>	26
3.3.2 <i>Structure and Mechanical</i>	28
3.3.2.1 <i>Structural Analysis</i>	29
3.3.3 <i>Thermal Subsystem</i>	30
3.3.4 <i>Electrical Power</i>	30
3.3.5 <i>Telecommunication Subsystem</i>	32
3.3.6 <i>Command and Data Subsystem</i>	33
3.3.6.1 <i>Commanding</i>	33
3.3.6.2 <i>Data Management</i>	33
3.3.6.3 <i>Observatory Time Management</i>	34
3.3.7 <i>Guidance, Navigation, and Control Subsystem</i>	34
3.3.7.1 <i>Observatory Spin Motion Effects on Star Tracker Performance</i>	36
3.3.7.2 <i>Spin Phase Synchronization</i>	36
3.3.8 <i>Propulsion Subsystem</i>	37
3.3.9 <i>Autonomy and Fault Management</i>	38
3.4 Development Approach	38
3.5 Risk List	39

<b>4</b>	<b>Development Schedule and Schedule Constraints</b>	<b>41</b>
4.1	Management Approach	41
4.2	Organization & Processes	42
4.3	High-Level Mission Schedule	43
4.4	Science, Technology Development Plan(s)	43
4.5	Development Schedule and Constraints	44
<b>5</b>	<b>Mission Life-Cycle Cost</b>	<b>46</b>
5.1	Cost Estimate Summary	46
5.2	Costing Methodology	46
5.3	Estimate Allocation	51
	<b>References</b>	<b>53</b>
	<b>Appendix 1: Master Equipment List (MEL)</b>	<b>55</b>

## Executive Summary

---

This report describes the motivation and implementation for **MAKOS** (Multi-point Assessment of the Kinematics Of Shocks), the first-ever spacecraft mission specifically designed and dedicated to the observation of both the terrestrial bow shock, as well as interplanetary shocks in the solar wind. Collisionless shocks are one of the main forms of energy conversion in space plasmas. They can directly or indirectly drive other universal plasma processes such as magnetic reconnection, turbulence, particle acceleration and wave phenomena. Despite their importance, and decades of observations and theoretical/simulation-based studies, the basic ability to predict how a shock with given upstream parameters will partition the incident energy amongst the various degrees of freedom available remains elusive.

The partitioning of energy downstream of collisionless shocks is not well understood, nor are the processes which perform energy conversion. Despite a wealth of observations of the terrestrial bow shock, previous instrument and mission-level limitations have made it impossible to quantify this partition. In order to understand these important, universal collisionless plasma processes and establish the physics within the shock layer, its dependence on upstream conditions, and its governance of downstream conditions, MAKOS must be implemented.

The MAKOS mission concept comprises four spacecraft (S/C) with varying spatial separations in high-altitude, slightly elliptical ( $22.1 \times 17 R_E$ ) five-to-one (5:1) lunar resonance orbits (LROs) with opposite lines of apsides to maximize the number of bow shock crossings, even when apogee is on the nightside. Each of the two orbits has two S/C with separations on the order of  $\sim 1000$  km to obtain the required simultaneous upstream and downstream shock observations and multipoint observations at ion-kinetic scales through every shock transition layer crossing. The separations between spacecraft on the different orbits range from  $\sim 4$  to  $7 R_E$ . This implementation provides year-round crossings of the bow shock with simultaneous multipoint separations ranging from ion kinetic ( $\sim 1000$  km; each pair) to MHD (several  $R_E$ ; the pair of pairs) scales, as well as prolonged dwell time in the solar wind, enabling MAKOS to simultaneously probe both ion-kinetic and MHD-scale processes during every shock crossing, including both Earth's bow shock and interplanetary shocks.

MAKOS requires each S/C to carry a comprehensive science payload of particles and field instruments specifically tailored to measure the *in situ* processes specific to collisionless shocks and their total energy budgets. The need to fully characterize the plasma populations upstream and downstream of the shock drives a mission requirement that the complete thermal and suprathermal electron and ion velocity distributions be sampled at very high temporal resolutions. This is achieved in the notional mission design by carrying multiple dedicated sensors targeting each species and energy range on a rapidly-spinning (10 RPM baseline) S/C.

The four-observatory configuration that we propose will require \$651 million (FY22) funding as a current best estimate. This includes \$601 million in Phase B–D development costs and \$50 million in Phase E–F operations and science cost. Recognizing that this is a preliminary concept study, we apply conservative reserves to all cost elements: 50% for all Phase B–D work and 25% for Phase E–F. This brings the baseline estimate to \$964 million including these reserves, with \$901 million allocated to Phases B–D and \$63 million for Phases E–F.

# MAKOS: Multi-point Assessment of the Kinematics Of Shocks

## MAKOS Science Objectives

1. Quantify the energy budget both upstream and downstream of collisionless shocks
2. Discern all processes governing energy conversion at and within collisionless shocks
3. Establish how and why those processes vary with shock orientation and driving conditions

## MAKOS Payload

### INSTRUMENTS

1. Solar Wind Ions (SWI): 2 sensorheads
2. Solar Wind Electrons (SWE): 4 sensorheads
3. Suprathermal Ions (STI): 4 sensorheads
4. Suprathermal Electrons (STE): 4 sensorheads
5. Energetic Particles (EP): 1 sensorhead
6. Fluxgate Magnetometer (FGM): 2 sensors
7. Search Coil Magnetometer (SCM): 3-axes
8. Electric Fields (EF): 3-axes

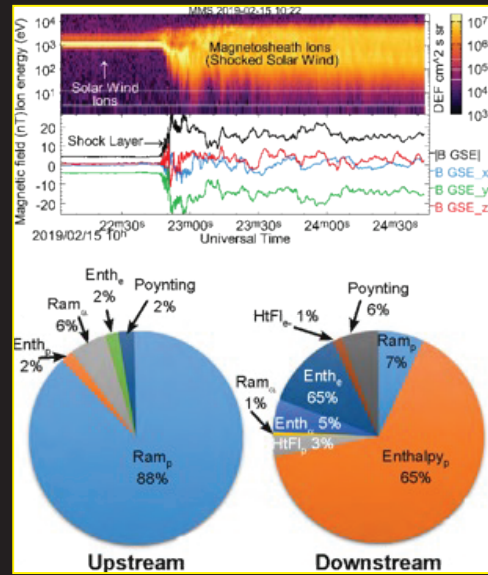
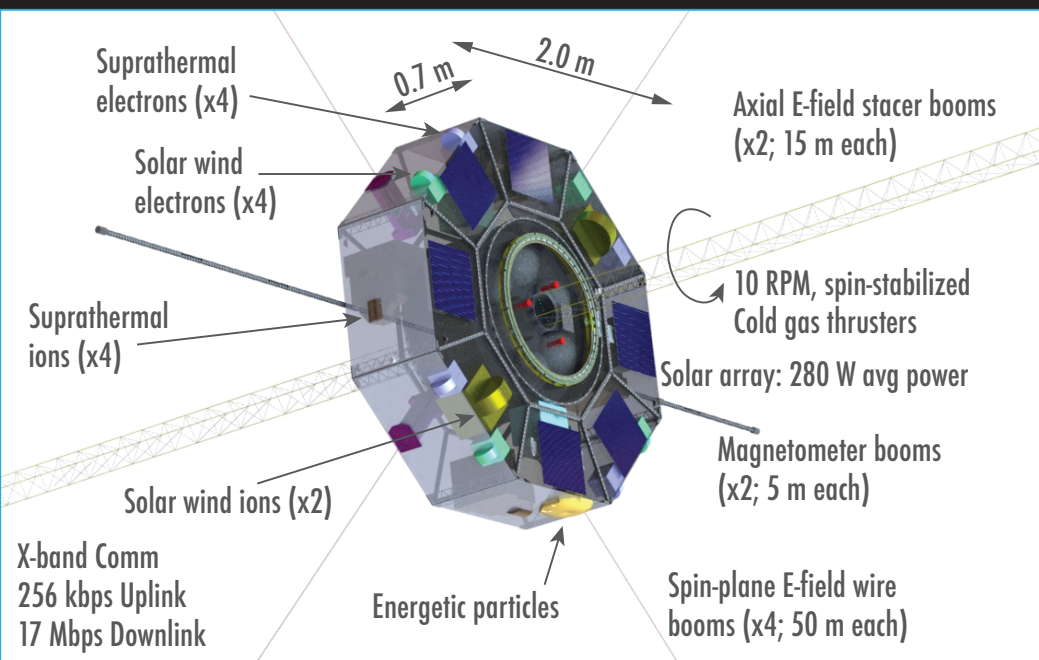
### MASS

- 3.5 kg x2
- 2.6 kg x4
- 11.4 kg x4
- 2.6 kg x4
- 3.9 kg
- 0.7 kg x2
- 0.8 kg
- 22.0 kg

### POWER

- 3.5 W x2
- 3.2 W x4
- 12.0 W x4
- 3.2 W x4
- 3.8 W
- 4.0 W x2
- 1.0 W
- 8.4 W

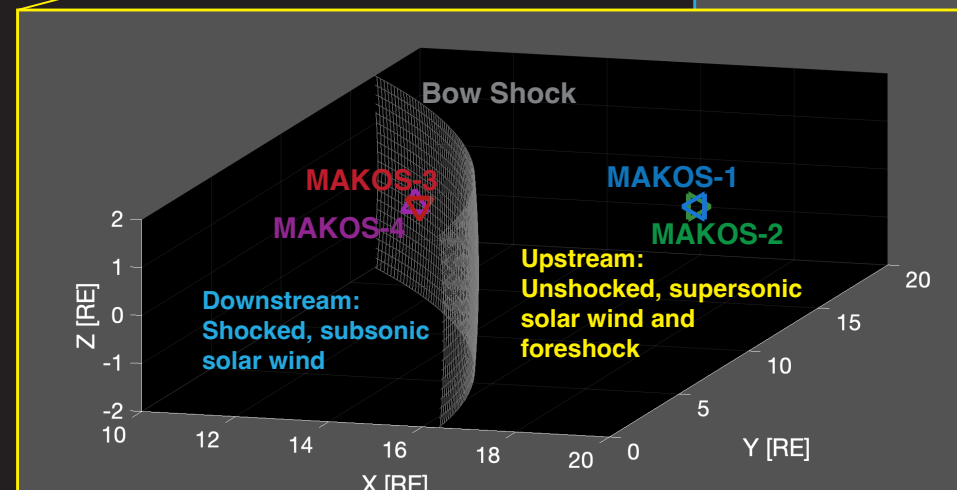
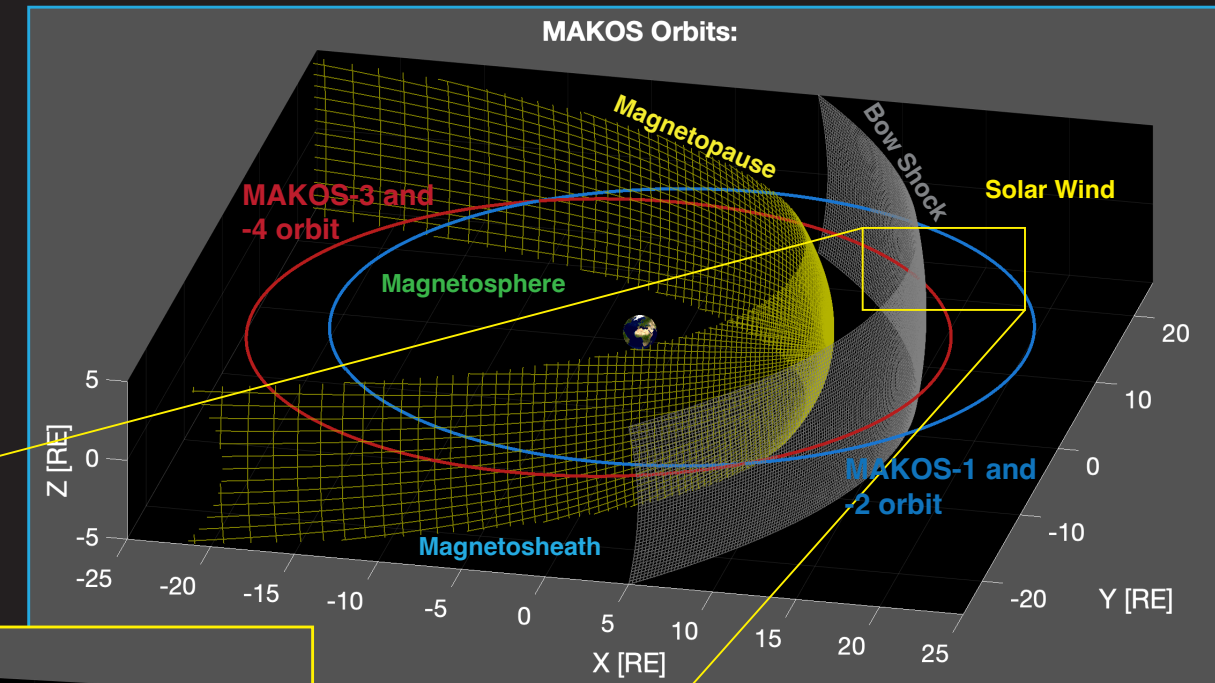
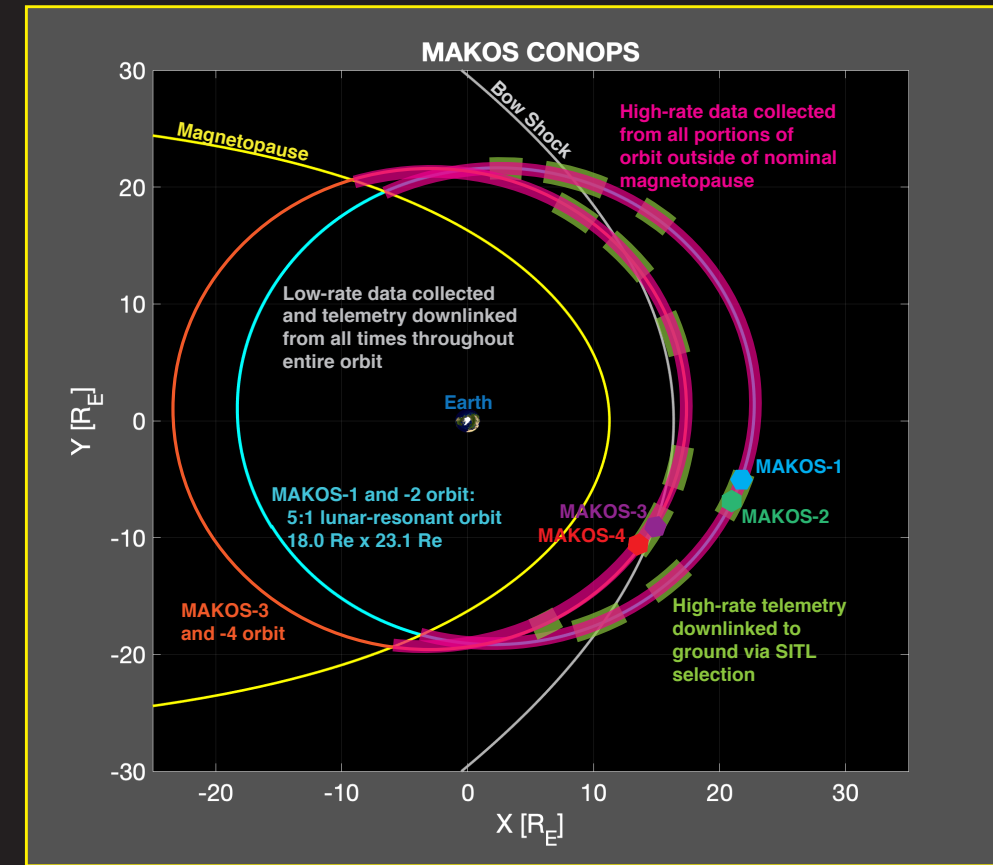
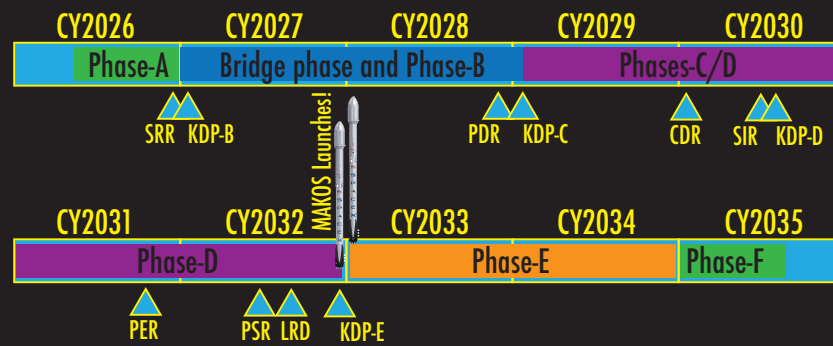
## MAKOS Observatories: 4x Identical



## Mission Overview

- 4 identically instrumented spacecraft in two common, 5:1 lunar resonant orbits
- Custom observatory and mission design to provide unprecedented measurements of collisionless shocks: Earth's bow shock and interplanetary shocks in the solar wind
- Multipoint formation ensures simultaneous measurements of upstream, downstream, and shock transition region with observatory pairs at ion kinetic and MHD scales
- Payload consisting of 8 science instruments for comprehensive plasma, particles, fields, and waves observations of collisionless shocks
- Solar wind pointed spinners at 10 RPM enabling unprecedented solar wind observations at 1 AU
- Cold gas propellant for attitude control and orbital delta-V
- X-band communications with DSN providing 17 Mbps downlink
- Straightforward CONOPS approach to reduce complexity and risk
- Scientist-in-the-Loop ensures return of 29 TB of prime science data for analysis
- Use of latest in small-satellite technology for efficient space vehicle design
- 2-year prime mission, with 3-year mission design life
- Cost: \$FY22 964M for Phases B-F, including 50% reserves (B-D) and 25% (E-F)

## Mission Timeline



## Enhancing Tech. Development

1. Electrostatic analyzer systems with reliable high-voltage optocouplers and responsive, precision-tuned HVPS for fast measurements
2. Optical communications from deep-space for highest-level of data availability for science analysis and discovery

# 1 Science Overview

---

## 1.1 Outstanding Science Questions

Understanding shocks in space plasmas is vital to the understanding of our universe, from the heating and deflection of bulk flows to the acceleration of cosmic rays. Moreover, collisionless shocks directly influence our own terrestrial space environment, e.g., solar wind-magnetosphere interactions. Vital questions regarding collisionless shocks remain unanswered:

- 1 What is the partition of energy across collisionless shocks?
- 2 What are the processes governing energy conversion at and within collisionless shocks?
- 3 How and why do these processes vary with macroscopic shock parameters?

## 1.2 Background and Motivation

Shocks are spatial discontinuities that form when a supersonic flow encounters an obstacle. If the medium travels faster than the speed of communication (i.e., information flow), the medium has no time to smoothly adjust its trajectory. A shock forms ahead of the obstacle and slows the supersonic flow to subsonic speeds in order for the medium to move past the obstacle. In high density media, the shock structure and evolution are governed by particle collisions, but shocks also act as a universal energy conversion mechanism in collisionless space plasmas. There is currently no known equation of state for collisionless shocks. Such an equation of state, if it could be found, would predict how the internal energy would be reconfigured as the plasma passes through a shock in response to the deceleration, deflection, heating, and compression demanded by the macroscopic shock initiation.

The most relevant collisionless shock to humans, and the one most often measured *in situ*, is the terrestrial bow shock. Earth's bow shock is also significantly more straightforward to observe relative to interplanetary (IP) shocks in the solar wind, as it remains in the same spatial position relative to Earth (to within a few Earth radii). Therefore, we derive the majority of our knowledge of collisionless shock dynamics from the terrestrial bow shock. The solar wind inputs primarily bulk proton ram energy upstream of the bow shock.

The shock outputs energy in several different forms, including, but not limited to, electron, proton, and heavy ion acceleration and heating, together with Poynting flux and turbulent fluctuations. Previous missions together with numerical simulations have provided invaluable insight to the overall structure and behavior of the terrestrial bow shock, as the next section discusses (e.g., Burgess et al., 2015). However, we will show that in order to observe the shock's detailed fundamental behavior, we require observations specifically designed to observe the terrestrial bow shock as a primary region of interest.

## 1.3 Current Knowledge of Collisionless Shocks

Past missions that have observed the terrestrial bow shock include MMS, THEMIS, Cluster, Wind, AMPTE, and ISEE. They confirmed that the shock can exist as a nonstationary discontinuity. It can act as a "breathing barrier" between the solar wind and the terrestrial magnetosphere, changing in response to varying upstream conditions. The spatial scale, energy conversion processes, and output of the shock are most heavily dependent on the orientation of the Interplanetary Magnetic Field (IMF) relative to the shock normal vector ( $\hat{n}$ ) and the fast magnetosonic Mach number ( $M_f$ ). Shocks are generally categorized as either Quasi-perpendicular ( $Q_{\perp}$ ) or Quasi-parallel ( $Q_{\parallel}$ ) depending on whether the angle between the IMF and shock normal ( $\theta_{Bn}$ )

is greater than or less than  $45^\circ$ . The terrestrial bow shock also tends to grow more turbulent in nature as  $M_f$  increases and as the plasma  $\beta$  decreases. Figure 1.1 illustrates the complexity of the terrestrial bow shock global structure.

At  $Q_\perp$  shocks (i.e., toward the top of the figure), particle motion in the shock-normal direction is restricted by the Lorentz force to within one gyroradius in the upstream direction. Thus,  $Q_\perp$  shocks tend to have short coherent transition regions, with quasi-static magnetic and electric fields making the largest contributions to the bulk particle dynamics.

Supercritical  $Q_\parallel$  shocks (Figure 1.1, bottom) permit particle traversals in both directions across the shock, including well into the upstream region and provide foreknowledge of the shock to the incident plasma (a feature entirely unique to collisionless plasma shocks). Such shocks exhibit an extended transition region and are dominated by strongly varying particle sub-populations, particle reflection with corresponding kinetic instabilities and turbulence, and particle acceleration. The nonlinear feedback enabled by the shock interacting with the upstream plasma can also lead to the development of foreshock transient events such as hot flow anomalies (Schwartz et al., 2018) and foreshock bubbles (Turner et al., 2013), which can locally generate their own shocks and foreshocks (Wilson et al., 2016; 2013) in poorly understood ways. Such complex, nonlinear behavior at  $Q_\parallel$  shocks and in the ion foreshock also contributes to, and further complicates, the total energy budget at collisionless shocks.

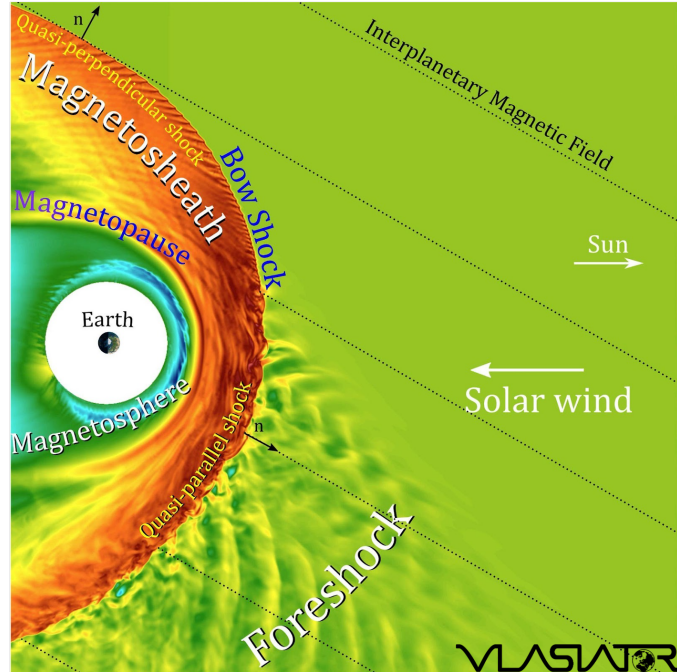


**Figure 1.1:** Global Vlasov Simulation of the terrestrial bow shock. Note the extended turbulent structure at the quasi-parallel shock (toward the bottom) by comparison to that at the quasi-perpendicular shock (toward the top). Figure courtesy of Prof. M. Palmroth and the Vlasior team at U. Helsinki.

#### 1.4 Outstanding Questions and Necessary Measurements

While it is known that collisionless shocks perform energy conversion, specifically to process the bulk flow kinetic energy density (Chen et al., 2018; Goodrich et al., 2018; Wilson et al., 2014a; 2014b), the details of this energy conversion and output remain unclear. The kinetic-scale processes that perform this energy conversion are not well known or well observed within the terrestrial bow shock. Moreover, it is not clear what the resulting energy budget is once the plasma traverses the shock or how it varies for different shock conditions. In this section, we describe the scientific motivation and the measurements necessary to address these questions.

##### 1) What is the partition of energy across collisionless shocks?

To understand how energy is partitioned in the shock, it is important to accurately resolve the types and weights of different energy inputs and outputs of the system. Simultaneously relating upstream and downstream conditions remains a persistent challenge in studying shock

physics as it necessitates simultaneous, complementary, and inter-calibrated upstream and downstream measurements of the plasma.

Important energy fluxes to measure include those related to particle bulk flow, thermal and energetic/non-thermal energy for multiple, relevant species (protons, alphas, heavy ions, and electrons), together with electromagnetic energy. These different energies require measurements of full velocity distribution functions. The thermal properties, anisotropies, and non-Maxwellian thermal features of the cool incident solar wind populations (i.e., electrons, protons, and alphas,  $<1$  keV) as well as higher energy particles (i.e., electrons, H, He, C, N, O, and Ne,  $>1$  keV) must also be resolved. Crucially, the cold thermal solar wind plasma beam must be fully resolved without compromising the measurement of the hot, shocked plasma or suprathermal reflected and accelerated particles.

The majority of the upstream energy flux consists of proton ram energy while proton enthalpy flux comprises the majority of the downstream partition (Schwartz et al., 2022) (Figure 1.2). The shock can also produce other significant energy fluxes including those in accelerated particles, nonthermal features, and DC/AC Poynting flux or turbulence. Although these energy fluxes are minor contributions to the energy partition, they can be significant to the overall dynamics of the shock, or to the nature of the shocked plasma with the magnetosphere interaction.

Two crucial factors must be considered. Firstly, the upstream and downstream plasma must be observed in correlation to ensure that the output energy fluxes are matched to the measured inputs. Secondly, the upstream plasma must be measured in such a way that it is clearly not perturbed by conditions of the shock itself (i.e., by reflected particles, ultra-low frequency waves, and foreshock phenomena). Historically, magnetospheric missions have lacked one or more capabilities to solve this problem. Those capabilities include matched up/downstream measurements, comprehensive inter-calibrated instrumentation, time resolution, velocity-space resolution, and spacecraft separations. Progress can be made with observations from NASA's Magnetospheric Multiscale (MMS) mission, but significant uncertainties plague our ability to find closure. These uncertainties are detailed in Schwartz et al. (2022) and are partially summarized in the following section.

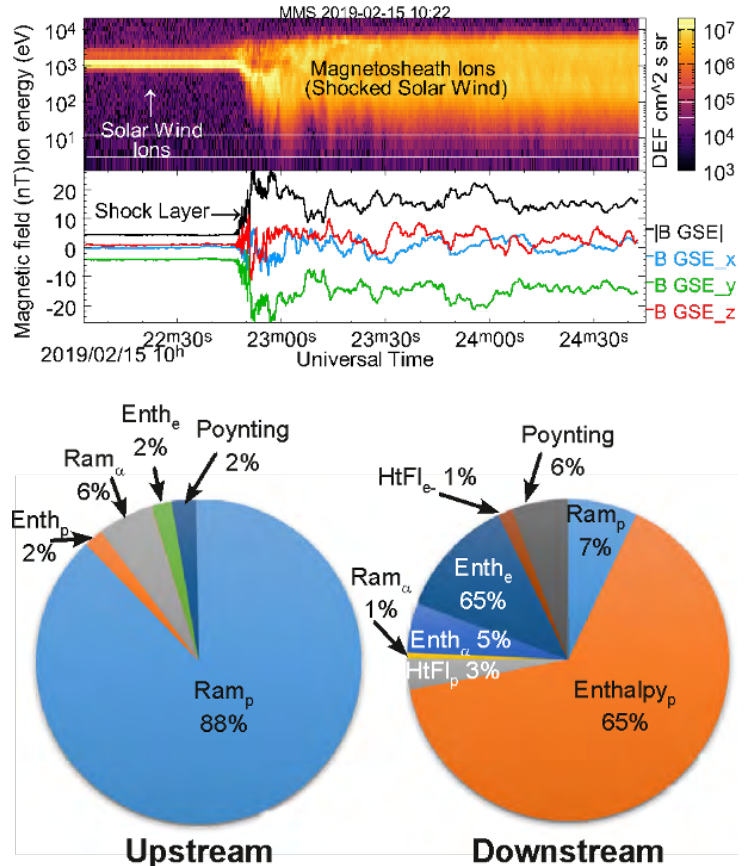


**Figure 1.2:** Documented energy partition upstream and downstream of an example shock. (Schwartz et al., 2022). Proton bulk flow ram energy dominates the upstream energy flux. It gets partitioned across the particle populations downstream. The relative proportions depend on the upstream parameters in unknown ways.

Without a full account of the energy partition, our modeling and simulation knowledge of shocks, and the applicability of that knowledge to more distant space environments, is at a significant disadvantage. Improvements can and must be made to allow for these observations. MAKOS will do this by engaging four spacecraft with varied spacing. Two of the four spacecraft (separated at ion kinetic scales,  $\sim 1000$  km) will act as upstream monitors with apogees up to  $25 R_E$ . The two remaining spacecraft (also spaced  $\sim 1000$  km apart) will be separated from the upstream monitors by several Earth radii anti-sunward to observe the resulting magnetosheath.

MMS shock observations, with high-temporal resolution, allow us to correlate wave and particle behavior like never before (Figure 1.3). Despite its capabilities, however, MMS has significant limitations in its capability to observe shock phenomena. Similarly, ESA's Cluster mission, while better spaced than MMS, was insufficiently instrumented to fully address MAKOS science objectives. We describe these limitations in detail within the following section.

To bring closure to this question, we must measure full velocity distribution functions at a high time resolution (tens of ms) with an energy and angular resolution specified for the solar wind ion distribution. The proposed MAKOS mission intends to develop and outfit such particle instruments. In addition to the DC fields that govern the lowest order particle dynamics, MAKOS will also measure high frequency electric and magnetic field oscillations to identify local plasma instabilities and estimate the amount of energy carried away from the shock region by plasma waves. Using these measurements, plasma instabilities and energy conversion mechanisms will be quantified and distinguished within the shock and then correlated with the energy budgets measured by the spacecraft situated upstream and downstream of the shock.

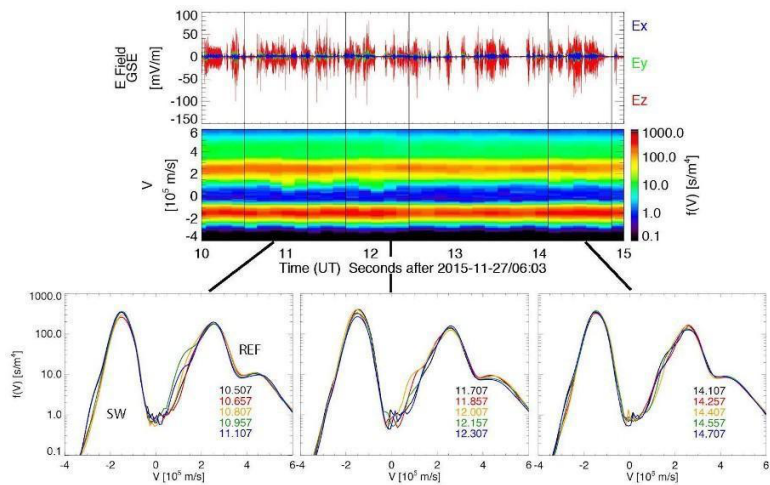


**Figure 1.3:** Comparison of 2D ion velocity distributions and electrostatic waves. Bursty electric fields (top) can be linked to fast time variations in particle reflection off the shock which manifests itself in fine scale structure in velocity. This illustrates the interplay between the macroscopic shock inputs and the processes responsible for ultimately converting that energy to other forms. (Taken from Goodrich et al., 2019)

## 2) What are the processes governing energy conversion at and within collisionless shocks?

The knowledge of several different conversion mechanisms include, but are not limited to, a cross-shock electrostatic potential (Chen et al., 2018; Tsurutani et al, 1981), current-driven instabilities such as the Buneman (Bale et al., 2007; Goodrich et al., 2016) and electron-cyclotron drift (Breneman et al., 2015), magnetic reconnection (Gingell et al., 2017), other wave-particle interactions (Chen et al., 2018; Goodrich et al., 2019; Wilson et al., 2014b) , and particle acceleration and reflection. We know, for example, that at even modest Mach number,  $Q_{\perp}$  shocks particle reflection initiates the dispersal in velocity space that results in a higher second moment (temperature). The balance between that mechanism and others within the

shock layer that act on both the incident protons and other species is not understood. It is also unknown how these mechanisms change with upstream conditions, or if the presence of one mechanism drastically alters the resultant downstream plasma.

Within the shock, energy is converted on the kinetic scale (see the references above). This inherently renders MHD modeling insufficient to accurately simulate collisionless shocks in their full complexity. We have learned much from PIC and Vlasov simulations, but we have yet to provide observational confirmation. Historically, *in situ* spacecraft have relied on particle detectors that can resolve full velocity distribution functions (VDFs) over one full spin period, on the order from one to tens of seconds. However, observed bow shock crossings can have observational lifetimes on the order of seconds, rendering most past particle instrument resolutions insufficient.

MMS shock observations, with high temporal resolution, allow us to correlate wave and particle behavior like never before. Despite its capabilities, however, MMS has significant limitations in its capability to observe shock phenomena. We describe these limitations in detail within Section 1.5.

To bring closure to this question, we must measure full velocity distribution functions at a high time resolution (tens of ms) with an energy and angular resolution specified for the solar wind ion distribution. The proposed MAKOS mission intends to develop and outfit such particle instruments. In addition to the DC fields that govern the lowest order particle dynamics, MAKOS will also measure high frequency electric and magnetic field oscillations to identify local plasma instabilities and estimate the amount of energy carried away from the shock region by plasma waves. Using these measurements, plasma instabilities and energy conversion mechanisms will be quantified and distinguished within the shock and then correlated with the energy budgets measured by the spacecraft situated upstream and downstream of the shock.

### **3) *How and why do these processes vary with macroscopic shock parameters?***

The final question is how the energy partitioning process and outputs are related to the shock's driving conditions. It is known that  $\theta_{Bn}$  can influence the geometry and size of the shock as well as its deviation from laminar behavior. It is not known, however, how  $\theta_{Bn}$  can influence the energy budget or energy conversion processes that may occur. The same can be said of the upstream fast magnetosonic Mach number ( $M_f$ ) and plasma beta ( $\beta$ ), the presence of  $\text{He}^{2+}$  and/or other minor ion populations, thermal anisotropies, temperatures of both electrons and various ion species, and contributions of energetic particle populations.

Implementing MAKOS will answer this question by observing a statistically significant number of shock crossings with a range of different driving conditions and shock geometries, enabling the quantification of parametric dependencies of various energy partitioning configurations and energy conversion processes vs. shock orientations and driving conditions. The MAKOS dataset will provide measurements of >500 quasi-parallel and quasi-perpendicular shocks each, assuming they are each observed with approximately equal probability. This will provide sufficient statistics to identify trends in the energy budget and identified energy conversion processes due to specific shock driving conditions and geometries. Furthermore, the MAKOS orbits offer year-round coverage in the solar wind, enabling MAKOS to study IP shocks and further bolster the statistics on various shock driving conditions and behavior from a regime of cases significantly different from that of Earth's bow shock.

## 1.5 MMS Limitations

MMS is the most sophisticated technology we currently have to measure space plasma *in situ* (Burch et al., 2016). It can measure full electron velocity distributions over a 30-ms cadence and partial distributions as low as 7.5 ms. It is the most capable mission we have to observe microscale phenomena in the bow shock, and indeed it has, opening up a completely new avenue into the discussion of collisionless shocks physics. However, MMS cannot provide scientific closure to the stated questions concerning collisionless shocks. In this section, we outline the most critical reasons behind this statement.

First and most critically, MMS cannot resolve the ion solar wind beam distribution. Due to its design, the MMS low-energy particle detectors – both the Fast Plasma Investigation (FPI; Pollock et al., 2016) and the Hot Plasma Composition Analyzer (HPCA; Young et al., 2016) – are not optimized to resolve the proton energy distribution of the solar wind. Figure 1.4 shows the MMS energy coverage of modeled solar wind populations in comparison to Wind. The proton core population is insufficiently resolved to determine even basic moments such as density and temperature. Nor can the strahl electron population above  $\sim 500$  eV be captured as count rates fall below statistical significance. Without accurate resolution of these populations, we cannot characterize the upstream plasma nor observe the solar wind development through the shock (Wilson et al., 2022).

Secondly, the electric field probes are too long to accurately measure high frequency wave phenomena (see Figure 3 in Goodrich et al., 2018). Observed short wavelength waves appear highly attenuated from the very long boom lengths, rendering them difficult to analyze. We can resolve this through careful interferometry and application of theory. However, assumptions will always be made to do so and we, therefore, cannot make significant progress to understanding the roles waves take in energy conversion within the terrestrial bow shock.

Finally, the MMS spacecraft separation distances do not allow for appropriate simultaneous upstream and downstream measurements. MMS has had an average of  $\sim 15$  km separation in the dayside magnetosphere, well within the solar wind gyroradius ( $\sim 1000$  km). This is not sufficient distance to determine the conditions of unperturbed solar wind. These scales can be adjusted, and plans are currently implemented to enable cross-scale measurements within the realm of the bow shock and magnetosheath. However, even if appropriate distances can be achieved, the two previous issues remain.

To summarize, MMS is insufficient to deliver accurately on MAKOS science objectives for the following reasons:

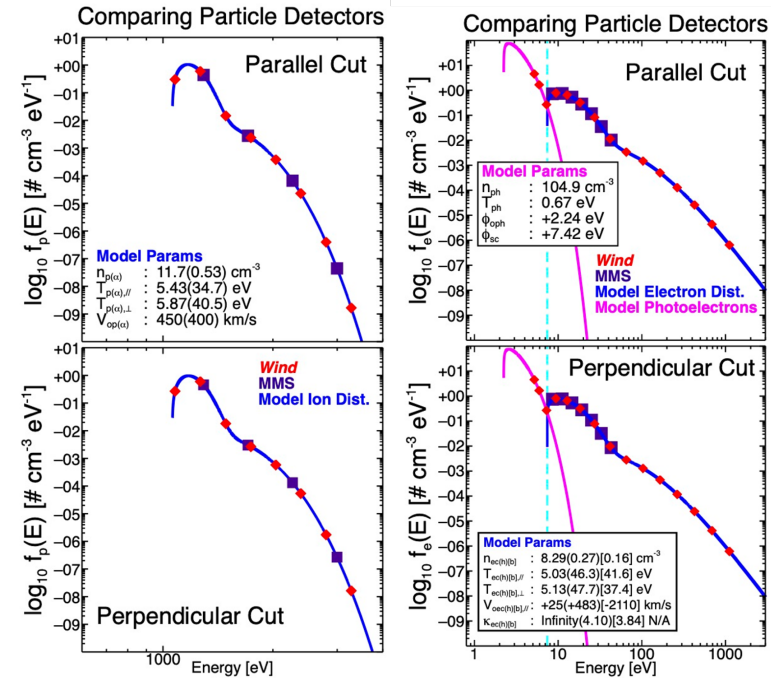


**Figure 1.4:** Comparison of MMS and Wind proton (left) and electron (right) energy resolution overlaid on model solar wind VDFs. Note MMS's inability to resolve the solar wind proton peak, and the lack of statistically significant

1. Insufficient particle instrument performance in the solar wind;
2. Limiting/restrictive assumptions concerning short wavelength E-field data inherent to the instrument design; and
3. Inadequate inter-spacecraft separations and orbital configuration.

Cluster is also insufficient to deliver accurately on MAKOS science objectives for the following reasons:

1. Insufficient particle instrument performance in the solar wind;
2. Insufficient temporal resolution; and
3. Sufficient spacing at ion kinetic scales but insufficient spacing at MHD scales.

The MAKOS mission and observatories are explicitly designed to provide the required multipoint spatial distribution, high temporal resolution, and energy and angular resolution (particles, particularly in the solar wind) to fully quantify the energy budget and characterize the dominant energy conversion mechanisms at collisionless shocks for the first time.

### **1.6 Expected Scientific Impact**

Collisionless shocks should be considered alongside turbulence and magnetic reconnection as ubiquitous and fundamental processes in collisionless plasmas. Both reconnection and turbulence have dedicated Heliophysics missions to study them, with MMS and HelioSwarm, respectively. MAKOS offers NASA a mission design to complete the trifecta and deliver answers to outstanding questions and fill gaps in our knowledge of collisionless shocks. Full knowledge of shock micro-processes will more firmly establish our knowledge of fundamental plasma processes. This will further enable collaboration with the laboratory plasma community, as they develop and experiment with similar scale and mechanisms. This will also enable interdisciplinary science and interdivisional collaboration within NASA, promising greater collaboration between the Heliophysics and astrophysical communities, since astrophysicists observe astrophysical shocks via remote sensing and are entirely denied the rich, *in situ* datasets afforded to Heliophysics. The radiation from these shocks observed by astronomers and astrophysicists stems from the post-energy conversion process. By acquiring an accurate knowledge of energy partitioning resulting from collisionless shocks, we will establish clearer connections to the processes at and implications of shocks in collisionless space plasmas far beyond our heliosphere and range of our *in situ* capabilities.

MAKOS Science Traceability Matrix					Instrument Requirements				
Science Questions	Science Objectives	Physical Parameters	Observable Quantities	Instrument	Instrument & Parameter	Measurement Req.	Exp. Data Volume per Orbit		
[Q1] What is the energy budget both upstream and downstream of a collisionless shock?	Quantify the contribution of proton and electron thermal and kinetic energy to the shock energy budget	Simultaneous upstream and downstream moments (density, velocity, pressure, heat flux) of particle sub-populations	Simultaneous upstream and downstream core 3D velocity distribution functions	SWI	SWI	Energy Range Energy Resolution FOV Angular Resolution Temporal Resolution	300 eV – 7 keV 10% 40° x 40° 6° 0.1 s	27 GB	
				SWE					
	Quantify the contribution of He and the CNO group thermal and kinetic energy to the shock energy budget		Simultaneous upstream and downstream suprathermal 3D velocity distribution functions	STI	SWE	Energy Range Energy Resolution Angular Coverage Angular Resolution Temporal Resolution	3 eV – 1.5 keV 10% 4π-ster 20° 0.01 s	314 GB	
				STE					
	Quantify the contribution of Poynting flux to the shock energy budget	Electric and Magnetic field contribution to the Poynting flux	Simultaneous upstream and downstream energetic particle energy, angular, and compositional distributions	Simultaneous upstream and downstream 3D DC- and AC-coupled electric and magnetic field	EP	STI	Energy Range Energy Resolution Angular Coverage Angular Resolution Temporal Resolution	700 eV – 30 keV 20% 4π-ster 20° 1 s	102 GB
					EFI				
	[Q2] What are the processes governing energy conversion at and within collisionless shocks?	Characterize the coherent and incoherent heating and acceleration of particle populations upstream, downstream, and within the shock front	Particle heating	Simultaneous upstream, within shock, and downstream core, suprathermal and energetic particle 3D Velocity Distribution Functions (VDFs)	FGM	STE	Energy Range Energy Resolution Angular Coverage Angular Resolution Temporal Resolution	500 eV – 30 keV 20% 4π-ster 20° 1 s	13 GB
					SCM				
					SWI				
					SWE				
Identify electric and magnetic field variations together with targeted local plasma instabilities and resulting waves within the shock		Non-Maxwellian features responsible for observed instabilities	Simultaneous upstream, within shock, and downstream core 3D VDFs	Simultaneous upstream, within shock, and downstream suprathermal 3D VDFs	STI	EP	Energy Range Energy Resolution Species FOV Angular Resolution Temporal Resolution	20 keV – 10 MeV 20% H, He, C, O, Ne, e 180° 30° 1 s	30 GB
					SWE				
Magnetic and electric field topology and wave modes		Simultaneous upstream, within shock, and downstream 3D DC- and AC-coupled magnetic and electric field	Simultaneous upstream, within shock, and downstream 3D DC- and AC-coupled magnetic and electric field	Simultaneous upstream, within shock, and downstream 3D DC- and AC-coupled magnetic and electric field	SWI	FGM	(DC) Dynamic Range Resolution Temporal Resolution	±500 nT 10 pT 0.03125 s	278 MB
					STI				
					STE				
					EFI				
Parameterize shock crossings according to the macroscopic, Rankine-Hugoniot relations	Particle-dependent macroscopic shock parameters.	Upstream, within shock, and downstream particle moments and 3D DC-coupled magnetic field	Upstream, within shock, and downstream particle moments and 3D DC-coupled magnetic field	SCM	SCM	(AC) Dynamic Range Resolution Temporal Resolution	±50 nT 0.1 pT 0.001 s	12 GB	
				EFI					
[Q3] How and why do these processes vary with shock orientation and driving conditions?	Tabulate and sort observed shock crossings according to the macroscopic shock parameters for statistical analysis of science objectives	Statistical parameterization of the processes in [Q1] & [Q2] versus calculated shock parameters	Upstream, within shock, and downstream particle moments and 3D DC-coupled magnetic field	All	EFI	(DC) Range Dimensions Resolution Temporal Resolution	±1000 mV/m 3 1 mV/m 0.5 s	115 GB	
				All					
						(AC) Range Dimensions Resolution Temporal Resolution	±2000 mV/m 3 1 mV/m 0.001 s		

Figure 1.5: The MAKOS science traceability matrix shows the flowdown of science questions to observables and subsequent measurement requirements, then to implementation requirements for instruments and mission.

## 2 Mission Concept Implementation

---

### 2.1 Overview

The baseline MAKOS mission concept (CML 4) comprises four spacecraft (S/C) with varying spatial separations in high-altitude, slightly elliptical ( $22.1 \times 17 R_E$ ) five-to-one (5:1) lunar resonance orbits (LROs) with opposite lines of apsides to maximize the number of bow shock crossings, even when apogee is on the nightside. Each of the two orbits has two S/C with separations on the order of  $\sim 1000$  km to obtain the required simultaneous upstream and downstream shock observations and multipoint observations at ion-kinetic scales through every shock transition layer crossing. The separations between the S/C on the different orbits range from  $\sim 5$  to  $12 R_E$ . This implementation provides year-round crossings of the bow shock with simultaneous multipoint separations ranging from ion kinetic ( $\sim 1000$  km; each pair) to MHD (several  $R_E$ ; the pair of pairs) scales, as well as prolonged dwell time in the solar wind, enabling MAKOS to simultaneously probe both ion-kinetic- and MHD-scale processes during every shock crossing, including both Earth's bow shock and IP shocks.

MAKOS requires each S/C carry a comprehensive science payload of particles and field instruments specifically tailored to measure the *in situ* processes at play in collisionless shocks. The need to fully characterize the plasma populations upstream and downstream of the shock drives a mission requirement that the complete thermal and suprathermal electron and ion velocity distributions be sampled at very high temporal resolution ( $\sim 1$  s). This is achieved in the notional mission design by carrying multiple dedicated sensors targeting each species and energy range on a rapidly-spinning (10 RPM baseline) S/C.

### 2.2 Technology Maturity

The baseline MAKOS mission is designed to be implemented with current technology and requires only minimal maturation of enabling technologies. In particular, the high-rate star tracker is at TRL 5 and its Technology Development Plan would require only in-house simulated spin-table testing to achieve the required TRL 6. However, there are several potential *enhancing* technologies that could optimize the MAKOS mission implementation and reduce costs and risk if they receive further development outside the scope of the mission. These include: 1) instrument development and 2) infrastructure.

**Instrument Development:** Obtaining more comprehensive 3D particle measurements at cadences even faster (e.g., 10 ms) than recent missions (e.g., MMS and Parker Solar Probe) – without relying on a high number of sensors – will require additional instrument development for traditional top-hat ESAs or development of new particle detection systems for low-energy space plasmas. Particular emphasis is needed in two key areas: 1) parts availability (e.g., reliable high voltage optocouplers) and 2) tuning and responsiveness of high voltage power supplies to ensure fast measurements are taken with sufficient accuracy. At least one vendor that has provided flight parts for previous NASA missions has existing custom optocoupler designs that can fulfill even the most ambitious high-resolution MAKOS measurement cadences.

**Infrastructure:** While MAKOS achieves its baseline science with current radio frequency (RF) communications infrastructure, it requires limiting high-rate data collection to only targeted portions of the orbit. Even downlinking data only when S/C are earthward of the magnetopause (i.e.,  $\sim 71$ -hr/orbit window) requires hours per day per S/C of Deep Space Network (DSN) time. Optical communications would drastically reduce required downlink, thus enabling significantly more science data to be downlinked and reducing SITL decisions and complexity. The much higher data rates afforded by optical downlink would enhance MAKOS by significantly

reducing resource competition and/or providing additional science data and reducing the need for SITL-based operations. Optical downlink would enable all MAKOS high-resolution science data to be transmitted to ground for scientific analysis, which would have profoundly positive impacts on the Heliophysics research community and extend the high impact of MAKOS science into magnetospheric physics as well.

### **2.3 Key Trades**

The baseline MAKOS concept (CML 4) presented here was achieved via execution of multiple trades. First, the science team finalized the Science Traceability Matrix (STM; Figure 1.5) to rigorously define measurement and mission requirements necessary to close on the proposed MAKOS science objectives. This led to careful consideration of potential heritage science instruments that could meet these measurement requirements with reasonable resource demands and minimal risk. Finalization of the measurement requirements and selection of the payload led directly to a trade between the number of sensors included in the payload versus the S/C spin-rate that could be achieved. This was largely driven by the high temporal resolution requirement on the thermal and suprathermal electrons and ions. Ultimately, it was decided that a baseline 10 RPM spin rate could be achieved, which would require multiple (1–4 per population) sensors to obtain the required temporal resolutions defined in the STM.

A trade was also evaluated on how the mission design would be implemented, specifically whether it could be achieved via a rideshare architecture or if it required dedicated launches. The size of the S/C and high-altitude orbit almost immediately led to the determination that dedicated launches were required. The dual-orbit nature also led to the conclusion that two launches – one per S/C pair – were the preferred configuration, with cold gas (as opposed to chemical) as a sufficient, and preferred, propellant. A single launch with increased on-board propulsion to achieve orbital spacing may also work, which can be evaluated in a future trade study; the current baseline concept implements separate launches with two standard medium-lift vehicles (e.g., SpaceX Falcon 9) as the lowest cost/risk option.

There are two primary trades for enhancement that can be considered for future work. The first is consideration of optical communications instead of the baselined RF (X-band) system downlinking through the NASA DSN. An optical solution would allow for significantly larger data downlink and would potentially simplify operations; however, currently, there are no commercial vendors nor operational ground stations that can provide or support optical communication compatible with MAKOS's design requirements. The second trade would focus on whether the current star tracker solution could be enhanced to operate faster than the 10 RPM currently baselined. This trade could come in two phases: 1) performing error analysis to see whether the current hardware can be operated at >10 RPM and 2) development of enhancing technology that achieves much higher spin rates.

### 3 Technical Overview

#### 3.1 Payload Description

The MAKOS payload design comprises eight instruments accommodated on each of the four spacecraft. Each instrument is based on a high-heritage (TRL  $\geq 6$ ) representative sensor from a previous mission. The notional baseline payload employs multiple dedicated solar wind and suprathermal sensors for each species (ions and electrons) to achieve the high temporal and angular resolutions required to achieve the MAKOS science objectives. Section 2.2 explores potential future instrument development that could be implemented to enhance and/or augment the representative heritage instruments to allow the MAKOS science objectives to be achieved without the high number of sensors currently implemented in the notional baseline payload. Table 3.1 provides the mass and power for the MAKOS payload with the instruments divided into two groups: particles and fields. For almost all of the MAKOS instruments, multiple potential high-heritage instrument alternatives were identified and considered; in every case, the instruments with highest resource (e.g., size, weight, and power) demand were selected for the baseline payload as a stress test (i.e., upper bound) for closure on the preliminary concept design.

**Table 3.1: Summary Payload Resource Table**

Instrument	Qty per S/C (#)	Mass				Average Power			
		CBE per unit (kg)	CBE Total (kg)	Cont.	MEV Total (kg)	CBE per unit (W)	CBE Total (W)	Cont.	MEV Total (W)
Solar Wind Ions (SWI)	2	3.5	7.0	10%	7.7	3.5	7.0	10%	7.7
Solar Wind Electrons (SWE)	4	2.6	10.4	15%	12.0	3.2	12.8	15%	14.7
Suprathermal Ions (STI)	4	11.4	45.6	10%	50.2	12.0	48.0	15%	55.2
Suprathermal Electrons (STE)	4	2.6	10.4	15%	12.0	3.2	12.8	15%	14.7
Energetic Particles (EP)	1	3.9	3.9	20%	4.7	3.8	3.8	10%	4.2
Fluxgate Magnetometer (FGM)	2	0.7	1.4	10%	1.5* <sup>^</sup>	4.0	8.0	15%	9.2 <sup>^</sup>
Search Coil Magnetometer (SCM)	1	0.8	0.8	10%	0.9* <sup>^</sup>	1.0	1.0	15%	1.2 <sup>^</sup>
Electric Fields (EF)	1	22.0	22.0	15%	25.3	8.4	8.4	15%	9.7
<b>Totals</b>			<b>101.5</b>		<b>114.3</b>		<b>101.8</b>		<b>116.6</b>

\* does not include two 5-kg, 50-m booms;  
<sup>^</sup> mass and power of common “fields” electronics carried in EF values

##### 3.1.1 Solar Wind Ions (SWI)

The Solar Wind Ions (SWI) instrument measures the core solar wind protons and alphas from 300 eV to 7 keV to investigate the energy budget and energy conversion processes across collisionless shocks. The MAKOS-concept SWI sensors are based on the heritage SWEAP/SPAN-I instrument (Figure 3.1) currently flying on the Parker Solar Probe mission (Kasper et al., 2014; Whittlesey et al., 2019). The SPAN-I instrument, which combines a top-hat electrostatic analyzer (ESA) with a time-of-flight (TOF) system, was chosen for its ability to clearly separate protons and alphas – the two primary ion constituents in the solar wind that comprise the vast majority of the solar wind ram energy. Two SWI sensor heads will be used on MAKOS, oriented such that their fan-like, planar ( $40^\circ \times \sim 6^\circ$ ) fields-of-view (FOVs) are orthogonal to each other and both parallel to the nominal solar wind direction (i.e., roughly parallel to the spin axis of the spacecraft). This orientation, in which the center of both FOVs is directed towards the solar

wind, will yield the required combined instantaneous FOV of at least a  $40^\circ \times 40^\circ$  that is necessary to resolve the solar wind beam with the required energy and high angular resolution to achieve the MAKOS science objectives. Only minor changes from heritage (e.g., FOV reduction, EEE parts updates, implementation-specific tailoring) would be required for the PSP/SWEAP/SPAN-I instrument to implement it for MAKOS/SWI.

Since the solar wind rarely deviates more than  $20^\circ$  from radial at 1 AU and the thermal speed is much less than the bulk flow speed, this detector system will not require significant rotation of the spacecraft to fully resolve the solar wind core. The system needs to resolve relevant ion kinetic scale phenomena like magnetosonic-whistler precursor waves (e.g., Wilson et al., 2017), which typically have frequencies of  $\sim 0.5\text{--}5$  Hz in the spacecraft frame. Thus, the time cadence of the instrument will need to be at least 100 ms.

Due to the extremely cold and fast beam profile of the solar wind, the MAKOS/SWI instruments will need to have high energy ( $\leq 10\%$ ) and angular ( $\leq 6^\circ$ ) resolutions to properly resolve the phase-space density peak for identification of non-Maxwellian features and secondary beams (e.g., Cara et al., 2017; De Keyser et al., 2018; De Marco et al., 2016). Based upon long-term statistics, the energy range of the SWI instruments must be able to cover the typical solar wind speeds (i.e.,  $\sim 300\text{--}600$  km/s for both protons and alphas), which results in an energy range requirement of 300 eV to 8 keV.



**Figure 3.1:** PSP/SWEAP/SPAN-I instrument (Kasper et al., 2016), as heritage for MAKOS/SWI.

**Table 3.2:** Solar Wind Ions Summary Table

Item	Value	Units
Type of instrument	Electrostatic analyzer with time-of-flight	
Size/dimensions (for each instrument)	$10 \times 10 \times 14$	cm
Instrument average science data rate <sup>^</sup> <b>without</b> contingency	45 (low-rate)	kbps
	897 (high-rate)	kbps
Instrument average science data <sup>^</sup> rate contingency	50	%
Instrument average science data <sup>^</sup> rate <b>with</b> contingency	68 (low-rate)	kbps
	1346 (high-rate)	kbps
Instrument field-of-view	$40^\circ \times \sim 6^\circ$ (per sensor)	$^\circ$
Pointing requirements (knowledge)	1	$^\circ$
Pointing requirements (control)	1	$^\circ$
Pointing requirements (stability)	1	$^\circ/\text{s}$
Representative Heritage Instrument	PSP/SWEAP/SPAN-I (Kasper et al., 2016)	

### 3.1.2 Solar Wind Electrons (SWE)

The Solar Wind Electrons (SWE) instrument measures the three primary solar wind electron populations – core, halo, and strahl (e.g., Wilson et al., 2019) – from 3 eV to 1.5 keV to investigate the energy budget and energy conversion processes across collisionless shocks. The MAKOS concept SWE sensors are based on the heritage 3DP/EESA-L instrument (Figure 3.2) currently flying on the Wind spacecraft (Lin et al., 1995). The EESA-L instrument, a top-hat ESA, was chosen as a reasonable (but more resource-demanding) representative from several similar

instruments that could fulfill the MAKOS objectives. Four SWE detector heads will each view the sky with a fan-like  $>180^\circ \times 3^\circ$  FOV (coplanar with the S/C spin axis) pointing radially outward at  $\sim 90^\circ$  spacing around the S/C. The acceptance angle (i.e., the direction perpendicular to the fan-like plane) of each sensor can be expanded up to  $\sim 120^\circ$  by an electrostatic deflection system. This feature combined with the distributed number of sensor heads will reduce the time (and spacecraft rotation) necessary to get the  $4\pi$ -ster coverage of the sky for all energy bins necessary to achieve the MAKOS science objectives. Only minor changes from heritage (e.g., FOV reduction, EEE parts updates for obsolescence, implementation-specific tailoring) would be required to the Wind/3DP/EESA-L instrument for MAKOS/SWE implementation.



**Figure 3.2:** Wind/3DP instrument including EESA-H and EESA-L (Lin et al., 1995), as heritage for MAKOS/SWE and STE.

To properly resolve the three primary solar wind electron populations – core, halo, and strahl (e.g., Wilson et al., 2019) – the MAKOS/SWE detectors will need to have an energy resolution of  $\sim 10\%$  and an angular resolution of no more than  $20^\circ$  in either direction. The minimum system energy must always fall below the spacecraft potential to ensure the measurement of the entire electron population (e.g., Lavraud & Larson, 2016). The electrostatic and electromagnetic cleanliness is expected to be similar to previous missions but will not include an active spacecraft potential control system, so the spacecraft potential should be  $\sim 3\text{--}6$  eV when in sunlight; this drives the minimum energy requirement of at least 2 eV. The MAKOS/EF instrument (Section 3.1.8) will obtain a DC-coupled measurement that will allow for the direct measurement of the spacecraft potential for every electron distribution.

The temporal resolution requirement is set by the necessity to resolve wave-particle interactions with high-frequency whistler modes (e.g., Giagkiozis et al., 2018). For nearly all observations, the spacecraft frame frequency of these modes falls below 80% of the local electron cyclotron frequency,  $f_{ce}$ , which is  $\sim 80\text{--}400$  Hz in the solar wind (e.g., Wilson et al., 2021) and up to a factor of four larger in the magnetosheath. The expected frequencies in the spacecraft frame are only  $\sim 0.3 f_{ce}$  (e.g., Giagkiozis et al., 2018), or  $\sim 24\text{--}120$  Hz in the solar wind and  $\leq 96\text{--}480$  Hz in the magnetosheath.

**Table 3.3:** Solar Wind Electrons Summary Table

Item	Value	Units
Type of instrument	Electrostatic analyzer	
Size/dimensions (for each instrument)	$31 \times 35 \times 25$ (plus electronics)	cm
Instrument average science data rate <sup>^</sup> <b>without</b> contingency	58 (low-rate)	kbps
	11444 (high-rate)	kbps
Instrument average science data <sup>^</sup> rate contingency	50	%
Instrument average science data <sup>^</sup> rate <b>with</b> contingency	87 (low-rate)	kbps
	17166 (high-rate)	kbps
Instrument field-of-view	$180 \times 120$ (w/ deflection)	$^\circ$
Pointing requirements (knowledge)	1	$^\circ$
Pointing requirements (control)	1	$^\circ$
Pointing requirements (stability)	1	$^\circ/s$
Representative Heritage Instrument	Wind/3DP/EESA-L (Lin et al., 1995)	

It is not feasible to measure the full electron velocity distribution function (VDF) in less than 3 ms in the solar wind as the signal-to-noise ratio (SNR) would be too low for any currently feasible instrument. However, it is possible to resolve the electron VDF on timescales comparable to the wave envelope of these modes. The wave packet duration of these modes tends to be more than 20 ms, thus the cadence over the full  $4\pi$ -ster for all energies will need to be at least 10 ms.

### 3.1.3 Suprathermal Ions (STI)

The Suprathermal Ions (STI) instrument provides measurements of the elemental composition, ionic charge state, and 3D velocity distribution functions of multiple key ion species within and around Earth's bow shock and IP shocks. Suprathermal ions represent a significant contribution to the energy budget at supercritical quasi-parallel shocks, where a non-negligible portion of the energy balance is maintained via accelerated and reflected suprathermal ions. The MAKOS concept STI sensors are based on the heritage PLASTIC instrument (Figure 3.3) currently flying on the STEREO spacecraft (Galvin et al., 2008). The PLASTIC instrument, a top-hat ESA paired with an energy-by-time-of-flight (ExTOF) system to enable energy and mass spectrometry, was chosen for its wide FOV as well as its high mass and charge-state resolution, which are necessary to achieve the proposed MAKOS science objectives. For MAKOS, four STI detector heads will each view the sky with a fan-like  $\sim 180^\circ \times 6^\circ$  FOV (coplanar with the S/C spin axis) pointing radially outward at  $\sim 90^\circ$  spacing around the S/C to achieve the  $4\pi$ -ster sky coverage and temporal resolution required to address the MAKOS science objectives. Only minor change from heritage (e.g., FOV reduction, EEE parts updates, implementation-specific tailoring) would be required to the STEREO/PLASTIC instrument for MAKOS/STI implementation.

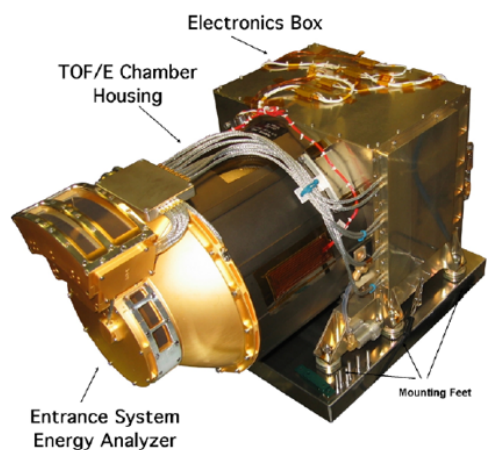


**Figure 3.3:** STEREO/PLASTIC instrument (Galvin et al., 2008), as heritage for MAKOS/STI.

**Table 3.4:** Suprathermal Ions Summary Table

Item	Value	Units
Type of instrument	Electrostatic analyzer with energy-by-time-of-flight subsystem	
Size/dimensions (for each instrument)	48 × 25 × 27	cm
Instrument average science data rate <sup>^</sup> <b>without</b> contingency	310 (low-rate)	kbits
	3104 (high-rate)	kbits
Instrument average science data <sup>^</sup> rate contingency	50	%
Instrument average science data <sup>^</sup> rate <b>with</b> contingency	465 (low-rate)	kbits
	4656 (high-rate)	kbits
Instrument field-of-view	175 × 6	°
Pointing requirements (knowledge)	0.1	°
Pointing requirements (control)	1	°
Pointing requirements (stability)	0.1	°/s
Representative Heritage Instrument	STEREO/PLASTIC (Galvin et al., 2008)	

### 3.1.4 Suprathermal Electrons (STE)

The Suprathermal Electrons (STE) instrument provides measurements of the 3D velocity distribution functions of suprathermal electrons within and around Earth’s bow shock and IP shocks. The MAKOS concept STE sensors are based on the heritage 3DP/EESA-H instrument (Figure 3.2) currently flying on the Wind spacecraft (Lin et al., 1995). The EESA-H instrument, a top-hat ESA, was chosen for its large geometric factor, energy range, and energy resolution, which are necessary to achieve the proposed MAKOS science objectives. For MAKOS, four STE detector heads will each view the sky with a fan-like  $\sim 180^\circ \times 14^\circ$  FOV (coplanar with the SC spin axis) – i.e., only half the EESA-H azimuthal range – pointing radially outward at  $\sim 90^\circ$  spacing around the S/C to achieve the  $4\pi$ -ster sky coverage and temporal resolution required to address the MAKOS science objectives. Only minor changes from heritage (e.g., FOV reduction, EEE parts updates for obsolescence, implementation-specific tailoring) would be required to the Wind/3DP/EESA-H instrument for MAKOS/STE implementation.

**Table 3.5:** *Suprathermal Electrons Summary Table*

Item	Value	Units
Type of instrument	Electrostatic analyzer	
Size/dimensions (for each instrument)	31 × 34 × 25	cm
Instrument average science data rate <sup>^</sup> <b>without</b> contingency	40 (low-rate)	kbps
	396 (high-rate)	kbps
Instrument average science data <sup>^</sup> rate contingency	50%	%
Instrument average science data <sup>^</sup> rate <b>with</b> contingency	60 (low-rate)	kbps
	594 (high-rate)	kbps
Instrument field-of-view	$\sim 180 \times 14$	$^\circ$
Pointing requirements (knowledge)	1	$^\circ$
Pointing requirements (control)	1	$^\circ$
Pointing requirements (stability)	1	$^\circ/s$
Representative Heritage Instrument	WIND/3DP/EESA-H (Lin et al., 1995)	

### 3.1.5 Energetic Particles (EP)

The Energetic Particles (EP) instrument provides measurements of energy and angular distributions of energetic ( $\geq 20$  keV) electrons and ions – including ion elemental composition for multiple key species – within and around Earth’s bow shock and IP shocks. Particle acceleration at collisionless shocks is a fundamental physical process relevant to both Heliophysics and Astrophysics, as shock acceleration is at least partially responsible for the generation of anomalous and galactic cosmic rays. The MAKOS concept EP sensor is based on the heritage ISØIS/EPI-Lo instrument (Figure 3.4) currently flying on the Parker Solar Probe mission (McComas et al., 2017; Hill et al., 2016). EPI-Lo is a TOF-by-total energy system consisting of eighty independent look directions that provide a simultaneous half-sky ( $2\pi$ -ster) FOV (much larger than required on the spinning MAKOS S/C). This instrument was chosen for its high mass resolution, which

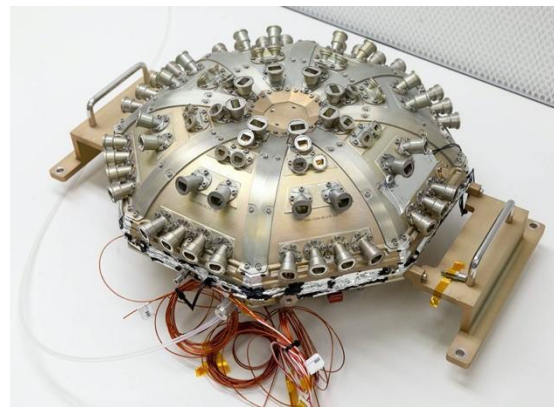


**Figure 3.4:** *Parker Solar Probe/ISØIS/EPI-Lo instrument (McComas et al., 2017; Hill et al., 2016), as heritage for MAKOS/EP.*

can deliver on the required energy range and resolution and angular range and resolution required for MAKOS to measure the energetic particle intensities expected in the solar wind, magnetosheath, and ion foreshock with only modest scaling of the instrument geometric factor. Only minor changes from heritage (e.g., scaling for increased geometric factor, EEE parts updates, implementation-specific tailoring) would be required to the PSP/ISØIS/EPI-Lo instrument for MAKOS/EP implementation.

**Table 3.6:** Energetic Particles Summary Table

Item	Value	Units
Type of instrument	Time-of-flight-by-total energy energetic particle telescope	
Size/dimensions (for each instrument)	30 × 30 × 13.5	cm
Instrument average science data rate <sup>^</sup> <b>without</b> contingency	305 (low-rate)	kbps
	465 (high-rate)	kbps
Instrument average science data <sup>^</sup> rate contingency	50	%
Instrument average science data <sup>^</sup> rate <b>with</b> contingency	458 (low-rate)	kbps
	698 (high-rate)	kbps
Instrument field-of-view	360 × 90	°
Pointing requirements (knowledge)	0.5	°
Pointing requirements (control)	1	°
Pointing requirements (stability)	0.5	°/s
Representative Heritage Instrument	Parker Solar Probe/ISØIS/EPI-Lo (McComas et al., 2017; Hill et al., 2016)	

### 3.1.6 Fluxgate Magnetometer (FGM)

The Fluxgate Magnetometer (FGM) instrument provides measurements of the 3D vector DC magnetic field up to 32 Hz within and around Earth’s bow shock and IP shocks. The MAKOS concept FGM sensor is based on the heritage FIELDS/FGM instrument (Figure 3.5) currently flying on MMS (Russell et al., 2016; Torbert et al., 2016). FIELDS/FGM is a tri-axial (orthogonal to within ~1°), fluxgate instrument and was chosen for its high performance and appropriate dynamic range. For MAKOS, two FGM sensors will be mounted on a common 5-m, single-hinged boom in a “gradiometer” configuration to characterize and eliminate S/C signals of electromagnetic interference. Only minor changes from heritage (e.g., EEE parts updates, implementation-specific tailoring) would be required to the MMS/FIELDS/FGM instrument for MAKOS/FGM implementation. It is assumed that the main FGM electronics will be housed in a common “fields” electronics box housing along with those for the SCM and EF instruments.

In order to achieve the necessary accuracy, the individual spacecraft must have a magnetic cleanliness of less than 10 nT and vary less than 0.5 nT per day. Thus, the FGM must be positioned at an appropriate distance from the S/C center with orthogonal axial components. This distance will depend on the assembly of the S/C; however, we shall use the distance implemented by MMS (5 meters) as a benchmark.

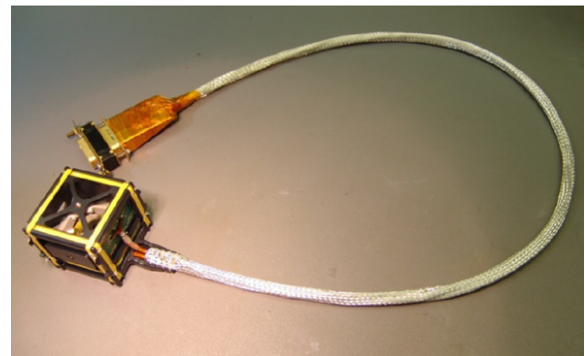


**Figure 3.5:** MMS/FIELDS/FGM instrument (Torbert et al., 2016; Russell et al., 2016), as heritage for MAKOS/FGM.

**Table 3.7:** Fluxgate Magnetometer Summary Table

Item	Value	Units
Type of instrument	3D fluxgate magnetometer	
Size/dimensions (for each instrument)	4.5 × 4.5 × 5	cm
Instrument average science data rate <sup>^</sup> <b>without</b> contingency	3 (low-rate)	kbps
	3 (high-rate)	kbps
Instrument average science data <sup>^</sup> rate contingency	50	%
Instrument average science data <sup>^</sup> rate <b>with</b> contingency	4.5 (low-rate)	kbps
	4.5 (high-rate)	kbps
Instrument field-of-view	n/a	°
Pointing requirements (knowledge)	n/a	°
Pointing requirements (control)	n/a	°
Pointing requirements (stability)	n/a	°/s
Representative Heritage Instrument	MMS/FIELDS/FGM (Torbert et al., 2016; Russell et al., 2016)	

### 3.1.7 Search Coil Magnetometer (SCM)

The Search Coil Magnetometer (SCM) instrument measures the 3D AC-coupled magnetic field to investigate the wave environment and energy conversion processes in the vicinity of the terrestrial bow shock and IP shocks. The MAKOS concept SCM sensor is based on three orthogonal (to within  $\sim 1^\circ$ ) instances of the WAVES instrument search coil magnetometer (Figure 3.6) currently flying on the Juno mission (Kurth et al., 2017). The Juno/WAVES instrument, a single-axis antenna holding thousands of turns of copper wire around a high-permeability core within a bobbin, was selected for its very high heritage and performance. For MAKOS, the three-axis SCM sensor will be mounted on a second 5-m, single-hinged boom (identical but oppositely mounted from the FGM boom). Only minor changes from heritage (e.g., expansion to three-axes, EEE parts updates, implementation-specific tailoring) would be required to the Juno/WAVES instrument for MAKOS/SCM implementation. It is assumed that the main SCM electronics will be housed in a common “fields” electronics box housing along with those of the FGM and EF instruments.



**Figure 3.6:** Juno/Waves instrument (Kurth et al., 2017), as heritage for MAKOS/SCM.

**Table 3.8:** Search Coil Magnetometer Summary Table

Item	Value	Units
Type of instrument	3D search coil magnetometer	
Size/dimensions (for each instrument)	20 × 20 × 20	cm
Instrument average science data rate <sup>^</sup> <b>without</b> contingency	16 (low-rate)	kbps
	389 (high-rate)	kbps
Instrument average science data <sup>^</sup> rate contingency	50	%
Instrument average science data <sup>^</sup> rate <b>with</b> contingency	24 (low-rate)	kbps
	584 (high-rate)	kbps
Instrument field-of-view	n/a	°
Pointing requirements (knowledge)	n/a	°
Pointing requirements (control)	n/a	°
Pointing requirements (stability)	n/a	°/s
Representative Heritage Instrument	Juno/Waves (Kurth et al., 2017)	

### 3.1.8 Electric Fields (EF)

The Electric Fields (EF) instrument will measure the three-dimensional AC- and DC-coupled electric field up to 1 kHz to investigate the field and waves environment and energy conversion processes in the vicinity of the terrestrial bow shock and IP shocks. The MAKOS concept EF instrument is based on the FIELDS/ADP (axial) and SDP (spin-plane) instruments (Figure 3.7) currently flying on MMS (Ergun et al., 2016; Torbert et al., 2016). The ADP & SDP instruments (double-probe sensors) were selected for their very high heritage and performance. For MAKOS, three-axis EF instrument will comprise twelve spherical voltage probes mounted on four 50-m wire booms in the spin-plane of the S/C (radial) and two 15-m stacer booms along its spin-axis (i.e., axial). The final lengths of these booms will be subject to the final length of the spacecraft body. Each probe will be mounted in a direction orthogonal (to within  $\sim 1^\circ$ ) to four booms, and anti-parallel to one boom thus enabling measurements across 3D space. The EF instrument will employ two probes (as implemented on the FAST mission; Ergun et al., 2001) – separated by 10 m – on each wire/stacer boom to accurately resolve wave phenomena with wavelengths  $\leq 100$  m. Only minor changes from heritage (e.g., introduction of double probe on each boom, EEE parts updates, implementation-specific tailoring) would be required to the FIELDS ADP and SPD instruments for MAKOS/EF implementation. It is assumed that the main EF electronics will be housed in a common “fields” electronics box housing along with those of the FGM and SCM instruments.

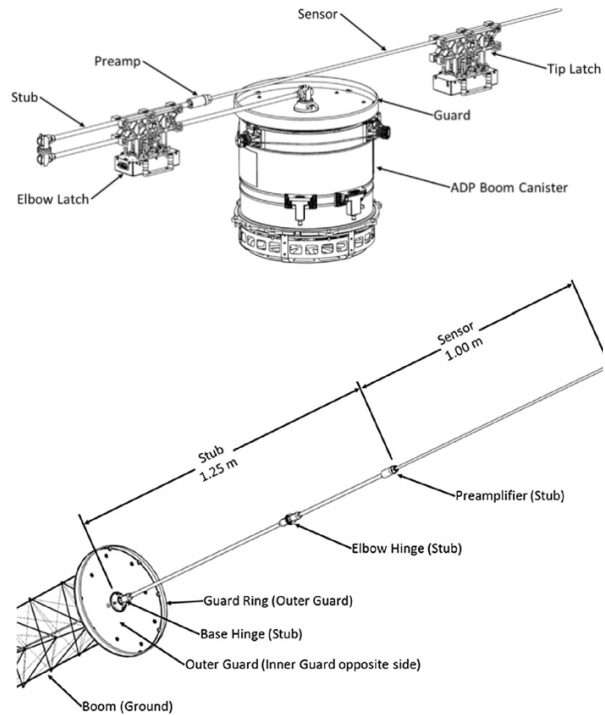


**Figure 3.7:** MMS/FIELDS/ADP & SDP (Ergun et al., 2016; Lindqvist et al., 2016; Torbert et al., 2016), as heritage for MAKOS/EF.

**Table 3.9:** Electric Fields Summary Table

Item	Value	Units
Type of instrument	3D electric field antennae	
Size/dimensions (for each instrument)	500	cm (radial)
	150	cm (axial)
Instrument average science data rate <sup>^</sup> <b>without</b> contingency	28 (low-rate)	kbps
	4176 (high-rate)	kbps
Instrument average science data <sup>^</sup> rate contingency	50	%
Instrument average science data <sup>^</sup> rate <b>with</b> contingency	42 (low-rate)	kbps
	6264 (high-rate)	kbps
Instrument field-of-view	n/a	°
Pointing requirements (knowledge)	n/a	°
Pointing requirements (control)	n/a	°
Pointing requirements (stability)	n/a	°/s
Representative Heritage Instrument	MMS/FIELDS/ADP & SDP (Ergun et al., 2016; Lindqvist et al., 2016; Torbert et al., 2016)	

We require the EF instrument to measure DC electric field to an accuracy of 1 mV/m and to resolve frequencies from DC to 1 kHz. Thus, the voltage probes must be positioned at a distance least 20 times the diameter length of the spacecraft body.

## 3.2 Concept of Operations and Mission Design

### 3.2.1 Mission Design

The MAKOS mission design consists of four identically instrumented spacecraft in 5:1 lunar-resonant orbits, which enable routine, year-round crossings of the bow shock at least twice per spacecraft during every orbit. Table 3.10 shows Keplerian orbital elements corresponding to these orbits at a generic time (true anomalies tuned to Moon’s location at initial condition), and Figure 3.8 shows the MAKOS orbits over the 2-year prime mission. These example orbits assume zero inclination of the orbital plane, but the inclination should be optimized considering launch vehicle capabilities and minimizing lunar perturbations. MAKOS’s 5:1 lunar resonance ensures that these orbits are stable over long time-periods (decades), since the lunar perturbations actually serve to balance out over each full lunar orbit, and that resonance condition locks in the orbital period (and corresponding elements) at 5 days, 11 hours, 8 minutes, and 40 seconds, or 5.4644 sidereal days.

MAKOS-1 and -2 share a common orbit and are separated along it only in orbit phase (i.e., true anomaly; “string-of-pearls” configuration); MAKOS-3 and -4 also share their own common orbit and are separated along it only in orbit phase. As seen in Table 3.10, the orbit for 1 and 2 is different from the orbit for 3 and 4 only via a 180° rotation in the argument of periapsis. The true anomalies of the MAKOS orbits have been configured such that the spacing between the MAKOS spacecraft are tuned for ion-kinetic (i.e., 100s to ~1000 km scales in the solar wind and magnetosheath) to magnetohydrodynamic (MHD, i.e., ~1 to 10  $R_E$ ) separation scales each time any of the MAKOS observatories are in the proximity of Earth’s bow shock. Figure 3.9 and Figure 3.10 show histograms of the MAKOS inter-satellite separations when MAKOS-1 and -3 (respectively) are within 1  $R_E$  of the average model bow shock (dark gray line from Figure 3.8). From these, it is clear that MAKOS-1 and -2 are typically separated by ~1000 to 3000 km, while MAKOS-3 and -4 are typically separated by ~300 to 1100 km, when the constellation is in the proximity of Earth’s bow shock. The two pairs (demonstrated with the middle panels of Figure 3.9 and Figure 3.10) are separated by ~5 to 12  $R_E$ .

**Table 3.10:** *Orbital elements corresponding to MAKOS orbit initial conditions*

Orbit Element	MAKOS-1	MAKOS-2	MAKOS-3	MAKOS-4
Semi-major axis [km]	1.3105e5	1.3105e5	1.3105e5	1.3105e5
Radius at perigee [ $R_E$ ]	18.000	18.000	18.000	18.000
Radius at apogee [ $R_E$ ]	23.139	23.139	23.139	23.139
Eccentricity	0.1249	0.1249	0.1249	0.1249
Inclination [°]	0.0	0.0	0.0	0.0
RAAN* [°]	0.0	0.0	0.0	0.0
Argument of Periapsis [°]	30.0	30.0	210.0	210.0

\* RAAN = “right ascension of the ascending node”

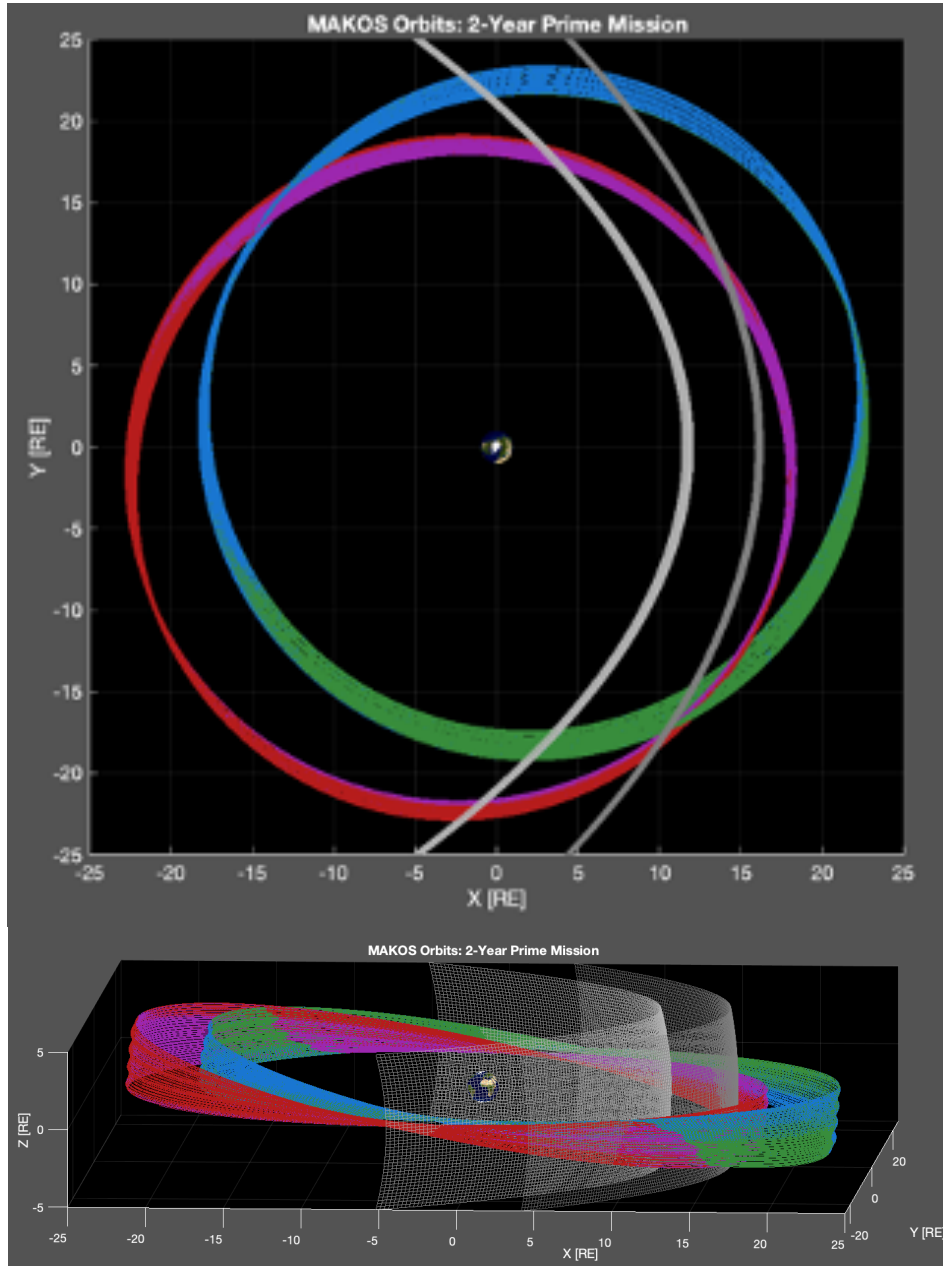


**Figure 3.8:** MAKOS orbits propagated over the 2-year prime mission. Orbits were initialized using the Keplerian orbital elements shown in Table 3.10, and they were propagated forward in time using Systems Tool Kit’s “Astrogator,” which critically for our purposes includes Earth’s moon as a third body. MAKOS-1, -2, -3, and -4 are shown in red, purple, blue, and green, respectively. Two model bow shocks are shown with the gray surfaces, one corresponding to average conditions (dark gray:  $MA = 5.0$ ,  $P_{dyn} = 1.2$  nPa) and the other for active conditions (light gray:  $MA = 10.0$ ,  $P_{dyn} = 5.0$  nPa). Bow shocks were generated in 3D using the Chapman and Cairns [2003] model. The orbits are shown in geocentric, inertial J2000 coordinates, and in this system, the bow shock rotates 360-degrees around the +Z axis as Earth completes one orbit around the Sun; thus, the bow shocks shown here are only snapshots from one point in time during the simulated 2-year period. Earth is shown to scale.

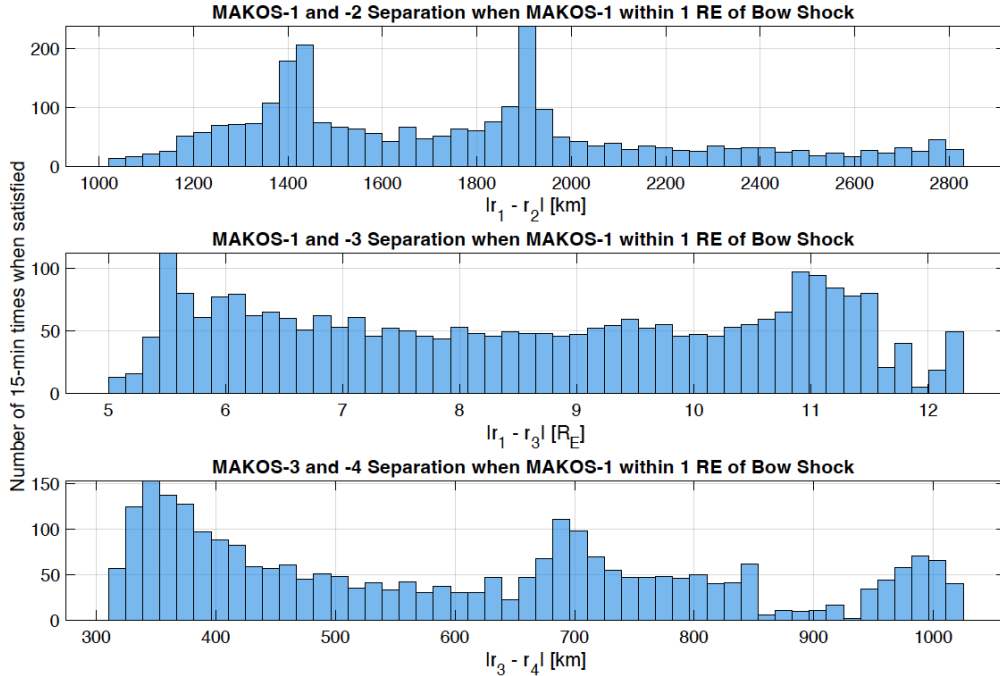


**Figure 3.9:** Distributions of MAKOS inter-spacecraft separations from all times during the 2-year mission when MAKOS-1 is within  $1 R_E$  of the average model bow shock. The top and bottom panels show separation between each pair on common orbits, MAKOS-1 and -2 (top) and -3 and -4 (bottom), while the middle panel shows separation between the two pairs quantified by the distance separating -1 from -3. These distributions exemplify how MAKOS promises to deliver dynamic, multipoint observations of collisionless shocks at ion-kinetic to MHD scales.

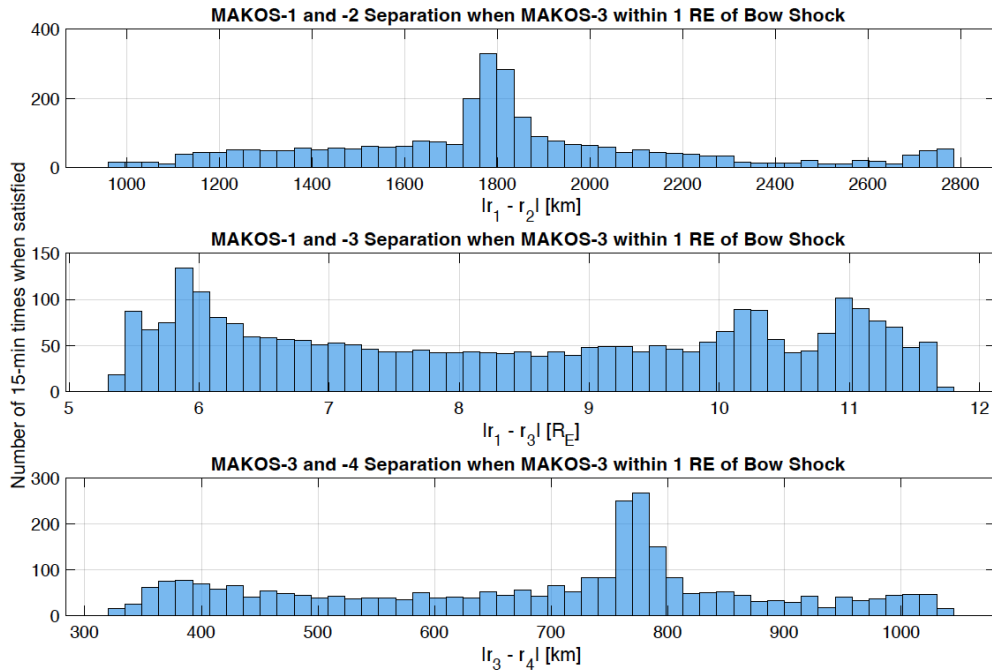


**Figure 3.10:** Distributions of MAKOS inter-spacecraft separations from all times during the 2-year mission when MAKOS-3 is within  $1 R_E$  of the average model bow shock (cf. Figure 3.9).

Figure 3.11 shows one example of the MAKOS constellation configuration during an example bow shock crossing. This example highlights the scientific advantages and value of the MAKOS orbits, which by design enable simultaneous, multipoint observations at and around (upstream and downstream) collisionless shocks (routinely Earth’s bow shock and also all IP shocks that occur when MAKOS are in the solar wind). In the example case (Figure 3.11), MAKOS-1 and -2 are located at the bow shock transition region, separated by  $\sim 1200$  km (ion-kinetic scales), while MAKOS-3 and -4 are located  $\sim 5 R_E$  (MHD scales) upstream in the solar wind (or ion foreshock) and are separated from each other by  $\sim 300$  km (ion-kinetic scales). Considering the MAKOS scientific payloads and 2-year prime mission, such collisionless shock crossings will enable unprecedented capabilities to quantify the full energy budget across the shock and detail the energy conversion processes active under a statistically significant number of different shock orientations and driving conditions (e.g., Alfvénic and fast magnetosonic Mach numbers, plasma beta, IMF orientation). Furthermore, Figure 3.12, including Earth’s magnetopause, showcases how MAKOS’s unique orbits enable year-round, multipoint observational coverage of Earth’s magnetotail and flank magnetopause, magnetosheath, bow shock, and upstream solar wind and ion foreshock.

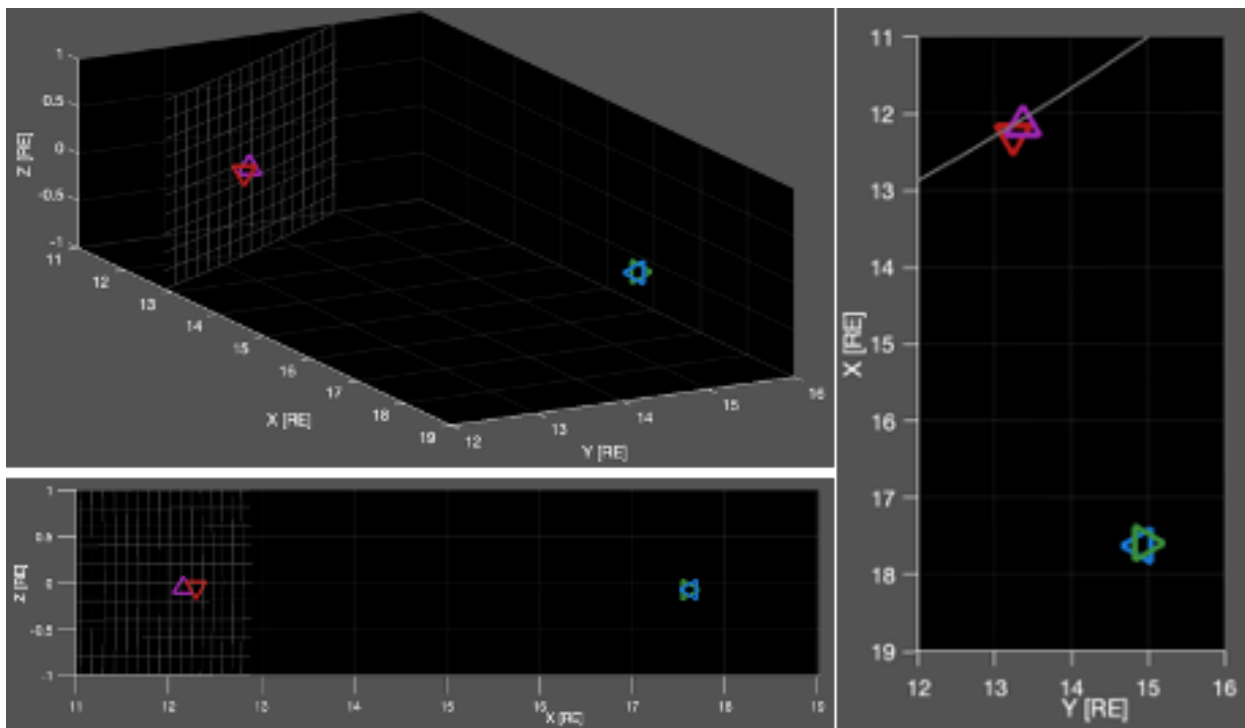


**Figure 3.11:** MAKOS constellation configuration during an example bow shock crossing. MAKOS-1, -2, -3, and -4 are shown in the same colors, respectively, as in Figure 3.8 and using different marker symbols (down, up, left, right pointing triangles, respectively). The average model bow shock is shown in the gray mesh. At the time shown, MAKOS-1 and -2 are at the bow shock and separated by 1,206 km. At the same time, MAKOS-3 and -4 are  $5.6 R_E$  upstream in the solar wind and separated from one another by 322 km. This exemplifies the unique, ideal, and opportune configurations offered by the MAKOS orbits and constellation for unprecedentedly detailed studies of Earth’s bow shock and interplanetary shocks at 1 AU.

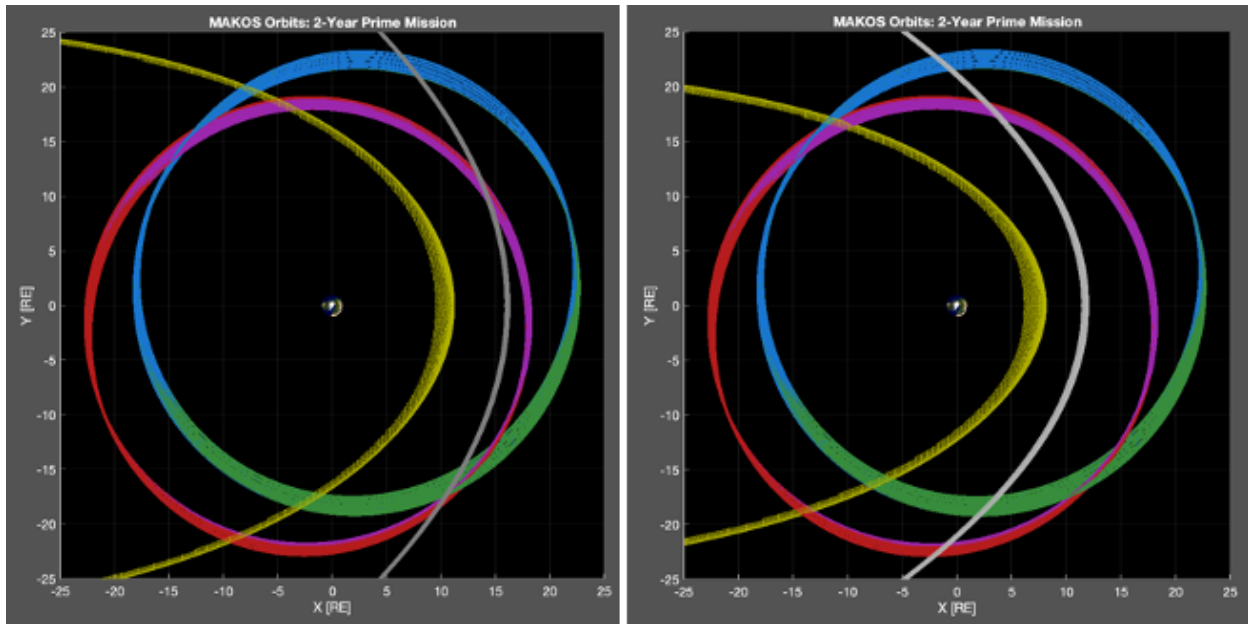


**Figure 3.12:** MAKOS orbits during its 2-year prime mission with “snapshots” of Earth’s magnetopause (yellow) and bow shock (gray) under average (left plot) and active (right plot) solar wind conditions. The magnetopause model is from Lin et al. [2010] using solar wind dynamic pressure, magnetic pressure, and  $B_z$  of 1.2 nPa, 0.1 nPa, and  $-1.5$  nT (average conditions) and 5.0 nPa, 0.5 nPa,  $-5.0$  nT (active conditions). The bow shock model is from Chapman and Cairns (2003) using  $M_A$  and dynamic pressure of 5.0 and 1.2 nPa (average conditions) and 10.0 and 5.0 nPa (active conditions). These plots demonstrate how MAKOS unique orbits enable year-round, multipoint observations of Earth’s magnetotail and flank magnetopause, magnetosheath, bow shock, and upstream solar wind and ion foreshock.

### 3.2.2 Concept of Operations

Telemetry is a major driver of the MAKOS conceptual mission design. MAKOS science requires very high data rates for observatory science telemetry at and around each collisionless shock crossing during the mission. Furthermore, MAKOS should also capture the highest rate data from any IP shocks that occur while MAKOS is upstream of the bow shock. All that considered, MAKOS CONOPS is simple by design and consists of collecting science data (telemetry) from each of the four identical observatories during the 2-year prime science mission. Each observatory shall record telemetry in one of two science modes for science data collection: i) high-rate mode and ii) low-rate mode. As seen in Figure 3.12, even under extreme solar wind driving conditions, the bow shock is consistently located outside the average (i.e., typical) magnetopause location. Thus, the average magnetopause location offers an opportune surface to use for routine orbit-to-orbit operations and systematically toggling the MAKOS spacecraft between high-rate and low-rate modes. Using the average magnetopause location and the orbit predications to schedule onboard science telemetry mode changes, each MAKOS observatory shall switch from low-rate to high-rate data collection when it transits from the magnetopause into the magnetosheath (i.e., outbound model magnetopause crossings) and from high-rate to low-rate data collection when it transits from the magnetosheath into the magnetosphere (i.e., inbound magnetopause crossings).

In low-rate mode, MAKOS's combined payloads generate new data at a rate of 807 kbps, while in high-rate mode, the payloads generate data at a rate of 20.875 Mbps, based on the temporal resolutions required for each observable as detailed in the STM. Operating the observatories in high-rate mode only when MAKOS S/C are *sunward* of the average magnetopause requires high-rate telemetry being recorded for approximately 60 hours out of each 5.4644-day orbit (i.e., 45.8% of the orbit). With the above data rates in the two operational modes (with low-rate data collected at all times, including during high-rate collection), this means that each MAKOS observatory generates ~611 GB of science data each orbit. During the course of the 2-year prime mission, the four MAKOS observatories combined will generate an expected total ~327 TB of science data.

To accommodate the MAKOS science data generation, each S/C includes 10.5 Tb = 1.3 TB of on-board storage, sufficient for more than two orbits' worth of data acquisition before data is overwritten. Data is downlinked over X-band radio frequency (RF) communication at a minimum baseline rate of 17 Mbps through the Deep Space Network (DSN), whenever the S/C spin axis is pointed within  $\pm 30^\circ$  of Earth. While downlink does not interrupt science data acquisition, we nonetheless baseline downlink during nightside only, to prioritize the dayside orbit for high-rate science observations; this then provides a precession-averaged ~21 hours per orbit of available downlink time, for a total baseline downlink capacity of ~161 GB/orbit.

Given this downlink capacity, not all of the ~611 GB/orbit per S/C of generated science data can or will be transmitted to ground. To ensure that all of the MAKOS transits of collisionless shocks are captured during the prime mission, MAKOS will employ a "scientist-in-the-loop" (SITL) strategy. Low-rate data will be produced onboard and telemetered to ground covering the entirety of each MAKOS orbit. Just as was successfully proven for MMS, the SITL is a trained expert in MAKOS science and data, who reviews the SITL-survey data and makes prioritized selections of which periods of the high-rate shall be telemetered from the onboard data recorders to ground. For obvious reasons, all collisionless shock crossings will carry the highest-level priority, and data from and around each shock crossing will be telemetered to ground to ensure closure of MAKOS prime science objectives. However, other events of interest (e.g., transient ion foreshock phenomena, magnetopause crossings, opportune conjunctions with other missions) will be noted and assigned some priority by the SITL. If additional bandwidth remains after telemetering the highest-priority shock crossings data, then those other SITL selections may be telemetered to ground for science data analysis. A SITL system for prioritized telemetry has been successfully employed by MMS since 2015.

We baseline 5 minutes of high-rate data around each SITL-selected shock crossing. Assuming 1000 shock crossings identified and downlinked over the 2-year prime mission, SITL selections comprise an average of ~1% of the total high-rate data. Together with the full complement of low-rate data, this yields an average downlink budget of ~54 GB/orbit, requiring ~7 hours (out of 21 hours available) for downlink, per spacecraft, providing significant margin on available downlink time to enable flexibility in the number or duration of shock crossings and/or downlink of additional events of interest. In the baseline budget, the total science data available for analysis from the MAKOS mission over its 2-year prime mission is ~7.2 TB/spacecraft, or 29 TB total from all four spacecraft. Of this, the low-rate data, which will form a foundational portion of the mission's standard data products, comprises ~6.4 TB/spacecraft for the 2-year prime mission, or 25.5 TB total.

### 3.3 Flight System (Spacecraft)

The four identical observatories meet MAKOS mission requirements as defined in Figure 1.5. The S/C uses a single-string hardware architecture with functional redundancy included for critical areas to increase mission reliability as illustrated in Figure 3.13. The MAKOS satellite design (Figure 3.14) comprises a central cylinder connecting two octahedral plates spanning 2 m across face-to-face (2.2 m corner-to-corner), with 0.62 m between the two separation interfaces.

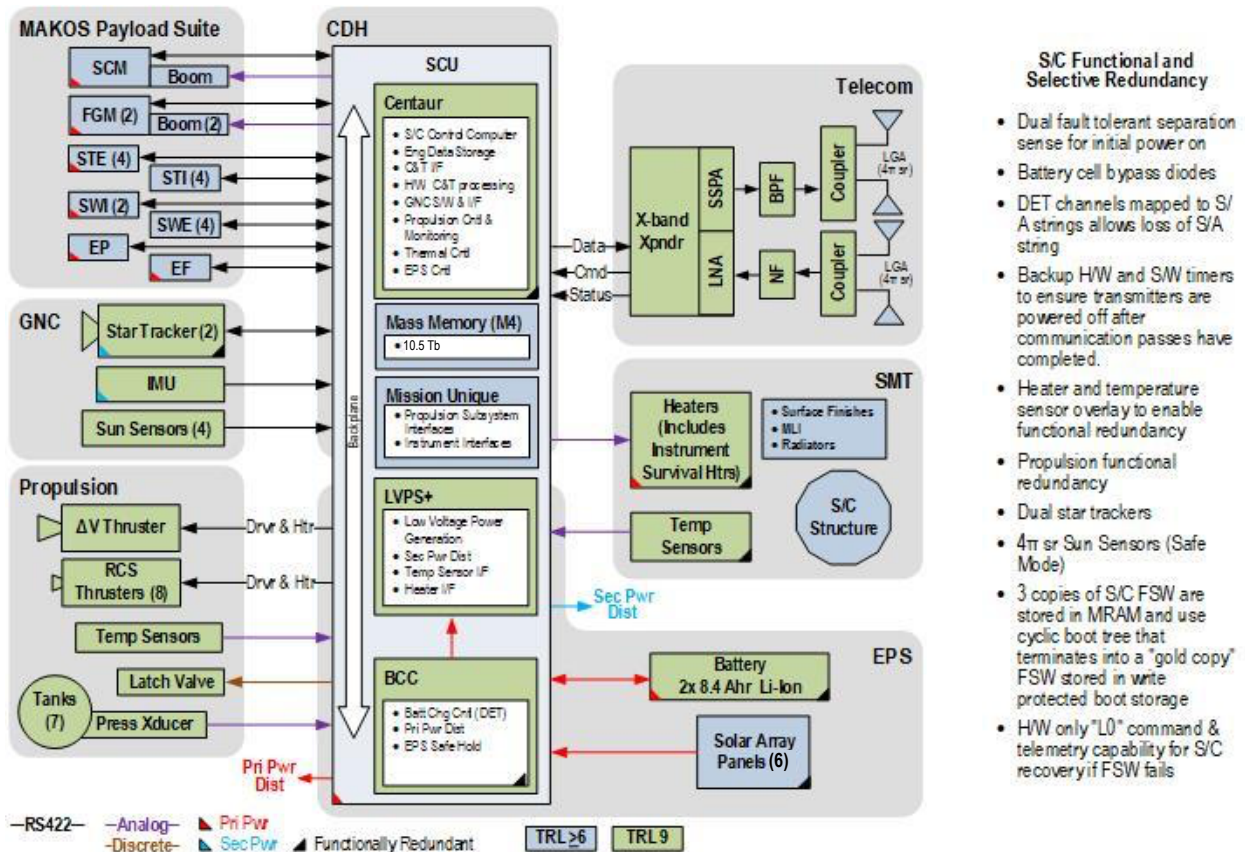


Figure 3.13: Functional block diagram of the MAKOS observatory architecture and definition of its functional redundancy attributes.

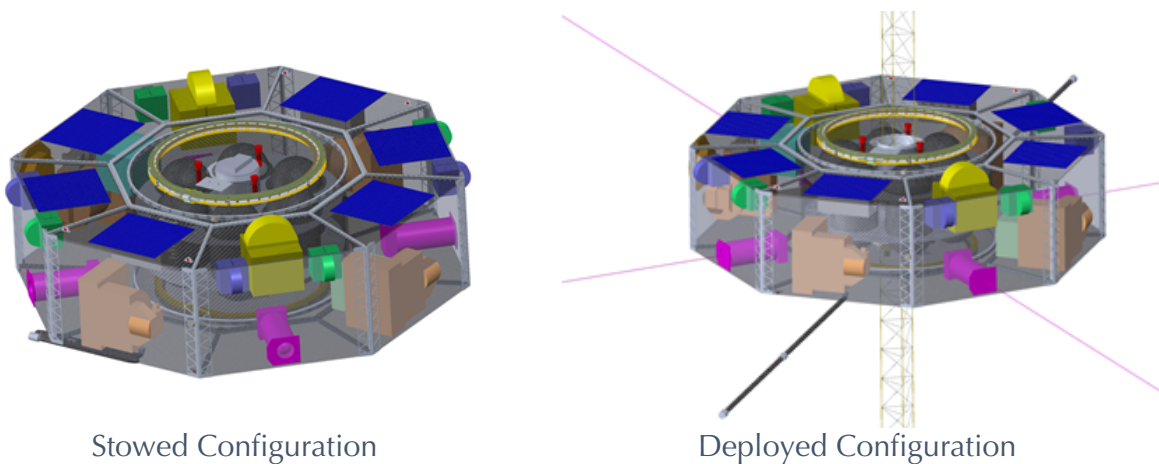


Figure 3.14: MAKOS Observatory flight configuration.

**Table 3.11: S/C Capabilities Summary**

Parameter/Item		Performance	Parameter/Item		Performance	
<b>Structure</b>	Type	CFRP panels with milled Al supports	<b>Space to Ground Communications</b>	Uplink	X-band 256 kbps	
	Size	Octagonal; 2.0m x 0.65m		Data Downlink	Science: 17 Mbps Engineering: 256 kbps	
	1 <sup>st</sup> Mode	>210 Hz		<b>Data</b>	Data Storage	1312 GBytes
	SV Mass (dry)	315.7 kg		<b>Attitude Knowledge</b>	Star Tracker	Dual, 20 arc-sec (1 $\sigma$ )
<b>Thermal</b>	Architecture	Cold bias	IMU		Bias Stability: 0.3°/hr	
	Control	Heaters, MLI, radiators	Performance	<30 arc-sec (1 $\sigma$ )		
<b>Solar Array</b>	Configuration	6-panel, body mounted	<b>Attitude Control</b>	Architecture	Spin stabilized, 10 rpm	
	Size	0.84m <sup>2</sup>		Pointing	<1.3 deg	
	Cell Type	Triple junction with AR coating		Nutation	<1.6 deg (p-p)	
	Cell Efficiency	28.4% (EOL)	<b>Orbital Knowledge</b>	GPS position	<100 m (1 $\sigma$ )	
	Full power output	283 W (EOL)		Velocity	<10 cm/s (1 $\sigma$ )	
<b>Battery</b>	Configuration	8 cells/10 strings (8p10s) (x2)	<b>Propulsion</b>	Type	Cold Gas (SF <sub>6</sub> )	
	Cell type	Li-ion		DeltaV Thrusters	1N, Isp: 45 sec (qty 3)	
	Capacity	56 Ahr		RCS Thrusters	120mN, Isp: 45 sec (qty 8)	
	DOD during full eclipse periods	<49% with no operational restrictions		Delta-V	>160 m/s when fully loaded	
	Average Load	149.5 W (cold case)		Reaction Control	6 degrees of freedom	
<b>Power</b>	Margin	90%				

### 3.3.1 Instrument Accommodation

The MAKOS S/C are designed to accommodate the science instruments via appropriate allocations for mass, power, and volume, as well as data storage and downlink. The instrument locations are shown in Figure 3.14 and the foldout mission summary (page iv). To ensure that the instruments meet science measurement requirements, additional requirements are flowed to the spacecraft and include the following accommodations and considerations.

**Configuration:** The reference S/C design has been specifically designed to enable AI&T flexibility. The S/C mechanical configuration must accommodate clear fields of view (FOV) and consider co-alignment of each of the instruments, accommodate launch loads, and consider pointing knowledge/control co-alignment where knowledge is the driver.

**Pointing and spin rate:** Each MAKOS observatory will be oriented along the solar wind direction (~7° off the Earth-to-Sun vector) and spin at a nominal rate of 10 RPM (6-sec spin period). A high-rate star tracker provides accurate knowledge of the spacecraft pointing vector, including roll angle, for use in reducing the science data.

**Thermal:** Multi-layer insulation (MLI), heaters, and dedicated radiators are accommodated as necessary to manage instrument thermal environments as required.

**Electrical:** Electrical power distribution and conditioning are key to successful operation of payloads. Power distribution electronics must address voltage management (especially critical to instruments with high voltages), power ripple, and spikes. Grounding is key to reliable and consistent operation of the observatory. The observatory uses a single point grounding architecture with primary electrical power returns galvanic isolation from secondary power return and chassis ground. Chassis ground integrity is maintained with all structural and mechanical parts, electronics boxes, enclosures, etc., of the observatory being electrically bonded to each other with a resistance of less than 2.5 mOhm at each joint. The solar array uses a ground strap with less than 250 mOhm across the interface.

EMI/EMC must be managed to ensure compatibility, mission safety, and technical performance. All components are tested to MIL-STD-461 then verified at S/C level to MIL-STD-461

per AIAA S-121-2009. Similarly, magnetic and electrostatic cleanliness are crucial to ensuring that MAKOS instruments meet measurement requirements. MAKOS uses mature electromagnetic processes and procedures consistent with MMS, Helios, GEOS, ISEE, Giotto, Ulysses, Cluster, STEREO, and THEMIS to develop magnetically and electrostatically clean Observatory. Table 3.12 discusses the magnetics and electrostatic cleanliness design features by various subsystems with dominant magnetic threats and primary design features to overcome them.

**Table 3.12: Magnetic and Electrostatic design features for cleanliness**

H/W or Function	Features and Mitigations
<b>Solar Array stray residual fields design</b>	Includes balanced cell layout (10 cells in one direction and 10 cells of same string in opposite direction) and back-wiring. Produces 0.7 nT at 1 m. (MMS requirement was 6 nT per panel at 1 m)
<b>Batteries</b>	Deperming cells before assembly limits residual fields. Battery layout cell connections in a “horseshoe” fashion and tight twisting the harnessing within the battery limit field strength when flowing current.
<b>Material selection</b>	Controlled w/ prohibited materials list & EMCCB approved soft magnetic materials.
<b>Magnetically clean flight hardware and tools</b>	<ul style="list-style-type: none"> <li>• Magnetic screening, tracking, and deperming of all flight HW and tools and tight control of cleanroom procedures.</li> <li>• Magnetically clean heaters; twisted pairs; cancellation magnets; opposing latch valves mounting; etc.</li> <li>• Single point ground strategy implemented</li> <li>• Limited chassis currents, using the same techniques and requirements from TRACERS and MMS; unbalanced returns are prohibited.</li> <li>• Magnetometer boom length set at 2 m, placing magnetometers at ~1.3 m and 2 m from the skin of SC. Boom length can be extended to 3 m, if required.</li> </ul>
<b>Heaters</b>	Magnetically clean heaters; on/off frequency computer commanded to be $\gg 0.1$ Hz
<b>Magnetic testing</b>	<ul style="list-style-type: none"> <li>• System level, powered testing using GSE and magnetometer EDU units appended to EMI/EMC testing.</li> <li>• Swing test (suspended on a hook and carefully moving the observatory through a range of motions) to detect stray DC fields.</li> </ul>
<b>AO-resistant GBK MLI</b>	Grounded and used for all insulated external surfaces. Avoids “charge islands” that occur on ITO-coated MLI (prior lesson from MMS).
<b>GBK tape w/ conductive adhesive</b>	Covers blanket buttons and other non-conductive surfaces.
<b>Optical Solar Reflectors (OSRs)</b>	<ul style="list-style-type: none"> <li>• Grounded, AO resistant, and ITO coated</li> <li>• Relatively rigid and used for all radiator surfaces.</li> </ul>
<b>Solar cells</b>	Use ITO-coated cover glass w/ Kovar cell interconnects (no view to ram AO) to form aperture covering non-conductive grout between cells & creates common ground.
<b>Grounding straps</b>	Used between all structures that are not otherwise conductively joined, with adequate margin; used for all external surface (MLI, OSRs, solar cell cover glass).
<b>Single-point ground strategy</b>	Employed with all external surfaces; only non-conductive surface on SC is T-0 37-pin connector insulator and only ungrounded conductive surfaces on SC are X-band antennas (both are out of FOV of science instruments).

**Instrument commanding and data handling (C&DH):** Complex suites of instrument payloads can drive requirements and costs for both the spacecraft and instruments. Spacecraft typically are not optimized for payload accommodations. Integrating mission-unique instrument C&DH causes changes that drive cost and schedule while rippling into core spacecraft subsystems that reduce heritage and reliability. Accommodating complex C&DH in the instruments

requires instrument providers to develop often unique capabilities for which they do not have necessary expertise. A solution that has proven successful is the use of a central instrument data processor as demonstrated on missions such as MMS, IMAGE, Cassini, JUNO, and CYGNSS. The use of a central instrument data processor, provided by a qualified vendor, allows the mission to efficiently centralize common command and data processing and storage capability, segregate mission unique functionality from the spacecraft, and address instrument specific unique requirements. Instrument operations on MAKOS are intended to be kept as simple as possible: turn them on, let them accumulate and record data, and activate/deactivate the two different modes based on a simple time- and/or position-dependent scheduler (low-rate vs. high-plus low-rate collect).

### 3.3.2 Structure and Mechanical

The MAKOS structure design consists of an octagonal shape designed for a balanced spin about the central axis (Figure 3.14) using an approach successfully employed in previous missions such as MMS and IMAGE. Though similar in function and instrument payload to MMS, the MAKOS concept is approximately one third the overall volume and mass of MMS satellites.

The MAKOS reference structural design emphasizes modular assembly resulting in better structural strength than large single panel top and bottom decks as used on MMS and IMAGE. This modular design also allows for various instrument packages to be integrated into the primary structure in parallel and without being located in the same facilities. Outer corners of the two panels are connected using aluminum T-brackets to maintain both axial and shear loads at the edges of the structure. The structure is comprised primarily of CFRP composite sandwich panels using aluminum honeycomb core and connected with lightweight aluminum inserts bonded into mating interfaces.

The MAKOS structure consists of three unique entities: a central column, two keystone plates, and eight outer wedges. The central column is a 1-m-diameter carbon-fiber-reinforced polymer (CFRP) sandwich tube structure with an aluminum honeycomb core. Milled aluminum rings bonded to the column ends facilitate mechanical fastening to the keystone plates at either end (Figure 3.15). The keystone plates are CFRP/aluminum honeycomb sandwich panels with a milled aluminum ring bonded to match the diameter of the center column. Additionally, the outer edges of the keystone plate have milled aluminum bars bonded to them for fastening to the outer wedges. The outer wedge assembly is where the majority of the spacecraft components and instruments are mounted.

Each of the eight wedges consists of two CFRP/aluminum sandwich panels with milled aluminum bars along three of the four edges that mechanically fasten to the keystone plate and its two neighboring wedge assemblies. Two triangular milled aluminum column supports

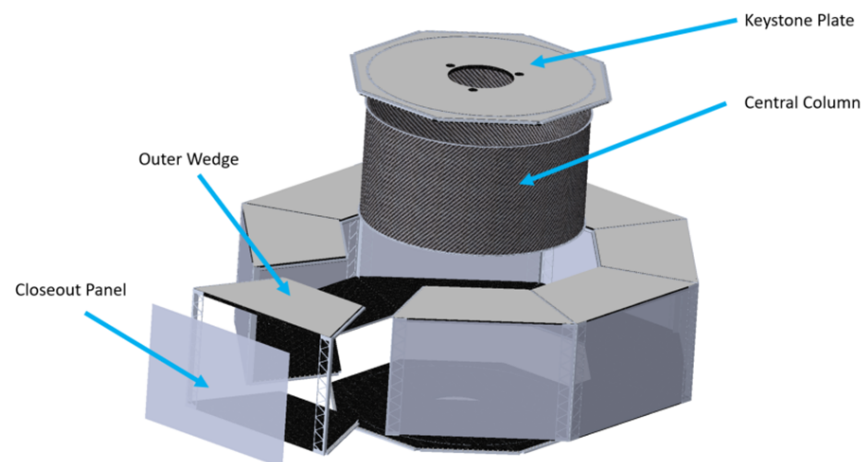


**Figure 3.15:** The MAKOS structure consists of only 3 unique entities: a central column, two keystone plates, and 8 outer wedges.

separate the upper and lower panels of each wedge. This design, using aluminum columns, withstands torsion as well as compression forces from the system. When assembled into the final spacecraft structure, these columns form a T-beam structure at every corner of the satellite. The wedge design provides component mounting options on the top, outer, and bottom decks, either internally or externally.

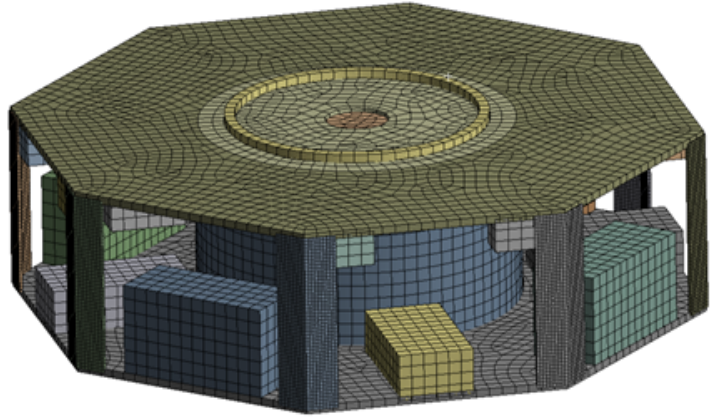


**Figure 3.16:** *MAKOS structural model mesh.*

Prior to mounting into the final assembly, each of the outer wedge assemblies can be utilized as its own standalone structure to perform component and instrument integration. This modularization allows integration activities to be performed at all locations and clean room levels consistent with instrument requirements prior to final integration of the observatories. Smaller panels and common inserts also serve to reduce overall structure fabrication costs and supply chain issues.

After final integration of the central core, keystone plates, and 8 outer wedges, the 8 radial sides of the structure are closed using reflective MLI over a CFRP mesh to protect the observatory internal components. The CFRP mesh serves to anchor the MLI and prevent MLI migration during launch such that it doesn't interfere with instrument FOVs or boom deployments. Actual MAKOS mission development may elect to replace these MLI closeouts with panels populated with additional instruments, solar cells, or RF antennas if the need arises.

### 3.3.2.1 Structural Analysis

Analysis of the MAKOS system was performed to determine the fundamental frequency of the reference observatory. A representative structural model was developed in the ANSYS analysis environment using primarily SHELL281 and SOLID186 elements; the completed model contained a total of 32,456 elements and 73,951 nodes (Figure 3.16).

Connections within the model use "bonded" contact regions to simulate joints between components and structure that assume zero gapping. The analysis performed was a linear eigenvalue modes analysis with a boundary condition set on the  $-Z$  separation ring. Figure 3.17 shows the first three modes, with the first mode being 118 Hz.

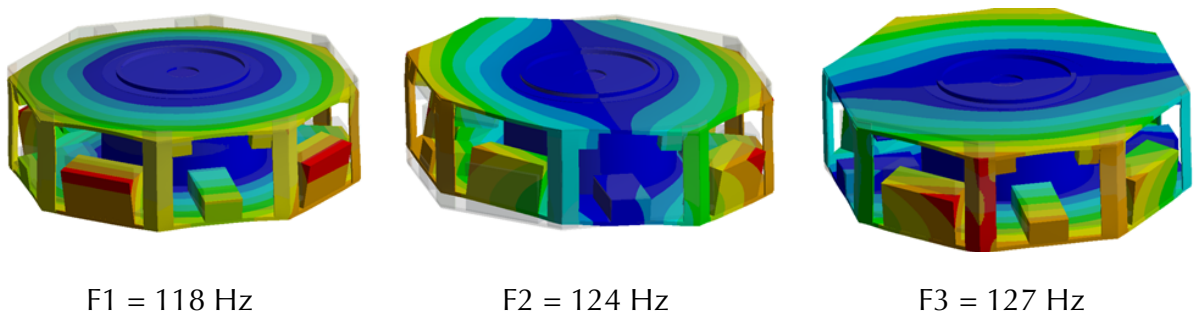


**Figure 3.17:** *MAKOS Modal prediction results.*

### 3.3.3 Thermal Subsystem

The MAKOS observatory reference design uses a standard flight-proven, cold-biasing approach to meet spacecraft and instrument thermal requirements using:

- Appropriately sized panel radiators and heaters to maintain internal components within temperature limits during all operational modes.
- An integrated design of component location, surface treatments, localized radiators, and MLI blankets to minimize supplemental heaters.
- A combination of hardware and FSW to control heater set points and thermal sensor-to-heater relationships.

Solar flux is blocked by MAKOS's solar array/top deck to fully shade the internal spacecraft components and instruments. Spacecraft and instrument thermal loads that do not require critical control are conductively coupled to the spacecraft structure. All spacecraft surfaces within view of the instruments are covered with MLI to minimize radiative coupling with the spacecraft. Components requiring critical control are isolated by titanium isolators and MLI, then thermally controlled by dedicated heaters. Deployed instrument components are thermally isolated from the deployed element and spacecraft; thermal control is implemented locally by the instrument.

All thermal control materials necessary for the MAKOS reference design are flight qualified and compatible with MAKOS contamination control requirements. Thermostat-type survival heaters are used to maintain critical components such as batteries, reaction wheels, propulsion module, and instruments within their survival limits during Observatory Safe Mode operation.

### 3.3.4 Electrical Power

The Electrical Power Subsystem (EPS) is required to provide primary and secondary power to the spacecraft subsystems and robust margins for payload accommodation (Table 3.13). Solar

**Table 3.13: MAKOS S/C Power by Subsystem and operational mode**

Observatory	Orbit Average Power				
	Safe Case	Orbit Phasing Case	Hot Science Case	Cold Science Case	Comm Downlink Case
<b>MAKOS Spacecraft</b>	<b>39.0</b>	<b>40.0</b>	34.6	<b>36.3</b>	<b>61.2</b>
<i>Structural/Mechanical Subsystem</i>	0.0	0.0	0.0	0.0	0.0
<i>Thermal Subsystem</i>	4.8	0.8	0.8	1.9	1.9
<i>Electrical Power Subsystem</i>	1.9	1.9	1.9	1.9	1.9
<i>Telecommunications Subsystem</i>	9.9	9.9	9.9	9.9	34.9
<i>Command and Data Handling Subsystem</i>	0.0	0.0	0.0	0.0	0.0
<i>Guidance, Navigation, and Control Subsystem</i>	18.7	18.7	18.7	18.7	18.7
<i>Propulsion Subsystem</i>	2.9	6.7	1.2	1.8	1.7
<i>Spacecraft Electrical Cables</i>	0.9	2.0	2.1	2.1	2.1
<b>MAKOS Payload Suite</b>	<b>8.2</b>	<b>37.1</b>	123.9	<b>123.9</b>	<b>123.9</b>
<i>Solar Winds - Ions</i>	0.00	0.00	8.75	8.75	8.75
<i>Solar Winds - Electrons</i>	0.00	0.00	16.00	16.00	16.00
<i>Suprathermal - Ions</i>	0.00	0.00	54.00	54.00	54.00
<i>Suprathermal - Electrons</i>	0.00	0.00	13.86	13.86	13.86
<i>Energetic Particles</i>	0.00	0.00	4.69	4.69	4.69
<i>Electric Fields</i>	6.18	0.00	13.21	13.21	13.21
<i>Fluxgate Magnetometer</i>	1.03	0.00	0.00	0.00	0.00
<i>Search Coil Magnetometer</i>	1.03	0.00	0.00	0.00	0.00
<i>Common Payload Instrument Electronics Unit (IEU)</i>	0.00	0.00	3.57	3.57	3.57
<i>Instrument Electrical Cables</i>	0.00	0.00	0.60	0.60	0.60
<b>Total Observatory Orbit Average PoXer</b>	<b>47.2</b>	<b>158.5</b>	158.5	<b>160.2</b>	<b>185.2</b>
Orbit Average Power Available (EOL)	283.2	283.2	283.2	283.2	283.2
<b>Orbit Average Power Margin</b>	<b>499%</b>	<b>79%</b>	<b>79%</b>	<b>77%</b>	<b>53%</b>

illumination during the MAKOS LRO allows use of a standard direct energy transfer (DET) power architecture. Detailed component level power information for the reference subsystem design is provided in the Master Equipment List (MEL; Appendix 1).

**Table 3.14:** Battery sizing provides 40% margin (beginning of life)

Battery Sizing Calculation	Value	Units	Notes
DOD	50%		Required DoD BOL
Eclipse duration	2.38	hours	Reference Orbit Parameters
Expected Nominal Case Power Consumption	248.5	Watts	Hot power should correlate to worst efficiency
Expected Watt-hours	592.6	Whr	As consumed by spacecraft
Nominal Battery Voltage	30	V	Average voltage during operation
Expected Amp*hours	19.8	Ahr	As consumed by spacecraft
Transmission Efficiency	0.9		Conservative value from SMAD
Required Battery Capacity	43.9	Ahr	Required Battery size at DoD BOL
Battery Capacity	56.0	Ahr	
Expected DOD	<49%		
Margin	40%		

Table 3.11 provides EPS characteristics. Dynamic EPS performance analysis includes the designated MAKOS reference orbit and seasonal solar Beta extremes. Power margin analysis includes projected worst-case RCS operation, communication transmitters active, and full heater loads. The EPS design is required to perform battery charging without interrupting payload data acquisition or data downlink. Maintaining full science operations during maximum eclipse to enable secondary science investigations drives battery sizing. Full instrument operational capability during eclipse can be traded for reduced battery size during Phase A.

The EPS solar panel reference design uses triple-junction solar cells arranged on solar panel substrates with anti-reflective coated cover glass to improve their thermal performance, radiation tolerance, and ground handling robustness. The solar array generates primary power (28±4 Vdc) for charging the battery. Available area on the reference design spacecraft allows all solar panels to be body mounted; no solar array deployment is required though options exist for solar array deployment if alternative mission designs require. The solar array is divided into 6 separate 0.14 m<sup>2</sup> panels, one mounted on the Sun face of 6 of the 8 outer wedges of the spacecraft structure resulting in a total solar array area of 0.84 m<sup>2</sup> to provide approximately 280 W of power.

Li-ion batteries connected directly to the primary power bus provide electrical power storage for eclipse operations. Orbital analysis identifies the maximum eclipse duration during a nominal MAKOS 2-year mission, conservatively using the sum of both umbra plus penumbra, to be approximately 2.4 hours. Given the limited number of eclipse periods during the MAKOS mission, a 50% maximum depth of discharge is allowed (Table 3.14), which results in the need for approximately 44 Ah of battery energy. Our reference design uses two standardly available 28 Ah batteries (56 Ah total) to provide >40% margin (beginning of life). Temperature sensors and bypass diodes (to withstand a failed cell) are included in the battery assembly. The S/C EPS battery charge is regulated by a direct energy charge regulator. The DET regulator operates in parallel to the solar array, charging the battery at prescribed charging rates using available power from the solar array. Excess solar array power is shunted to dissipative loads located near the solar arrays to minimize thermal impact of the shunt loads on the S/C design.

The battery charge control electronics includes a GSE interface that serves as the connection point for ground power, battery maintenance, and pre-launch battery charging. The reference EPS battery charging and power distribution hardware (H/W) operates independent of FSW except for configuration commanding and status reporting. Overcurrent protected switched power services are provided for payload loads.

### 3.3.5 Telecommunication Subsystem

The reference MAKOS Telecommunication (Telecom) Subsystem provides RF interface between the S/C and the NASA DSN. The interface provides for RF command uplink and RF telemetry downlink from the S/C and its payload. The Telecom Subsystem is compatible with the NASA DSN to transfer command, S/C telemetry, and stored mission data. The Telecom Subsystem design consists of an X-band transponder, RF couplers, filters, a receiver low noise amplifier, a transmitter solid state RF power amplifier, and antennas (Figure 3.13). The subsystem communication links are bi-directional and configured with the receiver always on so that flight operators can send commands whenever necessary.

During communication passes, payload and S/C data formatted by the Command Data Subsystem (CDS) routes to the Telecom transmitter for downlink. The transceiver is a software-defined radio forming the functional interface between S/C antennas and the command and data handling subsystem. The X-band uplink signal is directed to the receiver portion of the transceiver from the antennas via the appropriate RF components. The uplink data is BPSK modulated directly on the carrier, and the uplink rate is selectable up to 256 kbps (Table 3.15). The downlink S/C state-of-health and payload telemetry data is convolutional (Rate=1/2, K=7) plus Reed-Solomon encoded and 8PSK modulated by the transceiver directly onto the downlink carriers. Downlink data rates are selected from the ground up to 17 Mbps X-band (Table 3.15; baseline). The effective isotropic radiated power is adjustable, by command, such that it does not exceed the maximum power flux density at Earth per NTIA and ITU limits.

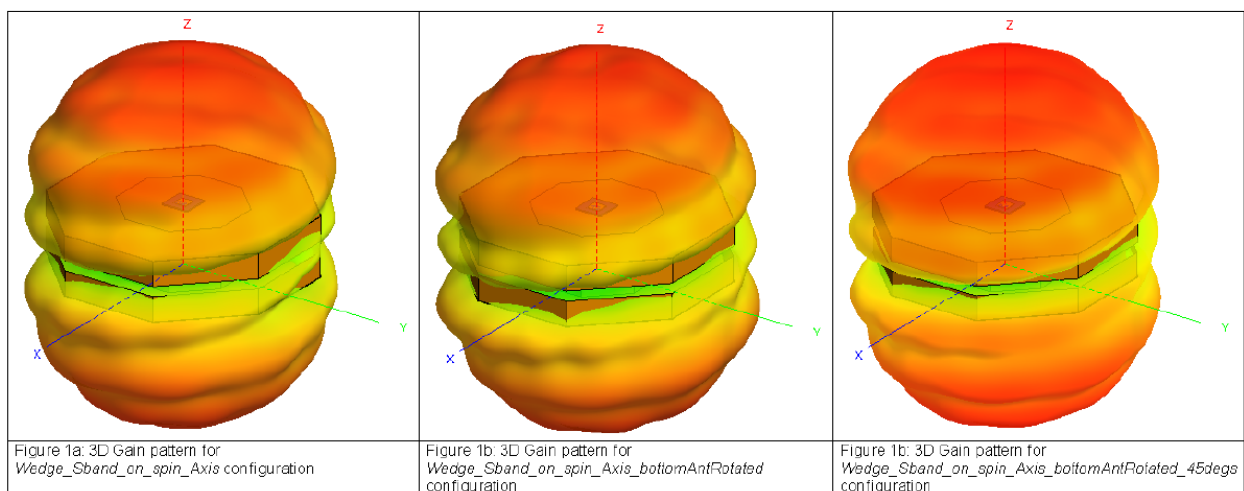
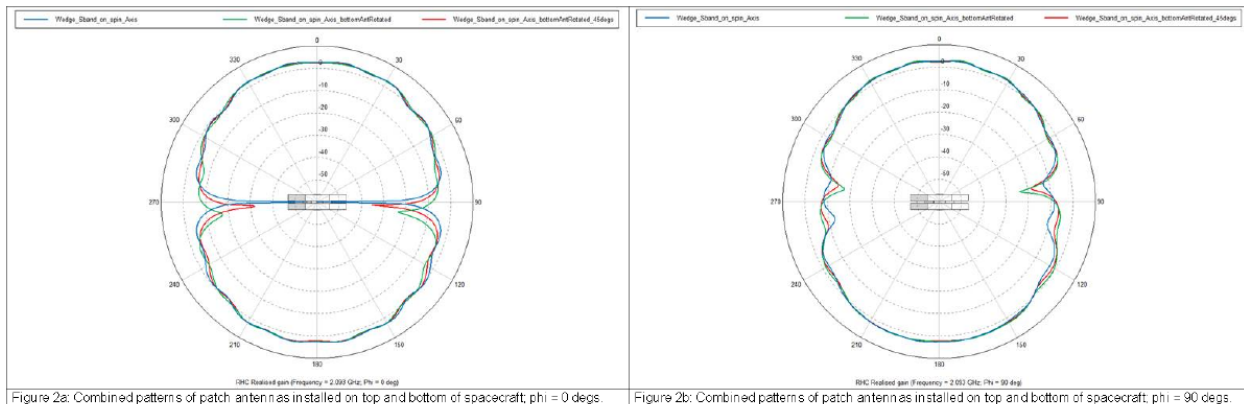


Figure 3.18: Combined RF Antenna Patterns

The Telecom Subsystem antennas consist of single frequency low gain antennas (LGA) that provide hemispherical coverage. There is an LGA pair for command and an LGA pair for telemetry. The individual LGAs in each pair are oriented opposite of each other normal to the S/C z-axis (spin axis) to provide coupled near  $4\pi$ -ster coverage with minor nulls about the S/C “equator” (Figure 3.18).

**Table 3.15: MAKOS RF Communication Characteristics**

<b>Band/Frequency</b>	X-band; Downlink: 7.5–8.5 GHz; Uplink: 7.0–7.2 GHz
<b>Data Rate</b>	Downlink: 17 Mbps (8PSK); Uplink: 256 kbps (BPSK)
<b>On-board Antenna Type and Gains</b>	Fanbeam +13.1 dBic (90deg boresight) +16 dBic (boresight)
<b>Transmit Peak power</b>	20 Wrf
<b>Ground Antenna Type and Gain</b>	34m DSN, 56 dBi (min)

### 3.3.6 Command and Data Subsystem

The Command and Data Subsystems (CDS) provides accommodation for on-board command data handling. The reference S/C CDS design localizes all on-board S/C processing on a single computer. The computer is space-qualified and supported by a CCSDS-compliant C&T interface, payload data interface, and GNC component data interfaces. The subsystem supports simultaneous command processing, real-time telemetry, playback of stored mission data, and mission data storage.

#### 3.3.6.1 Commanding

The operational nature of the MAKOS mission allows the CDS to be designed for autonomous control during all normal science and communications operations using only on-board command capabilities that include real-time command responses, stored command sequences, and CCSDS File Delivery Protocol (CFDP) processes. Command services of the reference design include NIST FIPS 197 CCSDS COP-0 uplink command processing with BCH error detect and correction. Cybersecurity requirements in the future will need to be addressed as they evolve.

The flight computer also provides FSW-independent execution of a limited command set used for ground-based fault management. This functionality serves as function redundancy to allow FSW issues to be addressed independent of FSW operation. All other commands are passed to the FSW Command Manager for execution or to the Stored Command Sequence Manager as onboard Absolute Time or Event-Based Sequences.

#### 3.3.6.2 Data Management

The CDS Telemetry Manager implemented in FSW provides collection and high-level formatting of housekeeping data which are either downlinked in real-time or passed to the FSW Storage Manager for later downlink. The Storage Manager software controls data acquisition, recording, and playback of housekeeping and payload data using the baselined 1.3 TB on-board flash memory for instrument and S/C data storage. Expected science data generated per S/C is ~611 GB/orbit, with ~54 GB/orbit downlinked. The 1.3 TB on-board data storage provides >2.1 orbits of science data storage to allow for recovery from downlink anomalies. The reference CDS design includes a hardware-based telemetry data formatter to form CCSDS source packets into transfer frames and while providing multiple separate virtual channel buffers to

enable optimized data routing and processing within the Ground Segment. This hardware functionality is designed to offload processing requirements from the FSW. An example allocation of these virtual channel buffers includes channel designation as real-time housekeeping data, stored payload data, and stored housekeeping data. CFDP is used for reliable delivery of stored data across the spacelink. The on-board memory data store allows for continuous science operations without downlink, providing significant margin for contingency operations.

### **3.3.6.3 Observatory Time Management**

Observatory time requirements are driven by science data synchronization within the constellation. Absolute time accuracy between spacecraft is a function of measuring the solar wind protons. Given a solar wind proton gyro-period of approximately 5 s, separation between the two MAKOS pairs of approximately 500 km, a maximum solar wind speed of 1000 km/s, and a budget margin of 10 yields a requirement of 50 ms. Onboard time resolution, captured within the timestamp of data measurements, is driven by E-field waveforms sampled at 200 kHz (5- $\mu$ s samples). Electron distribution measurement requires 10 ms resolution, given a factor of 2, yields a 5 ms time precision requirement. E-field data can be reconstructed during post-processing by dividing the 10-ms data by 2000 (5- $\mu$ s samples).

MAKOS uses high-side GPS as its baseline time source augmented with a chip scale atomic clock used during GPS outages. Nominal baseline time is distributed to the S/C and instruments with an accuracy error <100  $\mu$ s using a Time-of-Day packet synchronized with a Time-of-Day pulse every second.

### **3.3.7 Guidance, Navigation, and Control Subsystem**

The S/C Guidance, Navigation, and Control (GNC) subsystem meets performance capabilities (Table 3.11) by using a simple star tracker/cold-gas spin-stabilized design. The reference GNC attitude determination sensors consist of dual star trackers located opposite of the Sun vector and canted 15° from each other to preclude loss of both sensors due to Earth or Moon exclusions while meeting attitude determination performance requirements, a 3-axis inertial measurement unit for rate control, and sun sensors for Sun acquisition operations. The MAKOS baseline reference design uses high-side GPS measurements for navigation that are operationally augmented using optical navigation and ranging data from the Telecom subsystem. The GNC uses the Propulsion subsystem's reaction control thrusters to provide active nutation damping, precession control, and spin rate control. This hardware configuration provides flexible mission requirement accommodation.

The GNC has 5 operational sub-modes to support the observatory mode flow (Figure 3.19): nutation damping, Sun acquisition/precession control, spin-rate control, and science. After initial damping of launch vehicle separation rates is complete, the GNC transitions to Sun acquisition using the 4 $\pi$ -ster Sun sensors and a sky-searching algorithm to locate the Sun vector. The GNC then uses reaction control thrusters to point the S/C solar arrays at the Sun using the rate and Sun sensors. The star trackers are initialized followed by spin-up of the S/C to its operational spin rate of 10 rpm.

Spin control is accomplished by activating the reaction control thrusters continuously to generate torque about the spin axis until the targeted spin rate is achieved. Actual pulse width is a function of the disturbance environment and how closely the spin rate is controlled. The reference GNC design uses <5 sec pulse widths for spin rate control. Active nutation control removes nutation from the system by phasing reaction control thruster pulses as necessary at

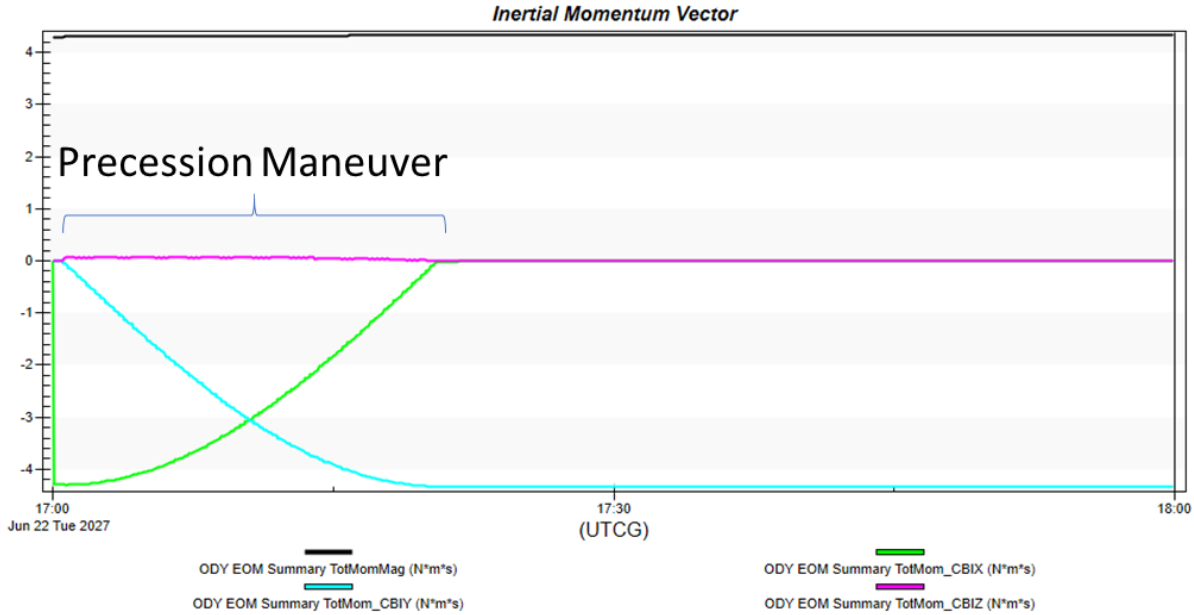


**Figure 3.19:** Spin vector precession performance example demonstrates ability of the reference GNC to control precession alignment.

nutations frequency to generate resistive torque to reduce the nutation amplitude until nutation is within budgeted pointing performance. Spin vector control is precessed to the desired inertial target by phasing reaction control thruster pulses at the spin period (60 s) to generate torques orthogonal to the spin vector until the vector is pointed at the commanded target (Figure 3.19). The reference design implements large precessions using a 1-s pulse width while small precession corrections use a 0.05 sec pulse width.

GNC has capability to perform small orbital corrections by aligning the spin-axis along the orbit velocity vector for  $\Delta V$  maneuvers. This capability is used for correction of post launch residual orbit insertion errors such as orbital altitude and eccentricities as well as phasing between the two MAKOS spacecraft within each of the MAKOS pairs.  $\Delta V$  maneuvers are stabilized using spin momentum and active nutation damping. After orbit corrections have been performed, the observatory spin-axis is oriented  $7^\circ$  offset from the Sun vector for science data collection (Figure 3.20). The GNC autonomously performs nutation damping, spin-rate, and orbital precession control during science operations. Orbital phasing corrections use uploaded scripts to instruct the GNC regarding specific  $\Delta V$  maneuver magnitudes and timing. This enables close monitoring of the maneuvers by ground controllers.

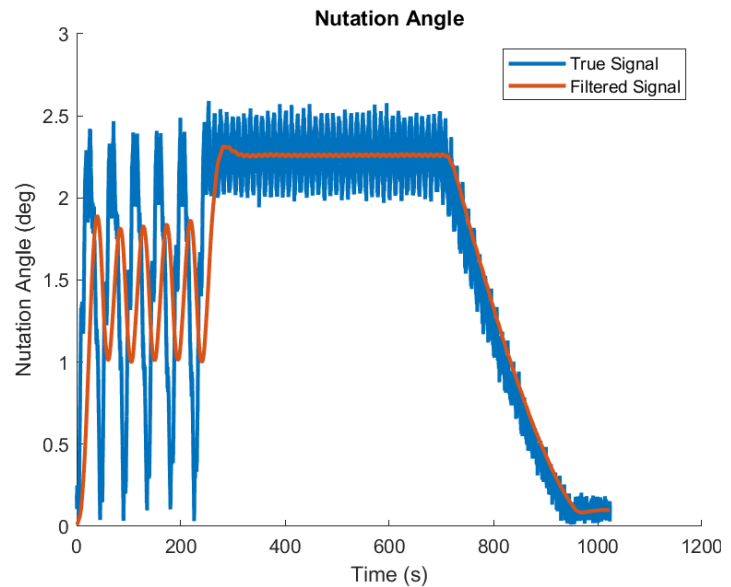


**Figure 3.20:** Projected pointing control of MAKOS reference GNC demonstrates ability to meet MAKOS science pointing control requirements.

### **3.3.7.1 Observatory Spin Motion Effects on Star Tracker Performance**

Generally, S/C rotation can be transformed into two different components of rotation as seen by the star tracker: cross boresight and about boresight rates. The cross-boresight rate is the most critical. The star tracker FOV is required to be oriented relatively close to the spin axis to be tolerant of the high rates. The higher the spin rate, the closer to the spin axis the FOV is required to point. Theoretical performance of star trackers presently available using an integration time of 0.25 s indicate attitude determination performance of 1.8" ( $1\sigma$ ) with >99% validity at spin-rates of 4 rpm. This performance has been validated by on-orbit operations on missions such as MMS. Indeed, MMS demonstrated reliable star tracker attitude determination at a spin rate of 7 rpm using 0.25-s integration time, albeit at reduced accuracies. The MAKOS 10 rpm spin rate requires star tracker image integration times of less than 0.1 s. Star trackers with 0.1-s integration times and compatibility with the MAKOS radiation environment are commercially available from vendors such as Optical Physics Company. These are at TRL 5 and require only straight-forward spin-table testing to achieve TRL 6 prior to mission PDR (see Section 4.4).

High rates of spacecraft motion have three impacts on attitude knowledge availability:

1. Decreased signal-to-noise ratio: In general, star tracker cameras are photon noise limited such that attitude determination accuracy is a function of the square root of the integration time. If the integration time is doubled, the accuracy is approximately doubled. When the star field is moving across the camera's FOV, the photons from a star are smeared over multiple pixels. The star smearing effectively results in a decreased signal-to-noise ratio. Higher rates of motion result in a decreased accuracy until the smearing effect becomes so large that fainter stars drop below the detection threshold, and the pointing knowledge degrades due to lack of stars. Additionally, the increased noise level causes the tracker to require more than one image to initially lock on the celestial pointing position because the data quality of any single image is too poor to allow for a robust solution of the lost in space problem. This is a dominant issue for trackers with an integration rate of 0.25 s and S/C motion greater than 4 rpm.
2. The effective system FOV is decreased. At very high rates, even bright stars that remain above the detection threshold are lost because they move outside the FOV during the integration time, thus efficiently decreasing the tracker FOV and limiting the accuracy further. The decrease in effective FOV is proportional to the rate of motion and inversely proportional to the integration time. Therefore, a short integration time is required to support high spacecraft spin rates.
3. The star tracker's centroiding function must cope with more complex star centroids.

Use of modern space-rated processors and FPGAs meets these requirements for integration times necessary for MAKOS 10-rpm spin rate. The high-rate star tracker will be matured to TRL 6 during development, well before mission PDR.

### **3.3.7.2 Spin Phase Synchronization**

MAKOS onboard measurement cycle is synchronous to the spin phase. This spin phase is traditionally derived from sun sensors, followed by integration of inertial sensors. The use of star trackers on spinning spacecraft offers a much higher accuracy of the derived spin phase, partly due to the intrinsic higher accuracy of star trackers and partly by eliminating divergence prob-

lems from the inertial sensors. The star tracker offers the ability to output a phase synchronization pulse each time the satellite spin reaches a certain inertially locked phase. Each time a reference vector in star tracker reference frames passes a reference vector in the inertial coordinate reference frame (ICRF) meridian, the pulse is output.

### 3.3.8 Propulsion Subsystem

The Propulsion subsystem design meets all MAKOS operational reaction and  $\Delta V$  control requirements by incorporating available flight proven components (Figure 3.21). The subsystem requirements enable use of a single fuel type (Sulfur hexafluoride, SF6) for both reaction control and  $\Delta V$  maneuvers. An additional benefit of using SF6 as a cold gas propellant is that it does not contribute to observatory electrical charging.

The design incorporates eight 120-mN reaction thrusters and three 3.6-N  $\Delta V$  thrusters along with necessary fuel storage tankage and management provisions. GNC baseline operation requires only 4 of the 8 reaction control thrusters. The addition of a secondary string of 4 thrusters develops redundancy and allows precession/nutation control without imparting  $\Delta V$  while using both strings. Use of only a single

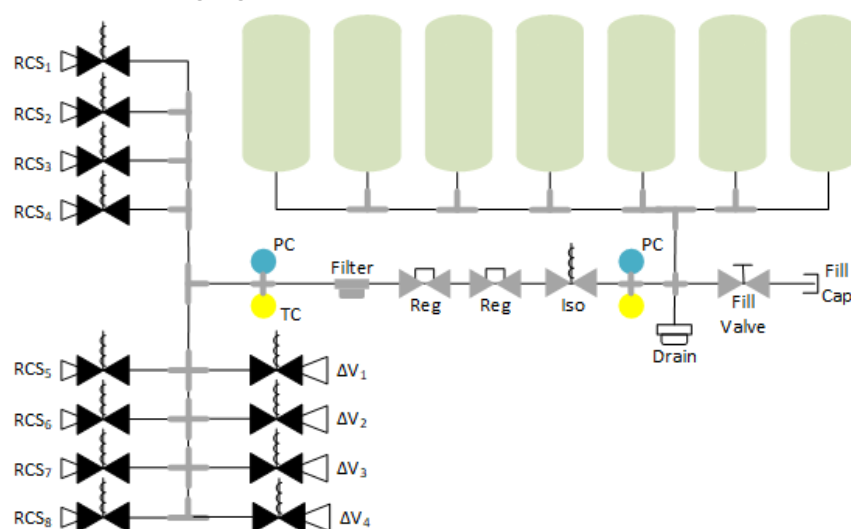


Figure 3.21: Simplified propulsion functional block diagram.

string during precession and nutation control will always impart delta-v. Canting of the reaction control thrusters within the spin plane provides for 3-axis control capability during launch vehicle separation recovery and initial solar orientation maneuvers.

The  $\Delta V$  thruster mechanical thrust axis is along the observatory z-axis (spin axis) and aligned to within 1 cm of the observatory center of gravity (CG) using an integrated machined cant during spacecraft baseplate design and manufacture. The mechanical thrust axis is then fine-tuned to within 0.5 cm of the observatory CG during final observatory AI&T mass property tests. The Mission Operations Team calibrates final alignment offsets during on-orbit spacecraft commissioning and programs them into the GNC onboard parameter table. Four separate  $\Delta V$  thrusters are used to allow the thrusters to be offset from the observatory centerline. This configuration accommodates the payload axial booms located on the spin axis while also accommodating co-manifest with the star trackers and Telecom antennas.

The propellant tanks and all pressure system components are designed to meet AFSPCMAN 91-710 Range Safety requirements. The Propulsion subsystem provides the performance necessary to perform orbit maintenance, nutation control, spin rate control, and spin-axis precession control for the MAKOS 2-year design reference mission. The propellant capacity (~15 kg) provides excess margins when fully loaded to enable mission design flexibility and mission extension options.

The MAKOS design uses existing manufacturer's data coupled with on-orbit calibration in conjunction with existing on-board thruster modeling and  $\Delta V$  accumulation software to meet the overall accuracy requirements. The combined thruster configuration and a low minimum impulse bit achieved with the SP6 cold gas approach exceed  $\Delta V$  acceleration and reaction control requirements while eliminating hazardous material handling safety concerns during AI&T, transport, and launch.

### **3.3.9 Autonomy and Fault Management**

On-board Autonomy and Fault Management (AFM) allows the S/C to perform payload and S/C operations autonomously while ensuring all observatory subsystems operate within their safety limits. If subsystem data exceeds predefined safety constraints, AFM performs the designed response. The S/C Sun Pointing mode doubles as Safe Hold mode providing power margins to address anomalous conditions. Autonomous and onboard fault management responses are implemented using telemetry monitoring logic and stored command sequence capabilities as demonstrated on previous missions such as the CYGNSS mission.

AFM implementation uses uploadable on-board command sequences tailored to new telemetry and command responses as part of the MAKOS accommodation flexibility. Reference design computer hardware includes Watchdog provisions to monitor processor and FSW operations in addition to "Level 0" hardware-only C&T capabilities that allow ground-based operators to monitor observatory low level status and issue primary commands to reset processor and shed power loads.

AFM is based on a time critical, layered approach to fault management. Faults that put the observatory in jeopardy in less than a few seconds are handled by built-in hardware measures (e.g., circuit breakers, WDTs). AFM addresses short term faults (e.g., resets or illegal state transitions) using onboard, uploadable event-driven deterministic command sequences. The GNC FSW application performs low level GNC component and algorithm performance fault management cooperatively with the S/C-level AFM to provide graceful performance degradation. S/C AFM is coordinated with the ATMS instrument's fault management to safely address excessive instrument power loads, requests from the instrument to be reset, or other similar fault responses. Faults that cannot be resolved without interrupting the operating mode result in the observatory transitioning to Safe Mode. S/C AFM is designed to synchronize with the instrument's safing sequences in the event the S/C needs to transition to Safe Mode. Finally, Mission Operations is responsible for faults that do not jeopardize the spacecraft for days.

The MAKOS S/C architecture includes specific functional and selective redundancy in critical areas (Figure 3.13) to increase observatory failure resilience. Besides aforementioned hardware Watchdog provisions to monitor processor and FSW operations, triple modular redundant FPGA implementation, memory EDAC, and hardware-only command and telemetry capabilities allow operators to monitor observatory low level status and issue primary commands to reset processor and shed power loads. Independent reliability analysis of the MAKOS design identifies a  $P_s$  of  $>0.88$  over a two-year operational life.

## **3.4 Development Approach**

An experienced systems engineering team with a toolset specifically tuned for NPR 8705.4 Class C multi-build applications is required to successfully manage MAKOS's development. The team should be led by technical experts with proven records, especially in the areas of Helio-physics instrumentation accommodation. A staff of engineers included for their expertise and

capabilities then supports leadership. Lesser experienced staff are included to provide mentoring opportunities. The MAKOS development philosophy is to incorporate existing component designs where applicable, use margins to manage technical risk, and incorporate innovative concepts when necessary to meet mission requirements, cost, and schedule.

The MAKOS systems engineering team, led by the Project Systems Engineer (PSE), is responsible for technical decision-making across MAKOS. The systems engineering team includes membership from each system element (e.g., spacecraft, instruments, ground segment). The systems engineering team’s primary responsibilities include requirements capture, synthesis, and verification management; system interface definition and control; technical performance measure management; and continuous risk management. The MAKOS Systems Engineering Management Plan (SEMP), based on NPR 7123.1C, defines the common technical processes.

### 3.5 Risk List

MAKOS employs SwRI’s Continuous Risk Management (CRM) practice, tailored to the requirements of NPR 8000.4A. For identifying, characterizing, analyzing, tracking, and trending risks, we use the web-based Project Information Management System (PIMS, first developed for IMAGE and in use on numerous flight projects since) CRM tool. The PSE is the CRM process owner and works closely with the Project Manager (PM) to identify, mitigate, control, track, and trend risks. Risks are weighted with both criticality (Cf, valued at 1 to 5; Table 3.16) and likelihood (Lf, valued at 1 to 5; Table 3.17) factors and reported to the NASA Program Office monthly.

Using the PIMS CRM tool, any resource on the project can enter an item into the risk database. During weekly Systems Engineering Team calls, the PSE evaluates all risks in the CRM database to first determine if the risk should be accepted and then statusing it with other accepted risks. Risk tracking involves establishing mitigations, monitoring implementation of mitigations, reporting risk retirement progress, and accepting a risk once all mitigations have been implemented. The PSE reports overall risk status during the Principal Investigator Monthly Review (PIMR).

**Table 3.16:** Candidate Consequence Factor Definitions

Consequence	Cost Impact	Schedule Impact
5 – Unacceptable	Exceeds project reserves	Affects Launch date
4 – Major	Exceeds segment reserves	Affects delivery date
3 – Significant	Within segment reserves	Affects critical path but not delivery date
2 – Moderate	Within allocated segment reserves	Reduces slack to the lesser of 1 month or 50% of the remaining schedule
1 - Minimal	No impact to cost reserves	Reduces slack, but still more than 1 month or 50% of remaining schedule

**Table 3.17:** Candidate Likelihood Factor Definitions

Likelihood	Definition
5 – Very High	Very likely to occur. Project’s progress cannot prevent this event, no alternate approach or process is available. Requires immediate management attention.
4 – High	Highly likely to occur. Project’s progress cannot prevent this event, but a different approach or process might prevent this event. Requires management attention.
3 – Moderate	Likely to occur. Project’s progress may prevent this event, but additional actions will be required.
2 - Low	Not likely to occur. Project’s progress is usually sufficient to prevent this type of event.
1 – Very Low	Very unlikely. Project’s progress is sufficient to prevent this event.

## Top Risks

Table 3.18 summarizes the top risks and planned mitigation approaches for MAKOS. Table 3.16 and Table 3.17 summarize preliminary risk definitions at this time. As no contributions of hardware or software are needed, there are no risks due to contributions. Science contributions in Phase E pose no risk to mission success.

**Table 3.18: MAKOS Top Risks & Mitigation Strategies**

#	Risk	Lf	Cf	Mitigation
1	IF a launch issue precludes all four S/C from achieving the necessary formation, THEN there could be delay to the science phase and/or impact to science closure.	1	5	Phase A trades will consider additional propulsion capacity in S/C design to potentially enable achievement of baseline MAKOS configuration from a single launch.
2	IF instrument cross-calibration requires more analysis to resolve known challenges and ensure data product adequacy, THEN additional effort will be required.	3	2	Use of advanced data analytic techniques to develop novel ways to cross-correlate the data using timing, position, and events to improve completeness of datasets for science would be required.
3	IF specialized component updates are needed for the EF instrument deployment mechanism, THEN additional development effort will be required.	2	2	Additional design, prototyping, and testing will be conducted to reduce likelihood of failure of the EF deployment mechanism.
4	IF flight optocoupler speeds do not align with science goals, THEN performance and/or reliability enhancements will be required.	2	3	While the necessary speeds have been demonstrated via prototyping, flight TRL will need to be developed during the mission Phase A.
5	IF spacecraft downlink budgets exceed planned X-band pass capacity, THEN either Ka-band or optical communications may be required to achieve higher data rates.	4	2	Phase A Telecom trades will include Ka-band (increased power, steerable antennas/beams) and Optical Communication options for higher data rates. Additional mitigations may include intelligent data selection (scientist in loop), on-orbit processing and data compression improvements.
6	Given that wire booms have been previously sheared on multiple missions (e.g., WIND, ISEE, IMAGE, STEREO, THEMIS, MMS) – there is a risk that high-TRL unshielded wire booms will be insufficient to prevent physical damage to the wires, resulting in degradation of instrument performance.	2	3	Mitigations will include Kevlar (or SS) shielding like Parker Solar Probe, Van Allen Probes. This concept has been previously studied ( <a href="https://interstellarprobe.jhuapl.edu/Interstellar-Probe-MCR.pdf">https://interstellarprobe.jhuapl.edu/Interstellar-Probe-MCR.pdf</a> ).
7	Given past performance of in situ space plasma instruments in the solar wind – there is a risk that electromagnetic interference and undesired environmental effects (i.e., photoelectrons and secondary electrons) will negatively impact MAKOS magnetic field, electric field and electron observations.	1	2	The application of best practices for instrument design (e.g., coatings, materials), and contamination control/cleanliness will be required. MAKOS will likely need to be a Class C mission.

## Descopes & Mission Resiliency

MAKOS's overall robustness (from large technical margins, high use of heritage subsystems, robust cost and schedule reserves, and low-risk implementation) all reduce the risk that descopes will be required. Should the project violate its reserve release schedule and find no viable workarounds, the Principal Investigator (PI) is prepared to descope to preserve the mission. Potential descopes will be developed in both Step 1 and Phase A – all of which can be taken while keeping the mission above threshold science.

## 4 Development Schedule and Schedule Constraints

### 4.1 Management Approach

The MAKOS management approach is based on decades of successful project management at SwRI, involving PI-led, cost and schedule capped projects ranging in size from single instruments to complete missions (IMAGE, IBEX, MMS, Juno, New Horizons, CYGNSS, and PUNCH). The foundations of our management approach are built on strong PI and PM leadership, a simple organizational structure with clear lines of authority and accountability, a well-defined and controlled set of scientific and engineering requirements with ample resources to meet requirements, controlled interfaces, and a trustworthy, timely, and accurate set of performance metrics. Our PM, safety and mission assurance (SMA), and systems engineering (SE) processes comply with the requirements of NPR 7120.5E, Explorer MAR, and NPR7123.1B, consisting of risk management, resource management, scheduling, earned value management (EVM), staffing, communications, reviews, and reporting. These processes are well honed and supported by a comprehensive set of tools, including the SwRI-developed PIMS.

The MAKOS management plan offers an efficient approach that controls mission cost through a commitment to and control of design, development, and operations costs. Our EVM and SM&A approaches are compliant with the requirements established in NPR-7120.5E and a range of specific category/mission payload classes (e.g., NPR 8705.4). MAKOS manages risks through the project's lifecycle in compliance with NPR 8000.4A. The investigation has large technical margins, a credible and complete schedule with considerable funded schedule reserve, robust cost reserves, and plans reasonable descopes to further reduce cost and mission complexity if necessary. MAKOS's substantial science return and high probability of success are achieved through a novel concept that is robust, low-risk, and will be well within an Announcement of Opportunity's (AO) established constraints. The MAKOS team is dedicated to mission success and will configure the investigation's implementation plan to control and minimize risk within the cost and schedule constraints established by the AO.

**Table 4.1:** *The MAKOS core team is established through the concept design.*

Role	Responsibility	Assumed for this study
Principal Investigator	Lead science effort and all aspects of investigation and provide overall management within contracted cost and schedule	K. Goodrich (WVU)
Program Manager	Lead the development and operations teams and manage project resources and risk	K. Smith (SwRI)
Mission System Engineer	Lead engineering team in overall technical aspects of development and mission operations	R. Rose (SwRI)
Deputy Principal Investigator	Assist PI in leading science effort and ensure instrument performance verification and calibration	L. Wilson (NASA/GSFC)
Project Scientist	Translate science goals into high-level implementation requirements and track progress toward completion	A. Caspi (SwRI)
Science Team	Conduct scientific analyses	I. Cohen, D. Turner (APL); S. Schwartz (CU/LASP); P. Whittlesey (Berkeley); F. Plaschke (Braunschweig)
Spacecraft	Design, fabricate, and test spacecraft and subsystems	SwRI
Payload Mgmt.	Manage payload elements	SwRI
Payload Elements	Design, fabricate, and test scientific instruments	APL, Berkeley, CU/LASP, Iowa, WVU
IA&T	Integrate, assemble, and test MAKOS observatories	SwRI
Mission Operations	Operate mission from launch through end of mission	SwRI

## 4.2 Organization & Processes

**MAKOS Organization:** MAKOS stands ready to respond promptly to a future AO. The core team is established through the MAKOS concept design, including science leadership (PI, PS), project management, instrument development, and mission design and implementation. Table 4.1 details the personnel and institutional roles and responsibilities assigned and assumed for this concept study.

These core MAKOS team members and institutions are well connected to the overall Heliophysics and Geospace communities. Additional team members and institutions to fill key roles will be determined during preparation of a Step-1 proposal to a future AO.

**Science Contributions:** MAKOS requires no foreign or U.S. unfunded contributions of flight hardware or software, contributing to the mission's overall low risk implementation approach. We do, however, benefit from the support and participation of the U.S. and international Heliophysics communities' expertise in MAKOS science and heritage systems. SwRI has a long and proven record of working with foreign and domestic contributors, and, as required, we operate in full compliance with ITAR and export laws and policies. MAKOS will comply with U.S. export laws 22 CFR 120-130 and 15.

The MAKOS team does not anticipate the need to have any foreign nationals access NASA facilities or information systems. The science contributions for MAKOS are discussed further in Section 1.6.

**Control Processes:** MAKOS's implementation plan contributes to the mission's robustness and low risk posture. Practices and strategies are in place for reserves and margin management coupled with tools for predicting problems before they arise. In addition to the mission's robust technical margins, the project is structured with considerable schedule and cost reserves. Inherent in the project's development schedule is over 120 working days of funded schedule margin – days of work scope on the project's critical path(s) not yet tasked but budgeted and included in the base costs for all activities. Additionally, most elements on the project have considerable unfunded schedule margins (i.e., slack) available prior to their final need dates. This combined technical, cost, and schedule margin position assures that MAKOS can achieve its science objectives within the time and cost profile proposed here.

Cost and Schedule Control: SwRI uses EVM practices to monitor and mitigate any potential cost or schedule risk. The MAKOS schedule and costs are tied to the project's work breakdown structure (WBS) thus we are able to use a variety of EVM metrics to monitor, trend, and predict cost and schedule performance. Cost and schedule updates are made monthly across the project. Reserve release is requested only via an engineering change request in PIMS and the appropriate subtools, triggering an established process for approval of the reserves release. Prior to releasing any cost or schedule reserves, the PI, PM, and PSE evaluate options (workarounds, requirements relaxation, etc.) to see if cost and schedule problems can be resolved by release of technical resources or non-critical schedule adjustments. Throughout this process, the PSE, using DOORs, manages the requirements process over the project's lifecycle to control any scope changes or growth.

Technical Reserve & Margin Control: The PSE tracks technical resources (mass, power, CPU usage, etc.) and trended monthly. Like cost and schedule reserves, technical reserves can only be released via the change review process. The PSE leads the effort to determine if reserves should or can be released, to evaluate alternatives, and to verify that any releases are within the

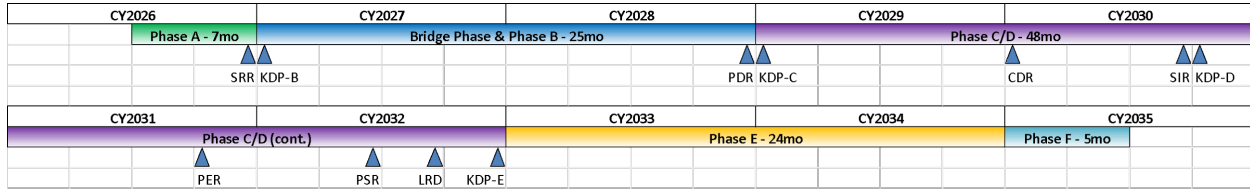


**Figure 4.1:** MAKOS High-Level Schedule

agreed release schedule. Should need for reserves exceed the release schedule, the possibility of descope is evaluated.

### 4.3 High-Level Mission Schedule

The baseline high-level mission schedule for Phases A–F is shown in Figure 4.1. This schedule includes the full duration needed to implement the MAKOS plan, with margin, based on schedules for prior missions of similar scope and cost. The baseline MAKOS mission requires no pre-Phase-A technology development or formulation work, only minor engineering development for the high-rate star tracker as noted in Section 2.2. Every MAKOS component is either already at TRL 6 or will be prior to Phase B under existing roadmap plans. The enhancing technologies discussed in Section 2.2 do require development but are not required for the baseline mission and are not included in the baseline schedule and cost.

This baseline schedule assumes an AO release in early 2026, approximately 18 months after the expected conclusion of the 2024–2033 Heliophysics Decadal Survey. Because the baseline MAKOS plan can be implemented effectively immediately, and because MAKOS launch considerations and science have no strict time window requirements, this schedule can be robustly moved forward or delayed to accommodate other AO release dates.

Table 4.2 lists the rough number of months anticipated for each mission Phase (A through F), Phase B Start to PDR, Phase B Start to CDR, and other key metrics for schedule analysis (Phase B Start to instrument(s) delivery, flight element(s) delivery, integrated flight system delivery, and launch). Note that instrument reviews (I-PDR, I-CDR) are planned approximately 4 months prior to the mission-level reviews but are not explicitly shown on the timelines. Flight model instrument development begins after I-CDR.

### 4.4 Science, Technology Development Plan(s)

The baseline MAKOS science employs currently existing analytical and modeling techniques and does not require any science maturation. Data products from the MAKOS instruments follow established precedent and do not require specific new development beyond the

**Table 4.2:** Key MAKOS Phase Durations

Project Phase or Milestone	Dur. (mos)
Phase A – Conceptual Design	7
Phase B – Preliminary Design (including Bridge Phase)	25
Phase C/D – Detailed Design, Integration & Test	48
Phase E – Primary Mission Operations	24
Phase F – Extended Mission Operations	5
Start of Phase B to Mission PDR	23
Start of Phase B to Mission CDR	37
Start of Phase B to Delivery of Solar Wind Ions	40
Start of Phase B to Delivery of Solar Wind Electrons	40
Start of Phase B to Delivery of Suprathermal Ions	42
Start of Phase B to Delivery of Suprathermal Electrons	40
Start of Phase B to Delivery of Energetic Particles	40
Start of Phase B to Delivery of Electric Fields	42
Start of Phase B to Delivery of Fluxgate Magnetometer	40
Start of Phase B to Delivery of Search Coil Magnetometer	40
Start of Phase B to System Level Integration & Test	44
Start of Phase B to Delivery of Observatory #1	59
Start of Phase B to Delivery of Observatory #2	60
Start of Phase B to Delivery of Observatory #3	61
Start of Phase B to Delivery of Observatory #4	62
Project Total Funded Schedule Reserve	6
Total Development Time Phase B–D	73

usual mission-specific engineering development. MAKOS science may proceed immediately when science data is retrieved and processed through the data pipeline.

The baseline MAKOS implementation is achievable with current technology, requiring only minimal maturation of enabling technologies. The high-rate star tracker on the spacecraft bus is currently at TRL 5 and requires only in-house simulated spin-table testing to achieve TRL 6. This activity requires only a few person-weeks upon receipt of the star tracker, and would be completed well before mission PDR. This maturation is straightforward and low-risk, leveraging concept heritage from prior TRL 9 implementations (e.g., RHESSI).

Additional development of enhancing technologies could benefit MAKOS but is not required for the baseline concept. High-performance optocouplers would help reduce the number of required sensors in some instruments. Appropriate custom designs already exist from at least one NASA-heritage vendor. Instruments would then need engineering development to incorporate these new optocouplers, but this engineering work could likely be incorporated into the EM build and development schedule without significantly affecting the baseline plan above.

#### **4.5 Development Schedule and Constraints**

The baseline Phase A–F mission schedule, detailed with key design reviews and critical path, is shown in Figure 4.2. It includes the development time to delivery required for each instrument, the spacecraft, as well as ground and mission/science operations.

The mission primary critical path runs through the development of the Suprathermal Ions instrument and its delivery to Spacecraft Integration & Test. In addition to known lead times for spaceflight-screened EEE parts (52–62 weeks), the suprathermal and energetic particle instruments rely on detector technology available from a small number of custom vendors. The mission secondary critical path runs through the Propulsion Subsystem, with tertiary tied between the Electric Fields instrument and Spacecraft Structure.

Standard laboratory facilities (e.g., APL, SwRI) can be used for calibration and performance validation, and there should be no expected schedule challenges as those required tests are coordinated well in advance. While tasks like optocoupler design implementation and calibration of MCP efficiency/gain will take time, budgeting for these events is understood.

MAKOS science objectives do not depend strongly on variations in solar activity and can accommodate observations during any part of the solar cycle. The MAKOS orbit is within the Earth-Moon system and requires no gravitational assists or other maneuvers that require precise timing except for needing to acquire resonance with the lunar orbit, all of which is achievable with the propulsion system designed for MAKOS. There are no science- or operations-based launch restrictions identified at this time, and MAKOS can robustly accommodate a launch slip of essentially any duration.

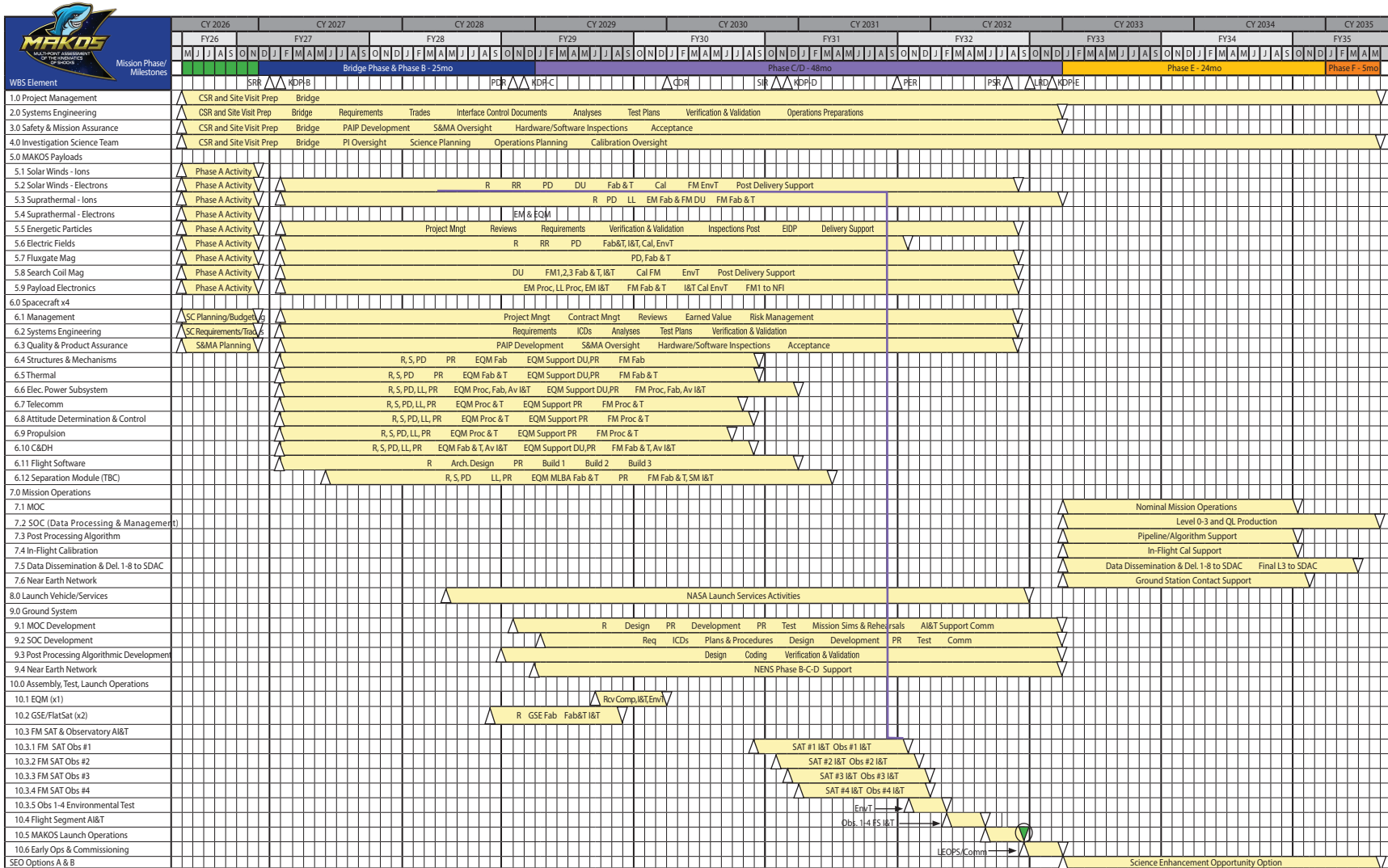


Figure 4.2: MAKOS detailed schedule

## 5 Mission Life-Cycle Cost

### 5.1 Cost Estimate Summary

The MAKOS team used a two-step process to develop a robust understanding of the cost and cost threats. First, SwRI commissioned an Independent Cost Estimate (ICE) using multiple parametric model sets in parallel. Taken together, these efforts define the concept’s baseline estimate. Second, the NASA Goddard Cost Estimating, Modeling and Analysis (CEMA) office independently prepared a separate estimate of the cost using a different model set according to their established office procedure. These cost estimates were developed from the current concept design and implementation plan, including a detailed flight system MEL, heritage-based instruments, a set of notional schedule milestones to define development intervals, and the instrument accommodation requirements. The baseline and CEMA results were reconciled to solidify a correct and complete definition of the input data set for modeling, and to further support the credibility and completeness of the estimate.

Table 5.1 presents a summary of the baseline cost estimate. The four-observatory configuration that we propose will require \$651 million (FY22) funding as a current best estimate. This includes \$601 million in Phase B–D development costs and \$50 million in Phase E–F operations and science cost. Recognizing that this is a preliminary concept study, we apply conservative reserves to all cost elements shown: 50% for all Phase B–D work and 25% for Phase E–F. This brings the baseline estimate to \$964 million including these reserves, with \$901 million allocated to Phases B–D and \$63 million for Phases E–F.

The baseline budget *excludes* costs for Phase A and launch, as these are typically outside PI-managed cost cap for such missions. Phase A costs can be reasonably assumed at \$2.0M. Launch costs for the proposed two vehicles, baselined as SpaceX Falcon 9, are estimated at \$90M (two vehicles at \$45M each) through NASA LSP with standard costs.

We included no funding for new development or technology maturation costs, as instruments and supporting hardware are assumed to be at TRL 6 prior to Phase A. The final report from CEMA supports a conclusion that this *MAKOS baseline budget with proposed reserves* is more than adequate to fund this project.

**Table 5.1:** MAKOS Concept Baseline Cost Estimate

MAKOS Concept Study	FY22 \$M
<i>Phase A</i>	<i>Not incl.</i>
Project Management	39.8
Systems Engineering	23.4
Safety & Mission Assurance	22.9
Science / Technology	77.4
Instruments	224.1
Solar Wind Ions	15.5
Solar Wind Electrons	22.8
Suprathermal Ions	81.3
Suprathermal Electrons	35.3
Energetic Particles	13.0
Fluxgate Magnetometer	6.5
Search Coil Magnetometer	4.4
Electric Fields	29.9
Payload Electronics	15.3
Spacecraft	143.4
Mission Operations	46.4
Launch Vehicles	0.0
Ground Systems	14.1
Observatory Integration & Test	59.5
<b>Subtotal before reserves</b>	<b>650.9</b>
Reserves @ 50% B-D, 25% E-F	312.9
<b>Total (excl. Phase A &amp; Launch Services)</b>	<b>963.8</b>

### 5.2 Costing Methodology

The MAKOS team has employed a comprehensive and conservative approach to developing the cost profile for our proposed mission concept. The proposed costs: 1) cover the full WBS over Phases A–F; 2) capture all elements and tasks to fully execute the mission as proposed; 3) are conservatively estimated using combined results from multiple independently run parametric cost modeling tools; and 4) are risk tolerant due to robust margins on all project elements (technical and programmatic). Table 5.1 shows details of the cost estimate to WBS level 2/3.

**Table 5.2: Cost Attributes & Assumptions**

Attribute	MAKOS Implementation
Mission Profile	4 identical observatories launched in co-orbital pairs on two LV to high-altitude elliptical orbits that are stable over the planned two-year baseline operational lifetime
Instrumentation	<ul style="list-style-type: none"> <li>• Each observatory instrumented with the same eight particle/fields instrument payload</li> <li>• Non-recurring engineering costs amortized across four identical flight units (and across multiple instruments, where feasible)</li> </ul>
High Heritage Payload Elements	<ul style="list-style-type: none"> <li>• All instruments are TRL 6, based on previously flown designs</li> <li>• Built by experienced institutional members of the MAKOS team</li> <li>• Common payload electronics built by SwRI, based on multiple prior flight units</li> </ul>
Simple Reliable spacecraft design	<ul style="list-style-type: none"> <li>• Four identical, modestly sized single-string Class C S/C optimized to carry 8 particles/fields instruments for two-year baseline mission</li> <li>• Non-recurring engineering costs amortized across four identical flight units</li> </ul>

### Key Assumptions

Key assumptions and attributes driving the MAKOS cost estimate are summarized in Table 5.2. Further detailed assumptions necessary to drive one or more of the model tools used can be found in the cost appendix.

### Cost Development

Costs were developed using the following set of ground rules:

- All mission-specific PI-managed costs (excluding Phase A and launch) are included in the NASA funding estimate.
- All costs are stated in fixed-year FY22 dollars (FY22\$).
- NASA standard WBS for flight projects (NASA/SP-2016-3404 – WBS Handbook) used as the Estimating Breakdown Structure for accumulating and identifying cost elements.

The MAKOS cost estimate covers all costs incurred from Phase A through Phase F, including:

- Phase A cost assumed at \$2 million (FY22\$), NOT included in the total PI-managed budget
  - This estimate is not included as it is typically funded separately. The \$2M estimate can be reinserted into the table without additional provision for reserve applied to the budgeted amount.
- Project Management
- Systems Engineering
- Safety and Mission Assurance
- Science & Technology
  - Science team support during development & operations.
  - Technology development if needed; note that, since high-TRL instruments are proposed for the complete payload, we do not anticipate that a technology development effort will be required.
  - Instrument development.
  - Payload control hardware and software.
- Spacecraft development
  - Flight system hardware, including adapters and any other supporting flight hardware as required.
  - Flight software
- Observatory Assembly, Integration, and Test

- Mission Operations
  - Development of ground system hardware and software.
  - Phase E, F operations
- Launch services
  - Launch vehicle costs for two separate launches; for deployment of pairs of observatories to two high orbits ( $r_P$  and  $r_A \geq 15 R_E$ ), assume a vehicle cost of \$45 million each.
    - Note that these costs are excluded from the total PI-managed costs in the above table as they are not typically part of the PI-managed cost cap. An estimate for standard launch services can be reinserted without additional provision for reserve applied to the budgeted amount for WBS 8.
  - Custom launch services if required; For a particles and fields payload that does not require special handling, this is expected to be a minimal/no cost item. The exact deployment configuration and sequence of events may require a small custom effort to ensure proper deployment without risk of collisions as the observatories separate and commence checkout activity but is not expected to significantly affect the total costs. Hydrazine loading will be required.
- Cost reserves as specified in the cost summary: 50% on all Phase B–D costs shown and 25% on all Phase E–F costs shown

### Modeling Tools

The MAKOS management team directed preparation of a cost estimate using parametric modeling tools. The tools used are:

- NASA's Project Cost Estimating Capability (PCEC, version 2.3)
  - Subsystem-level input estimates development cost for bus
  - Includes an estimate of operations cost using an embedded, scaled-down version of the SOCM operations model (see below)
  - Includes estimate of LV cost based on observatory sizing and mission characteristics
- NASA Instrument Cost Model, Contractor version (NICM9c)
  - Estimates instrument cost using either (i) system-level total mass and power or (ii) subsystem-level mass breakdown
  - Reports estimate of sensor hardware cost as well as instrument costs for I&T, management, systems engineering and product assurance
- Space Operations Cost Model (SOCM)
  - NASA-sponsored development of a two-level multi-attribute estimator for all costs of flight projects
  - Inputs are a mix of discrete values and subjective determinations of complexity/difficulty of various aspects of operations
  - Results are summarized as costs allocated among 13 categories among mission operations, science, and management
- Unison (formerly Price Systems) True Planning Space Missions (TPSM)
  - Estimates hardware cost of spacecraft and instruments using detailed component-level information
  - Commercial product built on an extensive modeling of modern manufacturing techniques, tools, procedures, and costs

- Consultant’s Cost Model (CCM)
  - Estimates hardware cost of spacecraft and instruments using detailed component-level information
  - Proprietary model derived from a database of cost elements from completed robotic science missions
- Aerospace Corporation Small Satellite Cost Model (SSCM19)
  - Subsystem-level input estimates the development cost for S/C bus

The models were combined to develop two separate and complete end-to-end estimates of MAKOS cost as shown in Table 5.3. Results of the two model combinations were averaged together to form our baseline estimate as described above.

**Table 5.3:** Cost models used for MAKOS

MAKOS Estimate	Models Used	
	Development	MO & DA
1	CCM	SOCM
2	TPSM	SOCM
3	PCEC + NICM	SOCM (embedded)
4	SSCM + NICM	SOCM

### CEMA Validation Exercise

The Goddard Space Flight Center CEMA office has created a cost estimate for the MAKOS mission primarily based on parametric models for the flight hardware. The purpose of this analysis is to help the MAKOS team identify areas in which to improve their bases of estimate (BoEs) and to help identify, quantify, reconcile, and explain potential risks before the formal TRACE process begins. Table 5.4 shows the high-level results of this effort, organized according to the NASA WBS. This estimate is not a complete lifecycle cost estimate (LCCE) as it does not include Science (WBS 4.0), Launch Services (WBS 8.0), Education and Public Outreach (WBS 11.0), Phase A, or launch vehicle (LV) adapters and LV deployment mechanisms. This independent cost risk analysis serves as a cross-check of the MAKOS team’s cost estimate. CEMA leveraged input distributions to account for technical and schedule uncertainty and to provide risk-adjusted results at the 50% and 70% Confidence Level (CL).

The NASA Project Cost Estimating Capability (PCEC) was used to estimate Phase B–D costs of flight system hardware at the subsystem level (WBS 6.0) and to estimate costs of most other NASA WBS Level 2 elements including Project Management (WBS 1.0), Systems Engineering (WBS 2.0), Safety & Mission Assurance (WBS 3.0), Mission Operations (MOS, WBS 7.0), and

**Table 5.4:** Comparison of MAKOS Baseline cost elements and CEMA probabilistic results

WBS Elements	Phases in Scope	WBS Description	Cost in FY 2022 \$ Millions		
			MAKOS Baseline*	CEMA (50% C.L.)	CEMA (70% C.L.)
1.0, 2.0, 3.0	B-D	Project Management, Systems Engineering, Safety & Mission Assurance	\$ 129.2	\$ 101.1	\$ 138.7
5.0	B-D	Payloads	\$ 336.1	\$ 256.9	\$ 325.3
6.0, 10.0	B-D	Spacecraft, Observatory Integration & Test	\$ 304.3	\$ 209.7	\$ 243.7
7.0, 9.0	B-D	Pre-Launch Development of Mission Operations & Ground Data Systems	\$ 69.6	\$ 18.1	\$ 22.6
Phase E,F	E-F	Mission Phases E-F	\$ 75.4	\$ 77.3	\$ 91.5
		* Each baseline item includes estimate plus reserve for equitable comparison with CEMA CL-based estimates			

Ground Data Systems (GDS, WBS 9.0) combined, and System Level Integration & Test (I&T, WBS 10.0). PCEC was also used to estimate Phase E–F costs of the MAKOS mission. NICM was used to estimate instruments at the system level (WBS 5.0). Argo was used to capture uncertainty and run the Monte Carlo analysis of cost risk. These tools are described in the NASA HQ Strategic Investments Division’s NASA Cost Estimating Handbook (Version 4.0, Appendix E: Models and Tools).

After preliminary results were developed by both the MAKOS in-house modeling work and CEMA, these results were compared to ensure consistent assumptions were applied to both efforts and to reconcile any major differences. Based on interaction with the CEMA office, the MAKOS team made several adjustments that resulted in the baseline estimate presented in this report. Listed below are these adjustments along with the impact to the baseline estimate [higher or lower]:

- [Lower] Revisions to design heritage cost savings applied to six components in the spacecraft Structure/Mechanisms subsystem.
- [Significantly Higher] Tracking network changed from NEN to DSN for operations.
- [Higher] Mission risk class input modified for operations cost estimate.
- [Higher] Management mode input corrected from PI mode to NASA-managed.
- [Higher] Science Team involvement level increased to include full sequence planning during operations.
- [Higher] Science team size increased.
- [Lower] Science team assumed to operate from a single SOC instead of one central SOC with satellite locations.
- [Higher] Spacecraft design characterized as requirements-driven instead of cost-capped.

The net result of these changes was to increase the MAKOS baseline estimate by ~\$40–50 million. Table 5.4 shows the revised baseline estimate for only the cost elements that were directly estimated by CEMA so that the results may be compared. Since CEMA results are probabilistic (shown with either 50% or 70% CL), the corresponding MAKOS cost elements each include the planned 50% cost reserve to permit an equitable comparison of model results. Table 5.4 shows that the MAKOS baseline estimate with the included 50% reserve presents a conservative view of the costs of implementing this ambitious mission, as modeled using a variety of estimating tools and two separate modeling efforts.

### **Forward Cost Threats**

The MAKOS risk assessment and the cost estimate combine to identify key risks likely to drive significant cost increases if not managed and mitigated. A four-observatory constellation, each carrying eight instruments, is within the overall experience base of the institutional partners but the need to deliver multiple flight units raises the criticality of certain common development issues: (1) claimed design heritage for payload element(s) cannot be obtained for any of a variety of reasons, increasing the cost and schedule to deliver; (2) the payload integration and test plan must be designed and managed across multiple institutions to ensure timely performance, and; (3) spacecraft parts issues (availability, performance, cost) across four flight systems could increase cost and time to final delivery.

The MAKOS instrument and spacecraft teams have completed a preliminary mission risk assessment, identifying more than 20 risks, some of which will be mitigated via technology developments discussed in Section 2.2. Those with cost impact potential were considered in the parametric modeling exercises, and the top 7 overall mission risks were further quantified in Section 3.5.

### 5.3 Estimate Allocation Work Breakdown Structure

Table 5.5 below captures the MAKOS development plan with the WBS adopted following NPR 7120.5E and tasks allocated to each WBS following standard SwRI practices.

**Table 5.5: MAKOS Development Plan**

WBS	WBS Owner & Summary Description
1.0 Project Management	Effort to manage, administer, plan and re-plan, control the project. Includes: risk management; resource management (personnel, cost, and schedule); cost & schedule control including EVM and EVM reporting; contracts; subcontracts and procurements; communications within team and to/from NASA; reporting and reviews, project travel.
2.0 Systems Engineering	Effort to plan, implement, oversee the project's SE function, including: requirements management and administration; trade studies, risk management; interface development, control, and compliance, verification, and validation.
3.0 Safety & Mission Assurance	Effort to plan, implement, oversee the project's S&MA in compliance with EXP-RQMT-003. Excludes effort/costs for quality inspections of discrete items, those are carried within the WBS for those items.
4.0 Science & Sci. Team	Effort for the PI to lead and oversee the project, plan, and implement the science investigation, reduce data, and report findings. Also includes activities of the MAKOS PS, Science Team, data analysis, oversight of data products, and archiving.
5.0 Science Payload	Effort to develop and support all instruments including PM, SE, S&MA, Science oversight of the instrument requirements flow down and management, design, development, fabrication, assembly, integration, test, calibration, delivery, and post-delivery support.
6.0 Spacecraft	Effort to develop & deliver four $\mu$ Sats. Includes: 6.1 SC PM; 6.2 SC SE; 6.3 SC S&MA; 6.4 Structures & Mechanisms Subsystem; 6.5 Thermal Subsystem; 6.6 Elec. Power Subsystem; 6.7 Telecomm Subsystem; 6.8 Attitude Determination & Control Subsystem; 6.9 Propulsions Subsystem; 6.10 CD&H; 6.11 FSW; 6.12 Separation Module.
7.0 Mission Operations	Effort to operate the MAKOS constellation in Phase E through the Mission Operations Center (MOC) and the Science Operations Center (SOC). Includes: 7.1 MOC; 7.2 SOC; 7.3 Post-Processing Algorithm; 7.4 In-Flight Calibration Activities; 7.5 Data Dissemination and Archiving; 7.6 Near Earth Network (Ground Station).
8.0 Launch Vehicle	Assumes AO- or HQ-directed costs for launch services (2x LV)
9.0 Ground Systems	Phase B/C/D effort to prepare the ground systems to operate the MAKOS constellation in Phase E and prepare the MOC, SOC, and data processing pipelines. The scope of this WBS includes the following sub-elements: 9.1 MOC Development; 9.2 SOC Development; 9.3 Post Processing Algorithmic Development; 9.4 Near Earth Network (Ground Station provider).
10.0 Systems Assembly, Integration, & Test	Phase B/C/D effort to prepare for and conduct the EQM, EM, and FM $\mu$ sat and integration, receive instruments and integrate Observatories, integrate and test Observatories with the Separation Module, conduct launch and early ops, and conduct Observatory deployment and commissioning on orbit. The scope of this WBS includes the following sub-elements: 10.1 EQM $\mu$ sat and observatory AI&T (1 unit); 10.2 GSE/FlatSat development (2 units); 10.3 FM $\mu$ sat and Observatory AI&T (4 units); 10.4 Flight Segment (Observatories + SM) AI&T; 10.5 Launch Ops; 10.6 Early Ops & Commissioning.

## **Basis of Estimate**

SwRI has an extensive array of recent experience in mission development and execution, and access to a large and diverse database of historical actual costs incurred for all of the MAKOS WBS elements. These multiple and analogous efforts to MAKOS include MMS-SMART, CYGNSS, and PUNCH. Given similarities between missions, actual efforts and costs incurred serve as the principal basis for cross-checking MAKOS resource estimates and cost models; this extensive cost database greatly mitigates estimating error. Note that SwRI has a history of delivering spacecraft with less expensive wrap factors (WBS 1–3), by leveraging the overlapping responsibilities between mission PM/SE/QA functions and the specific needs of spacecraft development team (WBS 6).

The management team evaluated the MAKOS work plan and compared it to inflated actual costs of CYGNSS and MMS-SMART. These calculations yield specific, evidence-based estimates for the MAKOS resource plan and proposed costs. Once these costs were assembled, they were reviewed internally. All costs will be loaded into the IMS to arrive at a final proposed cost profile. The costs proposed for MAKOS include all necessary fringe, overhead, and fee.

## References

---

- Bale, S. D., et al. 2007, *Phys. Rev. Lett.*, **98**, 205001, doi: [10.1103/PhysRevLett.98.205001](https://doi.org/10.1103/PhysRevLett.98.205001)
- Breneman, A. W., et al. 2013, *J. Geophys. Res.*, **118**, 7654, doi: [10.1002/2013JA019372](https://doi.org/10.1002/2013JA019372)
- Burch, J. L., et al. 2016, *Space Science Reviews*, **199**, 5, doi: [10.1007/s11214-015-0164-9](https://doi.org/10.1007/s11214-015-0164-9)
- Burgess, D., et al. 2015, *Collisionless Shocks in Space Plasmas* (Cambridge University Press)
- Cara, A., et al. 2017, *Journal of Geophysical Research: Space Physics*, **122**, doi: [10.1002/2016JA023269](https://doi.org/10.1002/2016JA023269)
- Chen, L.-J., et al. 2018, *Phys. Rev. Lett.*, **120**, 225101, doi:[10.1103/PhysRevLett.120.225101](https://doi.org/10.1103/PhysRevLett.120.225101)
- Ergun, R., et al. 2001, *Space Science Reviews*, **98**, doi: [10.1023/A:1013131708323](https://doi.org/10.1023/A:1013131708323)
- Ergun, R. E., et al. 2016, *Space Science Reviews*, **199**, doi: [10.1007/s11214-014-0115-x](https://doi.org/10.1007/s11214-014-0115-x)
- Gingell, I., et al. 2017, *J. Geophys. Res.*, **122**, doi: [10.1002/2017JA024538](https://doi.org/10.1002/2017JA024538)
- Gloeckler, G., et al. 1998, *Investigation of the Composition of Solar and Interstellar Matter Using Solar Wind and Pickup Ion Measurements with SWICS and SWIMS on the Ace Spacecraft*, Springer Netherlands, doi: [10.1007/978-94-011-4762-0\\_18](https://doi.org/10.1007/978-94-011-4762-0_18)
- Goodrich, K. A., et al. 2018, *J. Geophys. Res.*, **123**, 9430, doi: <https://doi.org/10.1029/2018JA025830>
- . 2019, *J. Geophys. Res.*, **124**, 1855, doi: [10.1029/2018JA026436](https://doi.org/10.1029/2018JA026436)
- Hill, M. E., et al. 2017, *Journal of Geophysical Research: Space Physics*, **122**, doi: [10.1002/2016JA022614](https://doi.org/10.1002/2016JA022614)
- Kasper, J. C., et al. 2016, *Space Science Reviews*, **204**, doi: [10.1007/s11214-015-0206-3](https://doi.org/10.1007/s11214-015-0206-3)
- Keyser, J. D., et al. 2018, *Annales Geophysicae*, **36**, doi: [10.5194/angeo-36-1285-2018](https://doi.org/10.5194/angeo-36-1285-2018)
- Kurth, W. S., et al. 2017, *Space Science Reviews*, **213**, doi: [10.1007/s11214-017-0396-y](https://doi.org/10.1007/s11214-017-0396-y)
- Lin, R. P., et al. 1995, *Space Science Reviews*, **71**, doi: [10.1007/BF00751328](https://doi.org/10.1007/BF00751328)
- Marco, R. D., et al. 2016, *Journal of Instrumentation*, **11**, doi: [10.1088/1748-0221/11/08/C08010](https://doi.org/10.1088/1748-0221/11/08/C08010)
- McComas, D. J., et al. 2016, *Space Science Reviews*, **204**, doi: [10.1007/s11214-014-0059-1](https://doi.org/10.1007/s11214-014-0059-1)
- Mozer, F. S. 2016, *J. Geophys. Res.*, **121**, 910, doi: [10.1002/2016JA022952](https://doi.org/10.1002/2016JA022952)
- Pollock, C., et al. 2016, *Space Science Reviews*, **199**, 331, doi: [10.1007/s11214-016-0245-4](https://doi.org/10.1007/s11214-016-0245-4)

- Russell, C. T., et al. 2016, *Space Science Reviews*, **199**, doi: [10.1007/s11214-014-0057-3](https://doi.org/10.1007/s11214-014-0057-3)
- Schwartz, S. J., et al. 2018, *Geophys. Res. Lett.*, **45**, 511, doi: <https://doi.org/10.1029/2018GL080189>
- . 2022, *Journal of Geophysical Research: Space Physics*, **127**, e2022JA030637, doi: <https://doi.org/10.1029/2022JA030637>
- Torbert, R. B., et al. 2016, *Space Science Reviews*, **199**, doi: [10.1007/s11214-014-0109-8](https://doi.org/10.1007/s11214-014-0109-8)
- Tsurutani, B. T., et al. 1981, *J. Geophys. Res.*, **86**, 4317, doi:[10.1029/JA086iA06p04317](https://doi.org/10.1029/JA086iA06p04317)
- Turner, D. L., et al. 2013, *J. Geophys. Res.*, **118**, 1552, doi:<https://doi.org/10.1002/jgra.50198>
- Vasko, I. Y., et al. 2018, *Geophys. Res. Lett.*, doi: [10.1029/2018GL077835](https://doi.org/10.1029/2018GL077835)
- Wang, S., et al. 2016, *Geophys. Res. Lett.*, **43**, 4850, doi: [10.1002/2016GL069406](https://doi.org/10.1002/2016GL069406)
- Whittlesey, P. L., et al. 2020, *The Astrophysical Journal Supplement Series*, **246**, doi: [10.3847/1538-4365/ab7370](https://doi.org/10.3847/1538-4365/ab7370)
- Wilson, L. B., et al. 2013, *J. Geophys. Res.*, **118**, 957, doi: <https://doi.org/10.1029/2012JA018186>
- . 2014a, *J. Geophys. Res.*, **119**, 6455, doi: <https://doi.org/10.1002/2014JA019929>
- . 2014b, *J. Geophys. Res.*, **119**, 6475, doi: <https://doi.org/10.1002/2014JA019930>
- . 2016, *Phys. Rev. Lett.*, **117**, 215101, doi: [10.1103/PhysRevLett.117.215101](https://doi.org/10.1103/PhysRevLett.117.215101)
- . 2017, *Journal of Geophysical Research: Space Physics*, **122**, doi: [10.1002/2017JA024352](https://doi.org/10.1002/2017JA024352)
- . 2019, *The Astrophysical Journal Supplement Series*, **243**, doi: [10.3847/1538-4365/ab22bd](https://doi.org/10.3847/1538-4365/ab22bd)
- . 2022, *Frontiers in Astronomy and Space Sciences*, **9**, doi: [10.3389/fspas.2022.1063841](https://doi.org/10.3389/fspas.2022.1063841)
- Young, D. T., et al. 2016, *Space Science Reviews*, **199**, 407, doi: [10.1007/s11214-014-0119-6](https://doi.org/10.1007/s11214-014-0119-6)

## **Appendix 1: Master Equipment List (MEL)**

---

The MAKOS master equipment list (MEL) is appended in the subsequent foldout pages. This MEL, v4.1, was provided to both of the independent cost modelers (internal and CEMA) evaluating MAKOS, and was used to generate the cost estimates in both cases. Additional information can be provided upon request.

Element/Subsystem/Component	# OF UNITS			FLIGHT HARDWARE MASSES					FLIGHT HARDWARE POWER										Thermal Limits				OTHER COMPONENT INFORMATION							
									Component					Safe		Orbit Phasing		Hot Ops		Cold Ops		Comm Downlink		Operational Component Limits		Survival Component Limits		TRL	Design Code	Design Maturity
	Power Mode	Unit Power, W CBE	Total Power, W CBE	PGA	Total Power, W MEV	Duty Cycle	Power (W)	Duty Cycle	Power (W)	Duty Cycle	Power (W)	Duty Cycle	Power (W)	Duty Cycle	Power (W)	Min (C)	Max (C)	Min (C)	Max (C)											
<b>MAKOS Spacecraft</b>																														
<b>Structural/Mechanical Subsystem</b>							108.99	24%	135.09	42.66%																				
Column	1	0	1	9.09	9.09	25%	11.37	3.59%	---	---	---	---	---	---	---	---	---	---	---	---	---	---	---	---	---	---	---	---	---	---
Tube section	1	0	1	4.74	4.74	25%	5.93	1.87%	---	---	---	---	---	---	---	---	---	---	---	---	---	---	---	---	---	---	---	---	---	---
Aluminum Inserts	1	0	1	3.92	3.92	25%	4.90	1.55%	---	---	---	---	---	---	---	---	---	---	---	---	---	---	---	---	---	---	---	---	---	---
Hardware	1	0	1	0.43	0.43	25%	0.54	0.17%	---	---	---	---	---	---	---	---	---	---	---	---	---	---	---	---	---	---	---	---	---	---
Center Plate	1	0	1	10.63	13.59	25%	16.98	5.36%	---	---	---	---	---	---	---	---	---	---	---	---	---	---	---	---	---	---	---	---	---	---
Upper Deck	1	0	1	3.51	3.51	25%	4.39	1.39%	---	---	---	---	---	---	---	---	---	---	---	---	---	---	---	---	---	---	---	---	---	---
Lower Deck	1	0	1	3.51	3.51	25%	4.39	1.39%	---	---	---	---	---	---	---	---	---	---	---	---	---	---	---	---	---	---	---	---	---	---
Bolt ring and edge closeouts	2	0	1	2.96	5.92	25%	7.40	2.34%	---	---	---	---	---	---	---	---	---	---	---	---	---	---	---	---	---	---	---	---	---	---
Hardware	1	0	1	0.65	0.65	25%	0.81	0.26%	---	---	---	---	---	---	---	---	---	---	---	---	---	---	---	---	---	---	---	---	---	---
Outer Wedge	8	0	1	4.91	41.58	25%	51.98	16.41%	---	---	---	---	---	---	---	---	---	---	---	---	---	---	---	---	---	---	---	---	---	---
Upper Deck	1	0	1	2.06	2.06	25%	2.58	0.81%	---	---	---	---	---	---	---	---	---	---	---	---	---	---	---	---	---	---	---	---	---	---
Lower Deck	1	0	1	2.06	2.06	25%	2.58	0.81%	---	---	---	---	---	---	---	---	---	---	---	---	---	---	---	---	---	---	---	---	---	---
Corner Column	2	0	1	0.29	0.57	25%	0.71	0.23%	---	---	---	---	---	---	---	---	---	---	---	---	---	---	---	---	---	---	---	---	---	---
Aluminum Inserts	1	0	1	0.26	0.26	25%	0.33	0.10%	---	---	---	---	---	---	---	---	---	---	---	---	---	---	---	---	---	---	---	---	---	---
Hardware	1	0	1	0.25	0.25	25%	0.31	0.10%	---	---	---	---	---	---	---	---	---	---	---	---	---	---	---	---	---	---	---	---	---	---
Secondary Structure	1	0	1	22.83	33.20	22%	40.35	12.74%	---	---	---	---	---	---	---	---	---	---	---	---	---	---	---	---	---	---	---	---	---	---
Propulsion tank support structure	2	0	0	5.65	11.30	25%	14.13	4.46%	---	---	---	---	---	---	---	---	---	---	---	---	---	---	---	---	---	---	---	---	---	---
RCS thruster bracket	8	0	0	0.30	2.40	25%	3.00	0.95%	---	---	---	---	---	---	---	---	---	---	---	---	---	---	---	---	---	---	---	---	---	---
Brackets and Fittings	1	0	0	6.25	6.25	25%	7.81	2.47%	---	---	---	---	---	---	---	---	---	---	---	---	---	---	---	---	---	---	---	---	---	---
Separation Mechanism	2	0	0	2.63	5.25	3%	5.41	1.71%	---	---	---	---	---	---	---	---	---	---	---	---	---	---	---	---	---	---	---	---	---	---
Balance Mass	1	0	0	8.00	8.00	25%	10.00	3.16%	---	---	---	---	---	---	---	---	---	---	---	---	---	---	---	---	---	---	---	---	---	---
Payload booms	1	0	1	4.80	11.53	25%	14.41	4.55%	---	---	---	---	---	---	---	---	---	---	---	---	---	---	---	---	---	---	---	---	---	---
Fields Axial Boom and Deployer	2	0	1	2.34	4.68	25%	5.85	1.85%	Nominal	---	---	---	---	---	---	---	---	---	---	---	---	---	---	---	---	---	---	---	---	---
Fields Radial Boom and Deployer	4	0	1	1.46	5.85	25%	7.31	2.31%	Nominal	---	---	---	---	---	---	---	---	---	---	---	---	---	---	---	---	---	---	---	---	---
Fluxgate Magnetometer Boom/Deployer (radial)	1	0	1	0.50	0.50	25%	0.63	0.20%	Nominal	---	---	---	---	---	---	---	---	---	---	---	---	---	---	---	---	---	---	---	---	---
Search Coil Magnetometer Boom/Deployer (radial)	1	0	1	0.50	0.50	25%	0.63	0.20%	Nominal	---	---	---	---	---	---	---	---	---	---	---	---	---	---	---	---	---	---	---	---	---
<b>Thermal Subsystem</b>				0.56	22%	0.69	0.22%			8.0	20%	9.6	4.8	0.8	0.8	1.9	1.9													
Multi-Layer Insulation (12 Layer)	1	0	0	0.15	0.15	20%	0.18	0.06%	---	---	---	---	---	---	---	---	---	---	---	---	---	---	---	---	---	---	---	---	---	---
Thermal Control Paints	1	0	0	0.10	0.10	20%	0.12	0.04%	---	---	---	---	---	---	---	---	---	---	---	---	---	---	---	---	---	---	---	---	---	---
Thermal Tape	1	0	0	0.05	0.05	20%	0.06	0.02%	---	---	---	---	---	---	---	---	---	---	---	---	---	---	---	---	---	---	---	---	---	---
Heaters	8	0	0	0.01	0.08	25%	0.10	0.03%	Nominal	1.0	8.0	20%	9.6	50%	4.8	9%	0.8	9%	0.8	20%	1.9	20%	1.9	---	---	---	---	---	---	---
Temperature Sensors	18	0	0	0.01	0.18	25%	0.23	0.07%	---	---	---	---	---	---	---	---	---	---	---	---	---	---	---	---	---	---	---	---	---	---
<b>Electrical Power Subsystem</b>				14.80	8%	16.00	5.05%			1.8	3%	1.9	1.9	1.9	1.9	1.9	1.9													
Solar Array Assembly	8	0	8	0.35	2.80	30%	3.64	1.15%	---	---	---	---	---	---	---	---	---	---	---	---	---	---	---	---	---	---	---	---	---	---
Battery	2	0	1	6.00	12.00	3%	12.36	3.90%	Nominal	0.9	1.8	3%	1.9	100%	1.9	100%	1.9	100%	1.9	100%	1.9	100%	1.9	10	25	-20	40	8	BA	A5
<b>Telecommunications Subsystem</b>				1.83	9%	1.99	0.63%			123.3	2%	126.1	9.9	9.9	9.9	9.9	34.9													
X-Band Transponder	1	0	1	0.88	0.88	3%	0.90	0.28%	Rcv	9.6	9.6	3%	9.9	100%	9.9	100%	9.9	100%	9.9	100%	9.9	0%	0.0	---	---	---	---	---	---	---
LNA	1	0	1	0.13	0.13	3%	0.13	0.04%	Nominal	Incl'd	---	---	---	---	---	---	---	---	---	---	---	---	---	---	---	---	---	---	---	---
SSPA	1	0	1	0.45	0.45	3%	0.46	0.15%	Nominal	85.0	85.0	3%	87.6	0%	0.0	0%	0.0	0%	0.0	0%	0.0	30%	26.3	-20	50	TBD	TBD	8	ES	A5
X-band Antenna	2	0	0	0.09	0.18	30%	0.23	0.07%	---	---	---	---	---	---	---	---	---	---	---	---	---	---	---	---	---	---	---	---	---	---
FRF Coax/Guides	4	0	0	0.05	0.20	30%	0.26	0.08%	---	---	---	---	---	---	---	---	---	---	---	---	---	---	---	---	---	---	---	---	---	---
<b>Command and Data Handling Subsystem</b>				3.67	3%	3.78	1.19%			18.0	18.0	10%	19.8	100%	19.8	100%	19.8	100%	19.8	100%	19.8	100%	19.8							
Centaur Single Board Computer	1	0	1	0.34	0.34	3%	0.35	0.11%	Nominal	Incl'd	---	---	---	---	---	---	---	---	---	---	---	---	---	---	---	---	---	---	---	---
Mission Unique Board	1	0	1	0.41	0.41	3%	0.42	0.13%	Nominal	Incl'd	---	---	---	---	---	---	---	---	---	---	---	---	---	---	---	---	---	---	---	---
Low Voltage Power Supply	1	0	1	0.42	0.42	3%	0.43	0.13%	Nominal	Incl'd	---	---	---	---	---	---	---	---	---	---	---	---	---	---	---	---	---	---	---	---
Battery Charge Electronics (DET)	1	0	1	0.50	0.50	3%	0.52	0.16%	Nominal	Incl'd	---	---	---	---	---	---	---	---	---	---	---	---	---	---	---	---	---	---	---	---
Electrical Interface Backplane	1	0	1	0.25	0.25	3%	0.26	0.08%	Nominal	Incl'd	---	---	---	---	---	---	---	---	---	---	---	---	---	---	---	---	---	---	---	---
Chassis	1	0	1	1.75	1.75	3%	1.81	0.57%	---	---	---	---	---	---	---	---	---	---	---	---	---	---	---	---	---	---	---	---	---	---
<b>Guidance, Navigation, and Control Subsystem</b>				2.91	3%	3.00	0.95%			18.2	3%	18.7	18.7	18.7	18.7	18.7	18.7													
Sun Sensor	4	0	1	0.04	0.14	3%	0.14	0.05%	---	---	---	---	---	---	---	---	---	---	---	---	---	---	---	---	---	---	---	---	---	---
IMU	1	0	1	0.75	0.75	3%	0.77	0.24%	Nominal	12.0	12.0	3%	12.4	100%	12.4	100%	12.4	100%	12.4	100%	12.4	100%	12.4	-40	85	-55	90	8	ES	A5
Star Tracker Camera (with Baffle)	3	0	1	0.57	1.71	3%	1.76	0.56%	Nominal	0.5	1.5	3%	1.5	100%	1.5	100%	1.5	100%	1.5	100%	1.5	100%	1.5	-65	20	TBD	TBD	8	ES	A5
Star Tracker DPU	1	0	1	0.31	0.31	3%	0.32	0.10%	Nominal	4.7	4.7	3%	4.8	100%	4.8	100%	4.8	100%	4.8	100%	4.8	100%	4.8	-40	70	TBD	TBD	8	ES	A5
<b>Propulsion Subsystem</b>				11.56	8%	12.54	3.96%			131.0	3%	135.3	2.9	6.7	1.2	1.8	1.7													
Tanks (dry)	6	0	0	1.20	7.20	3%	7.42	2.34%	---	---	---	---	---	---	---	---	---	---	---	---	---	---	---	---	---	---	---	---	---	---
deltaV Propulsion thruster	3	0	1	0.02	0.07	3%	0.07	0.02%	Hold open	1.3	3.9	3%	4.0	0%	0.0	100%	4.0	0%	0.0	0%	0.0	0%	0.0	---	---	---	---	---	---	---
								0.00%	Activate	30.0	90.0	3%	92.7	0%	0.0	0%	0.0	0%	0.0	0%	0.0	0%	0.0	---	---	---	---	---	---	---
								0.18%	Hold open	1.3	10.4	3%	10.7	25%	2.7	10%	1.1	10%	1.1	10%	1.1	10%	1.1	---	---	---	---	---	---	---
RCS Thrusters (dry)	8	0	1	0.07	0.66	3%	0.68	0.18%	Hold open	1.3	10.4	3%	10.7	25%	2.7	10%	1.1	10%	1.1	10%	1.1	10%	1.1	---	---	---	---			



Element/Subsystem/Component	# OF UNITS			FLIGHT HARDWARE MASSES					FLIGHT HARDWARE POWER														Thermal Limits				OTHER COMPONENT INFORMATION															
									Component				Safe		Orbit Phasing		Hot Ops		Cold Ops		Comm Downlink		Operational Component Limits		Survival Component Limits		TRL	Design Code	Design Maturity	Heritage	Vendor	Model #, Part #	Characteristics									
	Power Mode	Unit Power, W CBE	Total Power, W CBE	PGA	Total Power, W MEV	Duty Cycle	Power (W)	Duty Cycle	Power (W)	Duty Cycle	Power (W)	Duty Cycle	Power (W)	Duty Cycle	Power (W)	Duty Cycle	Power (W)	Min (C)	Max (C)	Min (C)	Max (C)																					
Preamp Electronics Unit	6	0	1	0.09	0.52	3%	0.53	0.17%	Nominal	0.4	2.3	3%	2.3	0%	0.0	100%	2.3	0%	0.0	0%	0.0	0%	0.0	0%	0.0										TC	A5		UNH		Low noise pre-amplifier electronic component with milled Al alodine finish chassis		
Electric Fields Cables	1	0	1	3.36	3.36	3%	3.46	1.09%	Nominal	0.5	0.5	3%	0.5	0%	0.0	100%	0.5	0%	0.0	0%	0.0	0%	0.0	0%	0.0										TC	A5		UNH		Cu with Teflon		
Heater	6	0	1	0.01	0.06	3%	0.06	0.02%	Nominal	1.0	6.0	3%	6.2	100%	6.2	100%	6.2	0%	0.0	0%	0.0	0%	0.0	0%	0.0										TC	A5		UNH		Internally redundant, wired in parallel		
Fluxgate Magnetometer				0.74	1.47	25%	1.84	0.58%			1.00		1.03		1.03		1.03		0.00		0.00		0.00														MMS/FIELDS/FGM (Torbert et al., 2016; Russell et al., 2016)	UCLA				
Sensor	2	0	1	0.73	1.46	25%	1.83	0.58%	Nominal	---	---	---	---	---	---	---	---	---	---	---	---	---	---	---	---										ST	E1			Electronic component with milled Al alodine finish chassis.			
Electronics (in Common Fields Electronics)	---	---	---	---	---	---	---	---	---	---	---	---	---	---	---	---	---	---	---	---	---	---	---	---										ST	E1			Electronic component with milled Al alodine finish chassis.				
Heater	1	0	1	0.01	0.01	3%	0.01	0.00%	Nominal	1.0	1.0	3%	1.0	100%	1.0	100%	1.0	0%	0.0	0%	0.0	0%	0.0	0%	0.0										TC	A5			Internally redundant, wired in parallel			
Search Coil Magnetometer				0.81	0.81	25%	1.01	0.32%			1.00		1.03		1.03		1.03		0.00		0.00		0.00														Juno/Waves (Kurth et al., 2017)	Iowa				
Sensor	1	0	1	0.80	0.80	25%	1.00	0.32%	Nominal	---	---	---	---	---	---	---	---	---	---	---	---	---	---	---										ST	E1		Roccor		Electronic component with milled Al alodine finish chassis.			
Electronics (in Common Fields Electronics)	---	---	---	---	---	---	---	---	---	---	---	---	---	---	---	---	---	---	---	---	---	---	---	---										---	---			---				
Heater	1	0	1	0.01	0.01	3%	0.01	0.00%	Nominal	1.0	1.0	3%	1.0	100%	1.0	100%	1.0	0%	0.0	0%	0.0	0%	0.0	0%	0.0											TC	A5			Internally redundant, wired in parallel		
Common Payload Instrument Electronics Unit (IEU)				3.36	3.36	10%	3.69	1.17%			3.12		3.57		0.00		3.57		3.57		3.57		3.57																			
Centaur Single Board Computer	1	0	1	0.34	0.34	3%	0.35	0.11%	Nominal	1.0	1.0	3%	1.0	0%	0.0	100%	1.0	100%	1.0	100%	1.0	100%	1.0	100%	1.0												ES	A5		SwRI		Single Board Computer
Payload Mission Unique Board	1	0	1	0.34	0.34	20%	0.41	0.13%	Nominal	1.0	1.0	20%	1.2	0%	0.0	100%	1.2	100%	1.2	100%	1.2	100%	1.2	100%	1.2												ES	C3		SwRI		128GB Flash storage; propulsion valve drivers
Mass Memory Board (M4)	1	0	1	0.34	0.34	20%	0.41	0.13%	Nominal	1.0	1.0	20%	1.2	0%	0.0	100%	1.2	100%	1.2	100%	1.2	100%	1.2	100%	1.2												ES	C3		SwRI		3.3Vdc, 5Vdc, ±12Vdc
Low Voltage Power Supply	1	0	1	0.42	0.42	20%	0.50	0.16%	Nominal	0.1	0.1	20%	0.1	0%	0.0	100%	0.1	100%	0.1	100%	0.1	100%	0.1	100%	0.1												ES	C4		SwRI		Battery charge control, SPG
Electrical Interface Backplane	1	0	1	0.25	0.25	20%	0.30	0.09%	Nominal	---	---	---	---	---	---	---	---	---	---	---	---	---	---	---	---												ES	C3		SwRI		4-board 3U cPCI connectors
Chassis	1	0	1	1.67	1.67	3%	1.72	0.54%	Nominal	---	---	---	---	---	---	---	---	---	---	---	---	---	---	---	---											ST	A5		SwRI		4-board 3U chassis; milled Al alodine finish	
Instrument Electrical Cables	1	0	1	1.50	1.50	55%	2.33	0.73%	Nominal	0.4	0.4	55%	0.6	0%	0.0	100%	0.6	100%	0.6	100%	0.6	100%	0.6	100%	0.6	-65.0	200.0	-65.0	200.0								WH	E1		SwRI		Cu with Teflon insulation
<b>Total MAKOS Payload Suite Mass/Power</b>					<b>113.34</b>	<b>24%</b>	<b>140.38</b>	<b>44.34%</b>					<b>114.32</b>	<b>18%</b>	<b>134.99</b>		<b>8.24</b>		<b>37.10</b>		<b>123.94</b>		<b>123.94</b>																			
<b>Total Observatory DRY Mass/Power</b>					<b>259.71</b>	<b>22%</b>	<b>316.63</b>								<b>67.04</b>		<b>96.88</b>		<b>178.32</b>		<b>180.03</b>		<b>204.96</b>																			

234.044